의학박사 학위논문

Regulation of glutamate release by presynaptic Ca^{2+} channels and K^{+} channels

전시냅스의 칼슘 이온 채널과 칼륨 이온 채널에 의한 글루탐산 분비의 조절 기전 연구

2021년 8월

서울대학교 대학원

의과학과 생리학 전공

이 병 주

A thesis of the Degree of Doctor of Philosophy

전시냅스의 칼슘 이온 채널과 칼륨 이온 채널에 의한 글루탐산 분비의 조절 기전 연구

Regulation of glutamate release by presynaptic Ca^{2+} channels and K^{+} channels

August 2021

The Department of Biomedical Sciences

Seoul National University

College of Medicine

Byoung Ju Lee

전시냅스의 칼슘 이온 채널과 칼륨 이온 채널에 의한 글루탐산 분비의 조절 기전 연구

지도 교수 호 원 경

이 논문을 의학박사 학위논문으로 제출함

2021년 4월

서울대학교 대학원

의과학과 생리학 전공

이 병 주

이병주의 의학박사 학위논문을 인준함

2021년 7월

위 원 장 _____

부위원장 _____

위 원 _____

위 원 _____

위 원 _____

Regulation of glutamate release by presynaptic Ca^{2+} channels and K^+ channels

by

Byoung Ju Lee

A thesis submitted to the Department of Physiology
in partial fulfillment of the requirements for the
Degree of Doctor of Philosophy in Physiology at
Seoul National University College of Medicine

July 2021

Approved by Thesis Committee:

Professor _____ Chairman

Professor _____ Vice chairman

Professor _____

Professor _____

Professor _____

ABSTRACT

Regulation of glutamate release by presynaptic Ca^{2+} channels and K^+ channels

Byoung Ju Lee

The Department of Biomedical Sciences

The Graduate School

Seoul National University

College of medicine

Neurotransmitter release occurs either synchronously to action potentials or spontaneously, yet whether molecular machineries underlying evoked and spontaneous release are identical, especially whether voltage-gated Ca^{2+} channels (VGCCs) can trigger spontaneous events has been in debate. To elucidate this issue, we characterized Ca^{2+} dependency of miniature excitatory postsynaptic currents (mEPSCs), in autaptic cultured hippocampal neurons. I found that spontaneous release shows Ca^{2+} cooperativity comparable to evoked release, and most of $[Ca^{2+}]_o$-dependent mEPSCs was attributable to Ca_V2 family VGCCs. Coupling distance between VGCCs and Ca^{2+} sensors was estimated as tight for both types of release. Moreover, I explored the experimental evidence for contribution of L-type Ca^{2+} channels (LTCCs) on spontaneous release. The spontaneous exocytosis mechanism of this channel was somewhat different from Ca_V2 family. The coupling distance

between LTCCs and Ca^{2+} sensors was longer than that of Ca_V2 family which was tested by 10 mM $[EGTA]_i$. Therefore, I suggested that the spontaneous release might be affected by global $[Ca^{2+}]$ which was regulated by LTCCs. In addition, the mechanism for global $[Ca^{2+}]$-dependent spontaneous release was mediated by calmodulin (CaM)-dependent synaptic vesicle exocytosis. In addition, I found that presynaptic voltage-gated K^+ channels (VGKCs) regulate spontaneous glutamate release. The role of K_V7 is mediated specifically by regulating LTCCs, while the role of K_V1 is mediated specifically by regulating P/Q-type VGCCs, suggesting the specific coupling between VGKCs and VGCCs. Taken together, my study reveals subtype-specific mechanisms of VGCCs and VGKCs in regulating spontaneous glutamate release.

Keywords: hippocampal autaptic pyramidal neuron, voltage-gated Ca^{2+} channels, resting $[Ca^{2+}]$, voltage-gated K^+ channels, spontaneous synaptic transmission, evoked synaptic transmission, Ca^{2+} nanodomain

Student Number: 2010-31172

CONTENTS

LIST OF FIGURES

Chapter 1

Chapter 2

Chapter 3

LIST OF ABBREVIATIONS

VGCC or Ca_v	voltage-gated Ca^{2+} channel
LTCC	L-type Ca^{2+} channel
VGKC or K_v	voltage-gated K^+ channel
I_M	M-type K^+ currents
I_D	D-type K^+ currents
I_{Ca}	Ca^{2+} currents
$[Ca^{2+}]_o$	extracellular Ca^{2+} concentration
$[Ca^{2+}]_i$	intracellular Ca^{2+} concentration
$[K^+]_o$	extracellular K^+ concentration
CaSR	calcium-sensing receptor
Syt1	synaptotagmin-1
mEPSC	miniature excitatory postsynaptic current
eEPSC	evoked excitatory postsynaptic current
PPR	paired-pulse ratio
RRP	readily releasable pool
AP	action potential
RMP	resting membrane potential
HP	holding potential
Aga	ω-Agatoxin-IVA

Cono	ω-Conotoxin GVIA
SNX	SNX-482
Nimo	nimodipine
Bay K	Bay K 8644
RYN	ryanodine
RyR	ryanodine receptor
2-APB	2-Aminoethyl diphenylborinate
Lino	linopirdine
XE	XE991
4-AP	4-Aminopyridine
PTX	picrotoxin
TTX	tetrodotoxin
CaM	calmodulin
CaM-iP	calmodulin inhibition peptide
CA1-PCs	pyramidal cells of CA1 hippocampus
CA3-PCs	pyramidal cells of CA3 hippocampus
DIV	day *in vitro*
Ctrl	control

GENERAL INTRODUCTION

Synaptic transmission is a major mechanism for information processing in neural systems. Excitation of a neuron can be transmitted to postsynaptic neurons by means of neurotransmitter release triggered by action potentials (APs) in the presynaptic nerve terminals. However, neurotransmitter release also occurs spontaneously at resting state with low frequency around 0.01 Hz per synaptic bouton (Murthy and Stevens, 1999; Sara *et al.*, 2005). This type of synaptic communication has pivotal roles in synaptic structure and function, including synapse maturation and maintenance, homeostasis, and plasticity. In spite of physiological importance of spontaneous release, its molecular mechanisms are poorly understood. Neurotransmitter release occurs when an increase in intracellular Ca^{2+} is detected by Ca^{2+} sensors at presynaptic terminals. During AP firing, Ca^{2+} influx mediated by VGCCs is captured by vesicular Ca^{2+} sensors, leading to synaptic vesicle fusion. Spontaneous release also involves Ca^{2+}-dependent processes, yet it is not clear whether extracellular Ca^{2+} ($[Ca^{2+}]_o$)-induced-spontaneous release utilizes the same Ca^{2+} sensors and sources with evoked release (Groffen *et al.*, 2010; Kavalali, 2015; Xu *et al.*, 2007; Xu *et al.*, 2009). In particular, the contribution of VGCCs to spontaneous release is controversial. It is generally accepted that stochastic VGCCs activity is a major trigger of spontaneous release at inhibitory synapses (Goswami *et al.*, 2012; Williams *et al.*, 2012), yet the contribution of VGCCs was denied in many studies at excitatory synapses (Courtney *et al.*, 2018; Dai *et al.*, 2015; Tsintsadze *et al.*, 2017; Vyleta and Smith, 2011).

Neuronal VGKCs have been shown to contribute to RMP, postsynaptic potentials, propagated action potentials, action potential firing patterns, and neurotransmitter

release (Hille, 1978; Rudy, 1988). Recent studies have shown that control of the presynaptic resting potential via resting K^+ channels conductance (e.g. $K_V7.2/3$ at hippocampus or $K_V7.5$ at Calyx of Held) can modulate the post synaptic signals in mammalian nerve terminals (Huang and Trussell, 2011; Sun and Kapur, 2012), and they are also known to be located at presynaptic terminals (Chung *et al.*, 2006). In addition, these channels are also known as slow activation, non-inactivation channels and activated at subthreshold potentials, so that they may be able to control the presynaptic potentials (Brown and Adams, 1980; Brown and Passmore, 2009). Recent studies reveal that K_V7 families are involved in the regulation of neurotransmitter release (Shah *et al.*, 2011; Vervaeke *et al.*, 2006). In addition, several studies report that K_V1 families are preferentially located at axons and axon terminals in hippocampal pyramidal neurons (Cooper *et al.*, 1998; Wang *et al.*, 1993). Also previous study explore that K_V1 channels are able to regulate spontaneous release in inhibitory synapses (He *et al.*, 2012).

The purpose of this study is to understand the mechanism of how VGCCs and VGKCs regulate spontaneous glutamate release. Using autaptic excitatory hippocampal synapse, I found that P/Q-, N-, R-, and L-type Ca^{2+} channels are involved in the spontaneous glutamate release and 53% of spontaneous glutamate release is mediated by a nanodomain coupling between Ca^{2+} sensors and P/Q-, N-, and R-type Ca^{2+}channels. L-type Ca^{2+}channels act as a facilitator on spontaneous release by regulating global $[Ca^{2+}]_i$. Furthermore, the role of presynaptic VGKCs in spontaneous glutamate release has been explored and this study suggests that the coupling between VGKCs and VGCCs with high specificity in the presynaptic terminals is the key factor to regulate spontaneous glutamate release. This configuration may allow K^+ channels to control Ca^{2+} channel activity strongly with a high specificity.

CHAPTER 1

The mechanisms of P/Q-, N-, and R-type Ca^{2+} channel mediated glutamatergic synaptic transmission

INTRODUCTION

Synaptic transmission is a major mechanism of information processing in neural systems. Neuronal excitation can be transmitted to postsynaptic neurons via neurotransmitter release triggered by action potentials (APs) in presynaptic nerve terminals. However, neurotransmitter release also occurs spontaneously at resting state with a low frequency of around 0.01 Hz per synaptic bouton (Murthy and Stevens, 1999; Sara *et al.*, 2005). This type of synaptic communication plays a pivotal role in synaptic structure and function, including synapse maturation and maintenance, homeostasis, and plasticity (Kavalali, 2015). Despite the physiological importance of spontaneous release, its molecular mechanisms are poorly understood.

Neurotransmitter release occurs when an increase in intracellular Ca^{2+} is detected by Ca^{2+} sensors at presynaptic terminals. During AP firing, Ca^{2+} influx mediated by voltage-gated Ca^{2+} channels (VGCCs) is captured by vesicular Ca^{2+} sensors, leading to synaptic vesicle fusion. Spontaneous release also involves Ca^{2+}-dependent processes, yet it is not clear whether Ca^{2+}-dependent spontaneous release utilizes the same Ca^{2+} sensors and sources as the evoked release (Groffen *et al.*, 2010; Kavalali, 2015; Xu *et al.*, 2007; Xu *et al.*, 2009). In particular, the contribution of VGCCs to spontaneous release remains controversial. It is generally accepted that stochastic VGCC activity is a major trigger of spontaneous release at inhibitory synapses (Goswami *et al.*, 2012; Williams *et al.*, 2012), yet many studies deny a contribution of VGCCs at excitatory synapses (Courtney *et al.*, 2018; Dai *et al.*, 2015; Tsintsadze *et al.*, 2017; Vyleta and Smith, 2011). It has been suggested that glutamatergic spontaneous release is independent of Ca^{2+} influx via VGCCs, but tonically activated by the calcium-sensing receptor (CaSR), which is a G-protein coupled receptor

whose activity depends on external Ca^{2+} concentration ($[Ca^{2+}]_e$) (Tsintsadze *et al.*, 2017; Vyleta and Smith, 2011). On the other hand, Ermolyuk et al. (2013) showed clear evidence that glutamatergic spontaneous release in cultured hippocampal neurons is triggered by local Ca^{2+} increases induced by stochastic opening of presynaptic VGCCs at the resting state. These contradictory results may imply that spontaneous release is mediated by multiple Ca^{2+} sensors and multiple Ca^{2+} sources, and their relative contributions are distinct among different cell types and differentially regulated by various cellular states or signaling mechanisms.

The coupling distance between Ca^{2+} sources and Ca^{2+} sensors of synaptic vesicles is a key determinant of the efficacy and speed of AP-triggered synaptic transmission (Eggermann *et al.*, 2012; Neher and Sakaba, 2008). In nanodomain coupling, a single or a few Ca^{2+} channel openings would lead to brief and local increases in Ca^{2+} concentration and directly trigger synaptic vesicle fusion, so that tight coupling has functional advantages, in terms of speed, temporal precision, and energy efficiency of synaptic transmission (Eggermann *et al.*, 2012; Schmidt *et al.*, 2013). On the other hand, loose coupling enables the control of initial release probability by fast endogenous Ca^{2+} buffers and the generation of facilitation by buffer saturation, providing the molecular framework for presynaptic plasticity (Vyleta and Jonas, 2014). The coupling configuration may also have implications for spontaneous release, but little information is available to date.

This study suggests that spontaneous glutamate release mediated by VGCCs uses common mechanisms with evoked release, while contribution of VGCC-dependent spontaneous release varies widely among different synapses and different experimental conditions.

MATERIALS AND METHODS

1. Autaptic neuronal culture

All preparations were carried out under the animal welfare guideline of Seoul National University (SNU), and approved by IACUC of SNU. Primary cultures of rat hippocampal neurons were prepared as described previously with slight adaptations (Bekkers and Stevens, 1991). Briefly, hippocampal neurons and astrocytes were obtained from Sprague-Dawley (SD) rats according to the protocols approved by the Seoul National University Institutional Animal Care and Use Committee. Astrocyte cultures were prepared from the Sprague-Dawley rat cortices P0 - P1 and grown for 10 days in 100-mm culture dish in glial medium [minimum essential medium (MEM; Invitrogen) supplemented with 0.6 % glucose, 1 mM pyruvate, 2 mM GlutaMAX-I (Invitrogen), 10 % horse serum (HS; Invitrogen), and 1 % penicillin-streptomycin (PS; Invitrogen)] before plating on the sprayed microisland coverslips in 30-mm petri dishes. 2 - 3 days before neurons being added in sprayed microisland dishes, astrocytes were removed from the 100-mm culture dish using trypsin-EDTA (Invitrogen) and plated on the microisland coverslips at a density of 60,000 cells/dish. Hippocampi from P0 - P1 SD rats were dissected in Hank's balanced salt solution (Invitrogen), digested with papain (Worthington, Freehold, NJ, USA), and then triturated with a polished half-bore Pasteur pipette. Immediately after removing glia medium in 30-mm dishes of microisland-shaped astrocytes, hippocampal neurons were added at a density of 6,000 cells/dish and were grown in neurobasal medium supplemented with B27 and glutamax (Invitrogen).

2. Electrophysiology

For recordings in autaptic cultured neurons, cells were visualized with an Olympus IX70 inverted microscope. Whole-cell voltage- or current-clamp recordings from hippocampal autaptic pyramidal neurons were performed at room temperature and continuously perfused with extracellular solution consisting of following composition (in mM): 135 NaCl, 2.5 KCl, 2 $CaCl_2$, 1 $MgCl_2$, 10 glucose, 10 HEPES, 0.1 EGTA, pH 7.3 adjusted with NaOH (295 - 300 mOsm), and maintained at 0.5 - 1 ml min-1. All recordings were done at least 23 days after neurons were plated on coverslips. The internal pipette solution for recording mEPSCs and resting membrane potential (RMP) was used K-gluconate based solution.

Whole-cell voltage- or current-clamp recordings were performed at 32 ± 1°C and the rate of aCSF perfusion was maintained at 1 - 1.5 ml min-1. For high $[K^+]_o$ experiments, NaCl was reduced to maintain osmolarity. Recordings were made in somata with an EPC-10 amplifier (HEKA Electonik, Lambrecht/Pfalz, Germany). Signals were low-pass filtered at 5 kHz (low-pass Bessel filter) and sampled at 10 kHz. Series resistance (Rs) was monitored, and only recordings with Rs remained constant (<30% change during a recording) were used. Rs was compensated to 50 - 70 %. The data were analyzed using IGOR software (Wavemetrics, Lake Oswego, OR, USA). Patch electrodes were pulled from borosilicate glass capillaries to a resistance between 3 and 4 MΩ when filled with pipette solution. The internal pipette solution for recording miniature excitatory postsynaptic currents (mEPSCs) contained the following composition (in mM): 130 Cs-methanesulfate, 8 NaCl, 4 MgATP, 0.3 NaGTP, 10 HEPES, 0.1 EGTA, pH 7.3 adjusted with CsOH (295 - 300 mOsm). For RMP recording, K-gluconate was substituted for Cs-methanesulfate, and pH was adjusted with KOH.

The mEPSCs of hippocampal autapses were recorded at holding potential of -70 mV. 0.5 μM TTX and 0.1 mM picrotoxin (PTX) was added during recordings in acute slices. Events exceeding 6 - 7 pA within a specified interval of three to four digitized points (0.5 - 0.8 ms) that showed a single exponential decay time course were identified as mEPSC. The rise time of mEPSC indicated the 20 - 80 % rise time. mEPSC frequency esd measured within 20 s bins. Synaptic activities were recorded at a holding potential of -70 mV. eEPSCs were recorded every 20 s after applying depolarization pulses from -70 to 0 mV for 2 ms. From the continuous recordings at -70 mV without stimulations, toxins and chemicals were typically applied for 5 - 20 min until a constant effect was observed.

3. Drugs

ω-Agatoxin-IVA, ω-Conotoxin GVIA, SNX-482, TTX, and ryanodine were purchased from Alomone Labs (Jerusalem, Israel). All other chemicals were purchased from Sigma (St. Louis, MO, USA). Toxin stock solutions were made at 1000-fold concentration with distilled water and stored at -20°C.

4. Estimation of the distance between Ca^{2+} sensors and VGCCs

Extensive theoretical studies assert that buffered calcium diffusion from open calcium channels make calcium microdomain of tens of micromolar concentration (Neher, 1998). Assuming that free buffer concentration does not change very much owing to rapid diffusional replacement of Ca^{2+}-bound buffer molecules with free buffer, the spatial profile of $[Ca^{2+}]$ as a function of distance from an open calcium channel (r) is given by:

$$[Ca^{2+}](r) = i_{Ca} / (4\ F\ D_{Ca}\ r) \exp(-r/\lambda)$$

, where i_{Ca} = calcium current; F = Faraday constant; D_{Ca} = diffusion constant of Ca^{2+} in cytosol.

Therefore, the ratio of $[Ca^{2+}]$ at a given distance from a Ca^{2+} channel (r) before and after the addition of BAPTA is as follows:

$$\text{Ca ratio} = \exp(-r/\lambda_b) / \exp(-r/\lambda_0)$$

, where λ_0 and λ_b are the length constants before and after BAPTA was added, respectively. Since the length constant, λ, in the presence of free calcium buffer [B] with Ca^{2+} binding rate constant, k_{on}, is given by

$$\lambda = \sqrt{}\ D_{Ca} / (k_{on}\ [B])$$

. Inserting this equation into the Ca ratio equation, we have dependence of calcium ratio as a function of $[BAPTA]_{total}$ (x, in mM) as follows:

$$\text{Ca ratio} = \exp[-r/\lambda_0\ (\sqrt{}(1+ (P_{b,1}/P_0)\ x) - 1)]$$

, where λ_0 = length constant in the presence of endogenous buffer (B_0) alone; P_0 and $P_{b,1}$ are buffer products (k_{on} [B]) of B_0 and 1 mM BAPTA, respectively. Finally, assuming that only the calcium influx through a calcium channel (or cluster) nearest to a vesicle is relevant to its release, and that glutamate release has the n-th power dependence on $[Ca^{2+}]$, the ratio of release (R_{rls}) before and after adding BAPTA has the relationship:

$$R_{rls} = \exp[\ n\ (-r\ /\lambda_0\ (\sqrt{}(1+ (P_{b,1}/P_0)\ x) - 1))]$$

. The n values for miniature and evoked EPSCs were obtained from Fig. 1D and 1F. $P_{b,1}$ is calculated as 300 $mM^{-1}ms^{-1}$ considering that k_{on} of BAPTA = 400 $mM^{-1}ms^{-1}$, and $[Ca^{2+}]_{rest}$ = 80 nM. Fitting the above equation to the plot of evoked or miniature EPSC frequency as a function of $[BAPTA]_{total}$ with setting r/λ_0 and P_0 as free

parameters, we estimated the distance of vesicles from the calcium source (*r*).

5. Calculation of VGCC coactivation for spontaneous or evoked glutamate release

The coactivation of VGCC on spontaneous or evoked release was estimated by simple arithmetic calculation of the VGCC contributions which were induced by single or a pair of VGCC blockers application. We assumed that cross reactivity of VGCC blockers on transmitter release was negligible (Fig. 11). The contribution of each VCGG to evoked release was calculated from the reduction of eEPSC amplitude in each VGCC blocker. The contribution of each VCGG to spontaneous release was calculated from the reduction of mEPSC frequency in each VGCC blocker, and then adjusted by the proportion of VGCC-dependent spontaneous release (divided by 0.53).

The contribution of coactivation of two VGCCs was calculated from the sum of the reduction in blocker 1 and 2, separately, (Fig. 4C), subtracted by the reduction in blocker 1 and 2, simultaneously (Figs. 12C and 12F). The sole contribution of each VGCC was obtained from the reduction in 3-mix (the total VGCC dependent portion) subtracted by the reduction in the other two VGCC blockers (colored arrows, Figs. 12C, 12F). The sum of coactivation portion and the sole contribution of a single VGCC was comparable to the reduction of the single VGCC blocker (Fig. 12Db). The contribution of three VGCC coactivation was calculated by subtracting the single VGCC contribution from the sum of each two blocker coactivations and the sole VGCC contribution (*e.g.* coactivation of P/Q + N + R = (coactivation of P/Q + N) + (coactivation of P/Q + R) + contribution of sole P/Q - total contribution of P/Q).

6. Statistical analysis

Data were expressed as the mean ± SEM, where *N* represents the number of cells studied. Statistical analysis was performed using IgorPro (version 6.1, WaveMetrics, Lake Oswego, OR, USA) and OriginPro (version 9.0, OriginLab Corp., Northampton, MA, USA). Significant differences between the experimental groups were analyzed using independent or paired Student's *t*-tests. $P<0.05$ was considered statistically significant.

RESULTS

1. Monitoring synaptic transmission in autaptic hippocampal pyramidal neurons

Prior to studying the effect of VGCCs on spontaneous or evoked glutamatergic synaptic transmission on hippocampal autaptic cultured neurons, we have explored autaptic circuits on 593 islands inhabited by single neurons. Fig. lA shows a representative image of hippocampal neurons in an autaptic culture system with a patch electrode on the somata for whole-cell patch clamp. This culture system, in which single neurons grow on small astrocyte islands so that neurons make synapses onto themselves and stimulation of presynaptic terminals and recording of postsynaptic events are accomplished by the same electrode for patch clamping (Augustin *et al.*, 1999; Lipstein *et al.*, 2017; Rhee *et al.*, 2002; Rosenmund *et al.*, 2002), was particularly useful for analysing the functional changes in synaptic transmission. To measure spontaneous glutamate release at excitatory synapses, we recorded synaptic activities at resting state (-70 mV) under the whole-cell voltage clamp condition using pipette solutions containing 0.1 mM EGTA from hippocampal

neurons grown isolated on astrocyte feeder islands at least for 3 weeks for synaptic maturation. (Fig. 1A). Neurons were identified as glutamatergic neurons firstly by the fast decay kinetics of synaptic currents (Fig. Bb, decay time constant: 3.02 ± 0.16 ms, $N = 64$), and then were confirmed by pharmacology. Postsynaptic currents which decayed within ~ 10 ms were not affected by 0.1 mM picrotoxin (PTX), but abolished by 10 μM CNQX (Fig. 1Ba). Frequencies of mEPSCs were variable among cells, ranging from 0.5 to 10 Hz (Fig. 1C, 3.87 ± 0.18 Hz, $N = 278$).

Synaptic activities evoked by step depolarization to 0 mV for 2 ms, called evoked excitatory postsynaptic currents (eEPSCs), represented action potential (AP)-induced transmitter release (Fig. 1Da). Neurons were identified as glutamatergic by the difference in pharmacology (Fig. 1Da). Postsynaptic currents that decayed within a few milliseconds and were selectively inhibited by 10 μM CNQX were regarded as glutamatergic excitatory postsynaptic currents (Fig. 1Db, decay time constant: 8.03 ± 0.68 ms). Amplitudes of eEPSCs were variable among cells ranging from 0.1 to 5 nA. To compare the eEPSC amplitudes by maturation, cells were divided into two groups DIV 8 - 13 and DIV 23 ~ by culture day (day *in vitro*), and there was no difference in amplitude between the two groups (Fig. 1E, DIV 8 – 13, 1.64 ± 0.29 nA, $N = 30$; DIV 23 ~, 1.57 ± 0.09, $N = 285$). In addition, we also analyzed the relationship between 1st EPSC amplitude and paired-pulse ratio (PPR). Fig. 1F showed that there was slightly negative correlation between 1st EPSC amplitude and PPR (slope = -0.02 ± 0.001, $N = 46$). Some cells were recorded mEPSC and eEPSC in the same cell as necessary. The relationship between 1st EPSC amplitude and mEPSC frequency showed slightly positive correlation (Fig. 1G, slope = 0.2 ± 0.04, $N = 54$). This data imply that the spontaneous and evoked release could not be regulated different molecular mechanisms.

2. Multiple Ca^{2+} channels contribute to spontaneous glutamate release in autaptic hippocampal neurons

To measure spontaneous glutamate release at excitatory synapses, we recorded synaptic activities at resting state (-70 mV) under the whole-cell voltage clamp condition using pipette solutions containing 0.1 mM EGTA from hippocampal neurons grown isolated on astrocyte feeder islands at least for 3 weeks for synaptic maturation (Fig. 1A). Neurons were identified as glutamatergic neurons firstly by the fast decay kinetics of synaptic currents (decay time constant: 3.02 ± 0.16 ms, N = 64), and then were confirmed by pharmacology. Postsynaptic currents which decayed within 10 ms were not affected by 0.1 mM picrotoxin (PTX), but abolished by 10 μM CNQX (Fig. 1Ba). These activities were not affected by TTX (Fig. 2A), confirming that none of the synaptic events were activity-dependent in voltage-clamped autaptic cultured neurons. We therefore regarded these events as miniature excitatory postsynaptic currents (mEPSCs) representing spontaneous glutamate release. Frequencies of mEPSCs were variable among cells, ranging from 0.5 to 10 Hz (3.87 ± 0.18 Hz, N = 278). Hereafter, mEPSC frequency obtained after applying any experimental conditions are normalized to the control level. To better represent the change of spontaneous frequency by the experimental treatment, five mEPSC traces were overlaid, and the duration of each trace was 500 ms. When external Ca^{2+} was removed (nominally Ca^{2+}-free), mEPSC frequency decreased to 0.42 ± 0.03 (N = 13) (Figs. 2Ba, Bd), while inhibition of internal Ca^{2+} release from endoplasmic reticulum (ER) via ryanodine receptors (RyRs) using ryanodine (RYN, 10 μM) reduced mEPSC frequency to 0.85 ± 0.04 (N = 6) (Figs. 2Bb, Bd). Ryanodine still reduced mEPSC frequency in Ca^{2+}-free condition (Fig. 3), suggesting that internal and external Ca^{2+} mediate spontaneous release by independent mechanisms. To rule out the effect of Ca^{2+} depletion from the internal Ca^{2+} store on the spontaneous release, recording was completed within 10 min after break-in. Inhibition of ER Ca^{2+}

release via IP_3 receptors (IP_3Rs) using 2-Aminoethoxydiphenylborane (2-APB, 10 μM) reduced mEPSC frequency (0.82 ± 0.04, $N = 9$, $P = 0.0002$) to the extent that was comparable to the effect of ryanodine (Figs. 2Bc, Bd). There was no additive effect when both ryanodine and 2-APB were applied (Figs. 2Bb-d), suggesting that RyRs and IP_3Rs share internal Ca^{2+} stores. Taken together, 27% and 15% of miniature events in autaptic cultured hippocampal neurons were attributable to Ca^{2+}independent and ER-dependent mechanisms, respectively, while 58% was $[Ca^{2+}]_o$-dependent (Fig. 2Be). mEPSC frequency changed according to $[Ca^{2+}]_o$ changes (Fig. 2C), with the slope of log-log plot for mEPSC frequency against $[Ca^{2+}]_o$ as 0.42 (black symbols and line, Fig. 2D), which is compatible to the value measured in cortical neurons, 0.63 (Vyleta and Smith, 2011). However, Ca^{2+} cooperativity shown in this slope is underestimated, since 42% of total mEPSCs is independent on $[Ca^{2+}]_o$. To obtain the actual Ca^{2+} cooperativity, we subtracted the $[Ca^{2+}]_o$-independent fraction and recalculated the slope. The result was 1.24 (red line, Fig. 2D), which turns out to be much higher than previous reports. It was in fact comparable to Ca^{2+} cooperativity of evoked excitatory postsynaptic currents (eEPSCs) obtained in hippocampal synapses (1.77: Vyleta and Jonas, 2014), suggesting that mechanisms underlying $[Ca^{2+}]_o$-dependent spontaneous release may not be substantially different from those of evoked release.

3. VGCCs contribute to spontaneous glutamate release

It is well known that evoked release is triggered by Ca^{2+} influx through presynaptic VGCCs during action potentials, but the contribution of presynaptic VGCCs to spontaneous glutamate release remains controversial (Ermolyuk *et al.*, 2013; Vyleta and Smith, 2011). To test this possibility, we examined the contribution of VGCCs to mEPSCs using blockers to specific VGCC subtypes. Blockade of P/Q-type (with 0.1 μM ω-Agatoxin-IVA, Aga), N-type (with 0.1 μM ω-Conotoxin GVIA, Cono), and R-type VGCCs (with 0.3 μM SNX-482, SNX, or 100 μM $NiCl_2$) significantly

decreased mEPSC frequency (Figs. 4Aa-c, C; Aga, 0.71 ± 0.02, N = 24, Cono, 0.73 ± 0.01, N = 18, SNX, 0.77 ± 0.06, N = 6, $NiCl_2$, 0.78 ± 0.02, N = 9). The mixture of Aga, Cono, and $NiCl_2$ (3-mix) decreased mEPSC frequency to 0.47 ± 0.02 (N = 10, Figs. 4Ad-e, C), suggesting that 91 % of $[Ca^{2+}]_o$-dependent mEPSCs is mediated by VGCCs. In the presence of 3-mix, changing $[Ca^{2+}]_o$ no longer affected mEPSC frequency (Figs. 4Ad-e, C), further confirming the role of VGCCs on $[Ca^{2+}]_o$-dependent miniature events.

One of the strongest pieces of evidence that supports a lack of the VGCC contribution to spontaneous glutamate release is that Cd^{2+}, a non-selective VGCC blocker, has no significant effect (Dai *et al.*, 2015; Tsintsadze *et al.*, 2017; Vyleta and Smith, 2011). We measured mEPSCs in the presence of Cd^{2+} (100 μM), and found that mEPSC frequency was reduced to 0.70 ± 0.03 (N = 4, Figs. 4B, C). This was a significant decrease, yet smaller than that by 3-mix, suggesting that Cd^{2+} did not completely block VGCC-dependent spontaneous release. This concentration of Cd^{2+} was potent to abolish depolarization-induced Ca^{2+} currents (Fig. 5, 0.04 ± 0.01, N = 3). Since VGCC blockade by Cd^{2+} is voltage-dependent and not as effective at hyperpolarizing potential (Swandulla and Armstrong, 1989), Cd^{2+}may not be suitable to assess VGCC dependency at resting membrane potential (RMP). We confirmed that mEPSC amplitudes were not changed by any VGCC blockers (Fig. 4D).

To further understand the role of VGCCs in glutamate release, we compared the effects of $[Ca^{2+}]_o$ and VGCC blockers on evoked release with those on spontaneous release. When evoked excitatory postsynaptic currents (eEPSCs) were recorded at different $[Ca^{2+}]_o$, amplitude of eEPSC changed according to $[Ca^{2+}]_o$ as did mEPSC frequency (Fig. 6A). The slope of log-log plot for eEPSC amplitude against $[Ca^{2+}]_o$

was 1.84 (black line, Fig. 6Ba), which was smaller than that obtained in neuromuscular junction, 3.8 (Dodge and Rahamimoff, 1967), but compatible to that obtained in hippocampal synapses 1.77 (Vyleta and Jonas, 2014). Removal of $[Ca^{2+}]_o$ completely abolished eEPSC (Fig. 7A), while ryanodine had no effect (Fig. 7B), confirming that evoked release was entirely dependent on Ca^{2+} influx via VGCCs. As expected, each of VGCC blockers decreased eEPSC amplitude significantly (Figs. 6C, D). The contribution of P/Q-, N-, and R-type VGCCs were 65 %, 40 %, and 40 %, respectively (Fig. 7E), which were slightly different from their contribution to mEPSCs (P/Q, 53 %; N, 49 %; R, 42 %; Fig. 4C and Fig. 6E). The linear sum of the contribution of the three VGCCs exceeds 100 % (145 % for eEPSCs and 144 % for mEPSCs, Fig. 6E), suggesting that the contribution of each type of VGCC is not entirely independent, but co-activation of multiple VGCCs contributes to the release. The effect of VGCC blockers on short-term plasticity was thought to imply the number and organization of VGCCs in the active zone (Scimemi and Diamond, 2012), so we analyzed changes in paired pulse ratio (PPR). We confirmed that PPR was unaffected when eEPSCs were reduced by submaximal concentration of CNQX (Fig. 8). In contrast, all VGCC blockers increased PPR significantly in association with the decreases in EPSC amplitude (Fig. 6F). These results are consistent with the previous study in rat Schaffer collateral synapses that suggests the contribution of multiple VGCC subtypes to trigger release (Wheeler *et al.*, 1994). However, when a single VGCC subtype remained active in the presence of other two blockers, PPR was unchanged by submaximal concentrations of a single blocker (Fig. 9).

4. Nanodomain coupling between Ca^{2+} sources and Ca^{2+} sensors for both spontaneous and evoked glutamate release

Above results demonstrated that presynaptic VGCCs contribute to both spontaneous and evoked release in autaptic hippocampal neurons. It is, however, not certain

whether Ca^{2+} influx upon stochastic openings of VGCCs at resting state directly triggers spontaneous release via increasing local [Ca^{2+}] near primed vesicles at active zone (Ermolyuk *et al.*, 2013) or indirectly modulates spontaneous release via increasing presynaptic global [Ca^{2+}] levels. This question is related to the question of how tightly vesicular Ca^{2+} sensors for spontaneous release are coupled to Ca^{2+} sources, VGCCs in this case. The distance between VGCCs and Ca^{2+} sensors can be probed using exogenous Ca^{2+} chelators with different kinetics, EGTA and BAPTA (Adler *et al.*, 1991; Neher, 1998). When the channel-sensor coupling is very tight, so called nanodomain coupling, the fast Ca^{2+} buffer such as BAPTA, but not the slow Ca^{2+} buffer such as EGTA, can interfere exocytosis, while when the coupling is loose, EGTA as well as BAPTA can interfere (Adler *et al.*, 1991; Neher, 1998). To estimate the coupling distance of VGCCs with vesicular Ca^{2+} sensors that operate for spontaneous release, we used pipette solutions containing different concentrations of EGTA and BAPTA. For comparison, we measured mEPSC frequency and eEPSC amplitude from the same cells, in a way that eEPSCs were recorded every 20 s starting immediately after patch break-in, while mEPSCs were recorded continuously in between eEPSCs (Fig. 11A). Sequential recordings for eEPSCs and mEPSCs continued until the effects of EGTA or BAPTA perfusion reached steady state. We performed these experiments in the presence of ryanodine to exclude the effects of exogenous buffer on RyR-dependent mEPSCs, which was mediated by loose coupling with Ca^{2+} sensors (Fig. 10). We first confirmed that with this experimental protocol eEPSCs amplitude remained stable for recording time up to 20 min when pipette solution was 0.1 mM EGTA-containing control solution (Fig. 11B). Frequency of spontaneous activities were increased after eEPSC recording due to asynchronous release, but this increase returned to the control level within a few s (Fig. 11Bb). So, we regarded the spontaneous activities recorded during 10 s before the next stimulation as mEPSCs. We then examined the effects of increasing EGTA or BAPTA concentration. Changes in eEPSCs or mEPSCs were small with 5 mM

EGTA (black symbols, Figs. 11Cb, Db left panel), while a significant reduction was induced in both eEPSC amplitude and mEPSC frequency with 5 mM BAPTA (blue symbols, Figs. 11Cb, Db left panel). Differential effects of EGTA and BAPTA suggest tight coupling between VGCCs and Ca^{2+} sensors both for spontaneous and evoked release. To estimate the distance between Ca^{2+} sensors and VGCCs, we recorded eEPSCs and mEPSCs with different concentrations of BAPTA and EGTA (Figs. 11Ea, Eb). Then, we subtracted $[Ca^{2+}]_o$-independent portion (0.26 ± 0.02, N = 5, in 5 mM EGTA and 0.25 ± 0.03, N = 7, in 5 mM BAPTA) from the measured mEPSC frequencies (Db, left panel) to obtain changes in $[Ca^{2+}]_o$-dependent mEPSCs, which were re-normalized to the first point (Fig. 11Db, right panel). The resulting curves (red lines) were superimposed to the changes in eEPSC amplitude for comparison (Figs. 11Ea, Eb). eEPSC amplitude (green lines) and mEPSC frequency (red lines) decreased as the concentration of each buffer increased (Figs. 11Ea, Eb) with time course and magnitude indistinguishable between eEPSCs and mEPSCs at all concentrations tested (Fig. 11E). The distance between Ca^{2+} sources and sensors was estimated by fitting these values to the following equation (see Methods).

$$\text{Mini frequency ratio} = \exp[n\,(-r/\lambda_0\,(\sqrt{(1+\,(P_{b,1}/P_0)\,x)} - 1))].$$

, where x = [EGTA] or [BAPTA] in mM; n = power dependence of vesicle release on $[Ca^{2+}]c$, λ_0 = length constant of calcium microdomain in the presence of endogenous buffer (B_0) alone; P_0 and $P_{b,1}$ are buffer products (k_{on} [B]) of B_0 and 1 mM EGTA or BAPTA, respectively. Since decreases in mEPSC frequency and eEPSC amplitude by EGTA and BAPTA were almost identical, we pooled the data for fitting. The best fit was obtained at r = 22 nm where n = 1.62 and P_0 = 3000 (Fig. 11F, mEPSCs, triangles; eEPSCs, circles). With the slopes of the Ca^{2+} cooperativity obtained in Fig. 1 (1.24 for mEPSCs and 1.84 for eEPSCs) regarded as n, r can be estimated as 19 nm and 29 nm for mEPSCs and eEPSCs, respectively. Taken together, both spontaneous and evoked glutamate release is mediated by nanodomain coupling between VGCCs and vesicular Ca^{2+} sensors in cultured hippocampal neurons.

5. Simultaneous activation of multiple type of VGCC subtypes contributes to spontaneous and evoked glutamate release

To further understand the role of VGCCs in glutamate release, I compared the effects of each VGCC blocker on eEPSCs and mEPSCs. All VGCC blockers decreased eEPSC amplitude significantly (Figs. 8A and B), which was associated with an increase in paired pulse ratio (Fig. 6C). The contribution of P/Q-, N-, and R-type VGCCs were 65 %, 40 %, and 40 %, respectively (Fig. 6E), which were slightly different from their contribution to mEPSCs (P/Q, 53 %; N, 49 %; R, 42 %; Fig. 6E). The linear sum of the contribution of the three VGCCs exceeds 100 % (145 % for eEPSCs and 144 % for mEPSCs, Fig. 6F), suggesting that the contribution of each type of VGCC is not entirely independent.

It has been debated whether VGCC-dependent spontaneous release is mediated by a stochastic opening of a single channel (Ermolyuk *et al.*, 2013) or simultaneous activation of multiple VGCC subtypes (Williams *et al.*, 2012). If the former is the case, the contribution of a VGCC subtype should be independent to each other. However, I showed that the linear sum of the reduction in mEPSC frequency by each VGCC blocker exceeded that by the mixture of the three blockers (Fig. 4C). This result was not caused by cross-reactivity of the blockers, because the linear sum of the reduction of Ca^{2+} currents induced by a depolarizing voltage step in each blocker was not significantly different from the reduction in 3-mix (22% (Aga) + 21.5% (Cono) + 40.8% (Ni^{2+}) = 84.3% *vs* 3-mix (80 ± 5.4%); Fig.12). Furthermore, the effect of each blocker was unaffected by the order of its application (Figs. 12Ac-d, D).

On the other hand, the potency of a blocker on mEPSC frequency was changed by the blocker applied beforehand. For example, Aga still can decrease mEPSC frequency by 25% in the presence of $NiCl_2$, while it reduced only little when applied in the presence of Cono (Figs. 13A, B), suggesting a different level of coactivation between P/Q type- and other Ca^{2+} channels. To investigate the extent of coactivation between the VGCCs, I measured the reduction of mEPSC frequency in the mixture of two blockers (Aga + Cono, Aga + Ni^{2+}, Cono + Ni^{2+}) (Figs. 13Ca-Cc), and compared them with the linear sum of those by each blocker (Fig. 13Da). The difference represented the contribution of coactivation of two channels (Fig. 13Da), showing that the level of coactivation is varying among which coactivation of P/Q- and N-type was largest. Then, I evaluated the contribution of each VGCC that is independent on other VGCCs by applying the third blocker in the presence of two blockers (Figs. 13Ca-Cc). Using these data, the contribution of each VGCC to mEPSCs can be reconstructed by the sum of independent activation and coactivation with other channels (Fig. 13Db). A summary graph showed that about 58% of VGCC-dependent mEPSCs was attributable to the activation of a single VGCC subtype (P/Q, 17%; N, 16%; R, 25%), while 42% was attributable to coactivation of two VGCC subtypes (Fig. 13E).

The profile of VGCC contribution to evoked release was evaluated (Figs. 13F-H) using the same method described in Figs 12A to E. Consistent with mEPSCs, eEPSCs were also mediated by both a single VGCC subtype (64%) and coactivation of VGCC subtypes (36%) (Figs. 13F, G). Contribution of coactivation of two VGCC subtypes was estimated to be 26, 23, and 15% for P/Q + N, P/Q + R, and N + R, respectively (Fig. 13Ga). The linear sum of these far exceeded 36%, suggesting coactivation of all three subtypes (Fig. 13Gb). Best fit was obtained with 14% of

total eEPSCs as coactivation of three subtypes (grey, Figs. 13Gb, H).

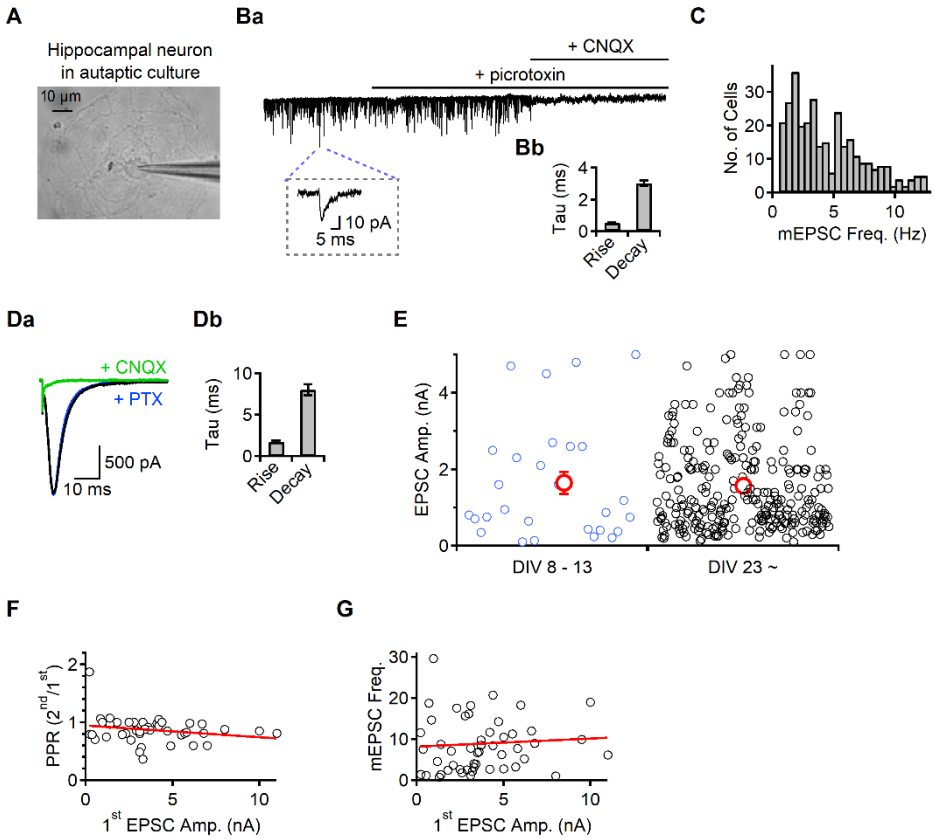

Figure 1. Monitoring synaptic transmission in autaptic hippocampal pyramidal neurons

(A) A representative image of hippocampal neurons in an autaptic culture system with a patch electrode on the somata for whole-cell patch clamp. (Ba) Top. A representative trace of mEPSC in the presence of PTX and CNQX. Bottom. inset box: an enlarged trace of a single mEPSC. (Bb) A bar graph indicating rise or decay time constant for mEPSC. Rise time was 0.53 ± 0.02 ms and decay time was 3.02 ± 0.16 (N = 62). (C) A histogram representing a mEPSC frequency distribution for total number of cells used in the present study. (Da) A representative trace of eEPSC in the presence of PTX and CNQX. (Db) A bar graph indicating rise or decay time constant for eEPSC. Rise time was 1.74 ± 0.15 ms and decay time was 8.03 ± 0.68

(N = 50). (E) A bar graph indicating the distribution of eEPSC amplitude between DIV 8 - 13 and DIV 23 ~. The average amplitude (red circle) was 1.64 ± 0.29 nA (N = 30) in DIV 8 – 13 and 1.57 ± 0.09 nA (N = 285) in DIV 23 ~. (F) A bar graph indicating the relationship between PPR and 1st EPSC amplitude. The line was fitted by the equation of 0.94 -0.02x. N = 46. (G) A bar graph indicating the relationship between mEPSC frequency and 1st EPSC amplitude. The line was fitted by the equation of 3.53 + 0.02x. N = 54.

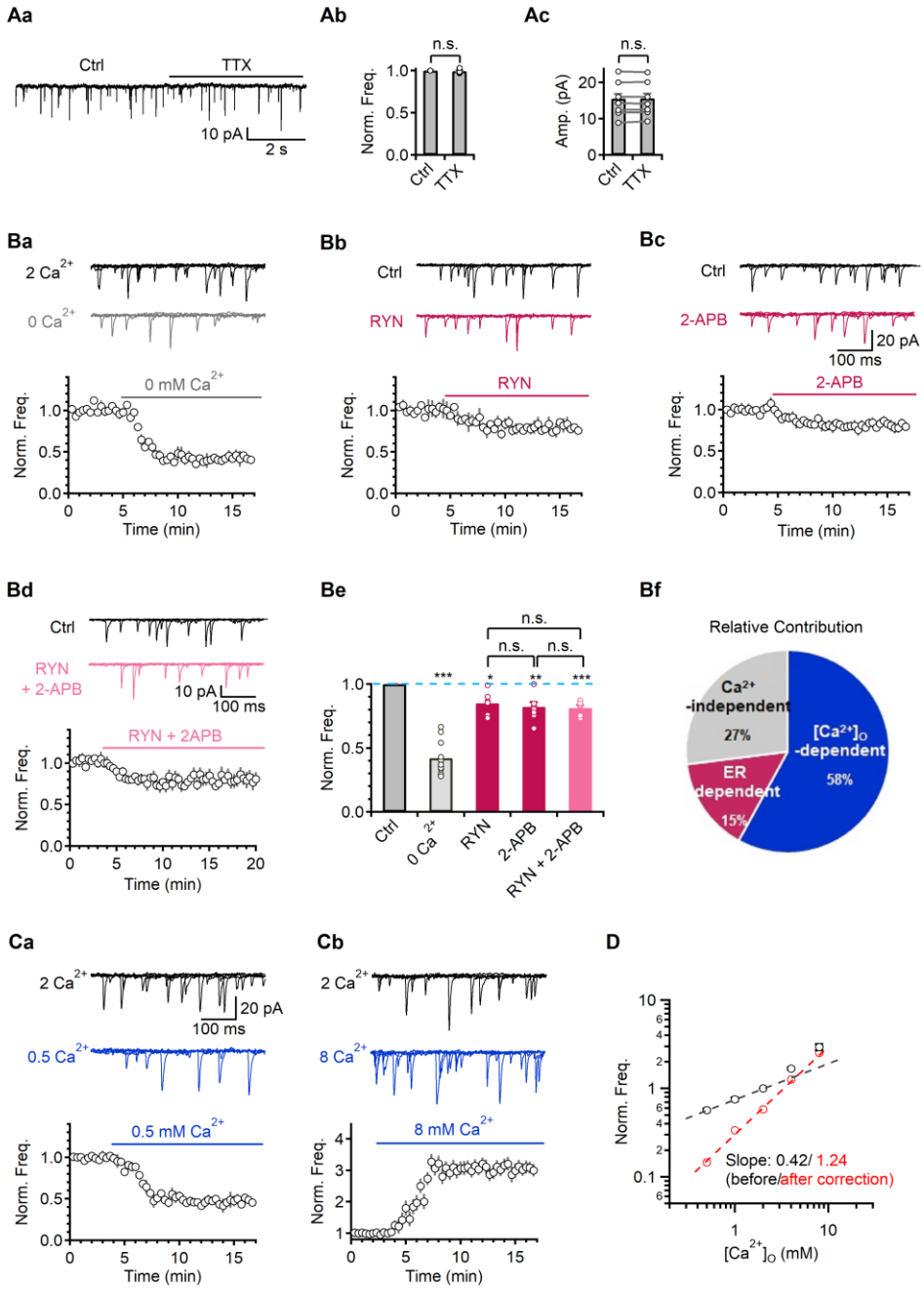

Figure 2. Ca^{2+} co-operativity for spontaneous glutamate release

(Aa-c) A representative trace of mEPSC before (Ctrl) and after the application of 0.5 μM tetrodotoxin (TTX) (N = 7, frequency; 0.99 ± 0.01 compared to control,

amplitude; 15.57 ± 1.3 *vs* 15.63 ± 1.3 pA). (B) Ba-Bc. Top. Representative traces of mEPSC in the control condition, containing 2mM Ca^{2+} and in different experimental conditions during removal of external Ca^{2+} (Ba), and application of ryanodine (RYN) with 2-aminoethoxydiphenylborane (2-APB) (Bb) or 2-APB with RYN (Bc), respectively. Five 500 ms-long mEPSC traces were overlaid. Bottom. An average time course of normalized mEPSC frequency. In each time course plot, the upper solid line indicates an application point for 0 Ca^{2+}, RYN or 2-APB, respectively. The normalized values were calculated from the mean frequency of the control condition. (Bd) A bar graph of average values of normalized mEPSC frequency from Ba-Bc, such as external Ca^{2+}-free ($N = 13$, 0.42 ± 0.03, $P < 0.001$), RYN ($N = 6$, 0.85 ± 0.04), 2-APB ($N = 9$, 0.82 ± 0.04) or RYN with 2-APB ($N = 6$, 0.81 ± 0.02). (Be) A pie chart evaluating the relative contribution of external Ca^{2+} -dependent (blue), Ca^{2+}-independent (grey) or internal Ca^{2+} release (magenta) to mEPSC. (C) Top. Representative traces of mEPSC in different $[Ca^{2+}]_e$ from 2 to 0.5 mM (Ca) and from 2 to 8 mM (Cb). Five 500 ms-long mEPSC traces were overlaid. $[Mg^{2+}]_o$ was 1 mM for these recordings. Bottom. An average time course of the normalized mEPSC frequency (0.5 *vs* 8 mM Ca^{2+}; 0.56 ± 0.02 *vs* 2.94 ± 0.24, compared to the control condition containing 2 mM Ca^{2+}, $N = 28$ *vs* 17). (D) A log-log plot for mEPSC frequency against $[Ca^{2+}]_e$. The slope of mEPSC frequency was 0.42 which was fitted from 2 mM to lower concentration (black circles and dash line). To overcome underestimated slope value, external Ca^{2+}-free fraction from the measured mEPSC frequency was subtracted and the slope was recalculated (red circles and dashed line, Slope; 1.24). All data are represented as mean ± S.E.M., $*P < 0.05$, $***P < 0.001$, single group mean *t*-test or paired *t*-test (Bd); n.s. = not significant.

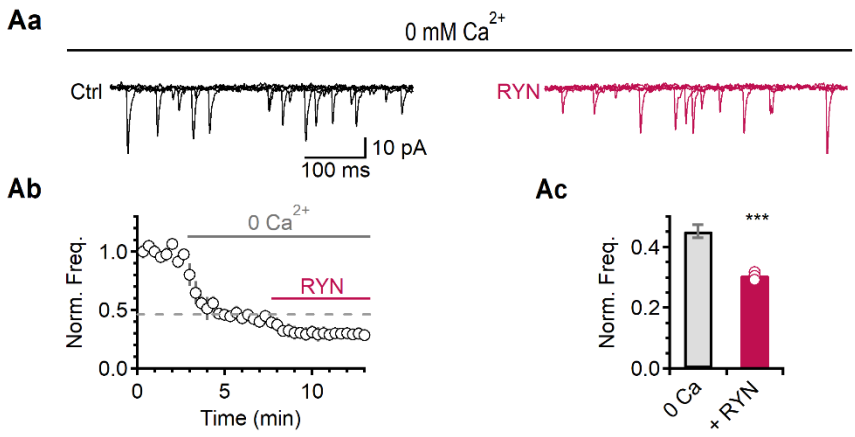

Figure 3. The effect of RYN on mEPSC frequency in the Ca^{2+}-free extracellular solution

(Aa) Representative mEPSC traces before (control) and 5 min after applying RYN. (Ab) An average time course of mEPSC frequency applying RYN in the Ca^{2+}-free extracellular solution. The normalized values were calculated from the mean frequency of the 2 Ca^{2+} control condition. (Ac) A bar graph of the effects of RYN on mEPSC frequency in the Ca^{2+}-free external solution (0.45 ± 0.02 *vs* 0.31 ± 0.01, compared to 2 Ca^{2+} control, $N = 4$). All data are represented as mean ± S.E.M., ***$P < 0.001$, single group mean *t*-test.

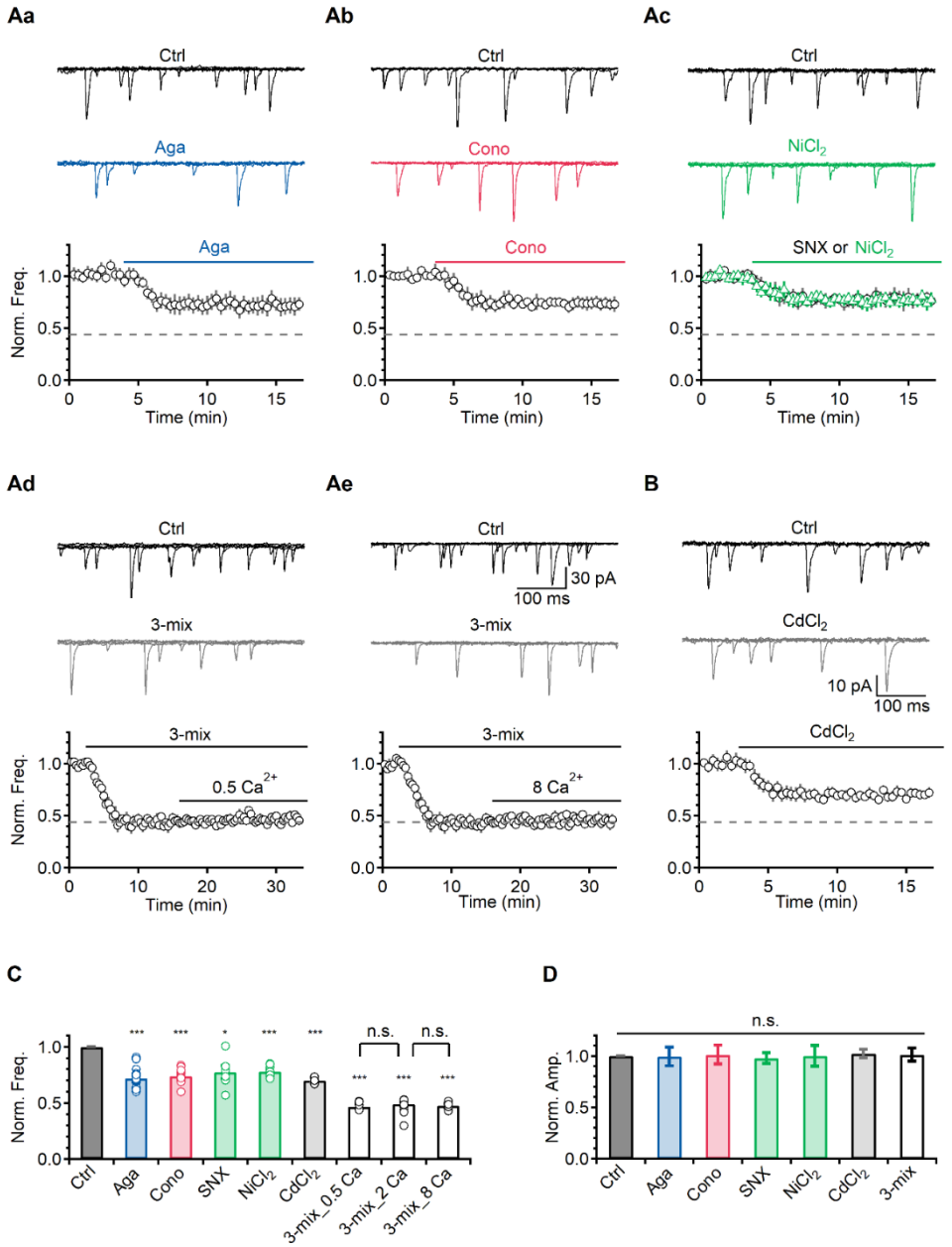

Figure 4. VGCCs contribute to spontaneous glutamate release

(Aa-c, B) Top. Representative traces of mEPSC frequency before (Ctrl) and after the application of Aga (Aa), Cono (Ab), $NiCl_2$ (Ac) or $CdCl_2$ (B), respectively. Five 500

ms-long mEPSC traces were overlaid. Bottom. An average time course of the normalized mEPSC frequency. The normalized values were calculated from the mean frequency of the control condition. The top solid line indicates an application point for each VGCC blocker. The grey dashed line (0.42) indicates a division of $[Ca^{2+}]_e$-dependent and -independent mEPSC. (Ad-e) Representative traces of mEPSC (Top) and average time courses of mEPSC frequency (bottom) before (Ctrl) and after the application of 3-mix (Aga+Cono+$NiCl_2$) in 2 mM $[Ca^{2+}]_e$ or different conditions of $[Ca^{2+}]_e$ (2 Ca^{2+}, 0.47 ± 0.02, N = 10; 0.5 Ca^{2+}, 0.47 ± 0.01, N = 5; 8 Ca^{2+}, 0.48 ± 0.02, compared to control, N = 4). (C, D) Bar graphs showing the normalized mEPSC frequency (Aga, blue, 0.71 ± 0.02, N = 24, $P < 0.001$; Cono, red, 0.73 ± 0.01, N = 18; SNX, green, 0.77 ± 0.06, N = 6; $NiCl_2$, green, 0.78 ± 0.02, N = 9; $CdCl_2$, 0.70 ± 0.03, N = 4, compared to control; C) and amplitude (D). All data are represented as mean ± S.E.M., *$P < 0.05$, ***$P < 0.001$, single group mean t test or paired t-test (C); n.s. = not significant.

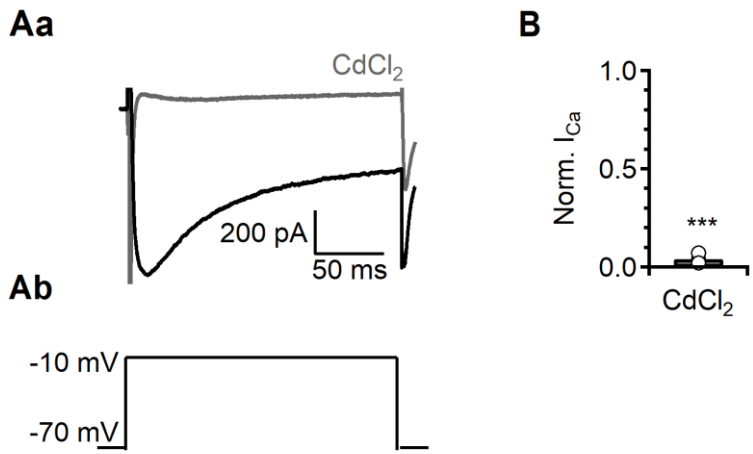

Figure 5. The effect of $CdCl_2$ on I_{Ca}

(Aa) Representative traces of I_{Ca} in the control condition and applying 100 μM $CdCl_2$. (Ab) The pulse protocol for recording I_{Ca}. The VGCC currents were recorded by changing clamed voltage from -70 to -10 mV via step-mode in bath solution containing 25 mM tetraethylammonium (TEA), 5 mM 4-AP, 1 μM TTX, 10 μM CNQX and 100 μM PTX. (B) A bar graph of normalized I_{Ca} in $CdCl_2$ (0.04 ± 0.01, $N = 3$). All data are represented as mean ± S.E.M., ***$P < 0.001$.

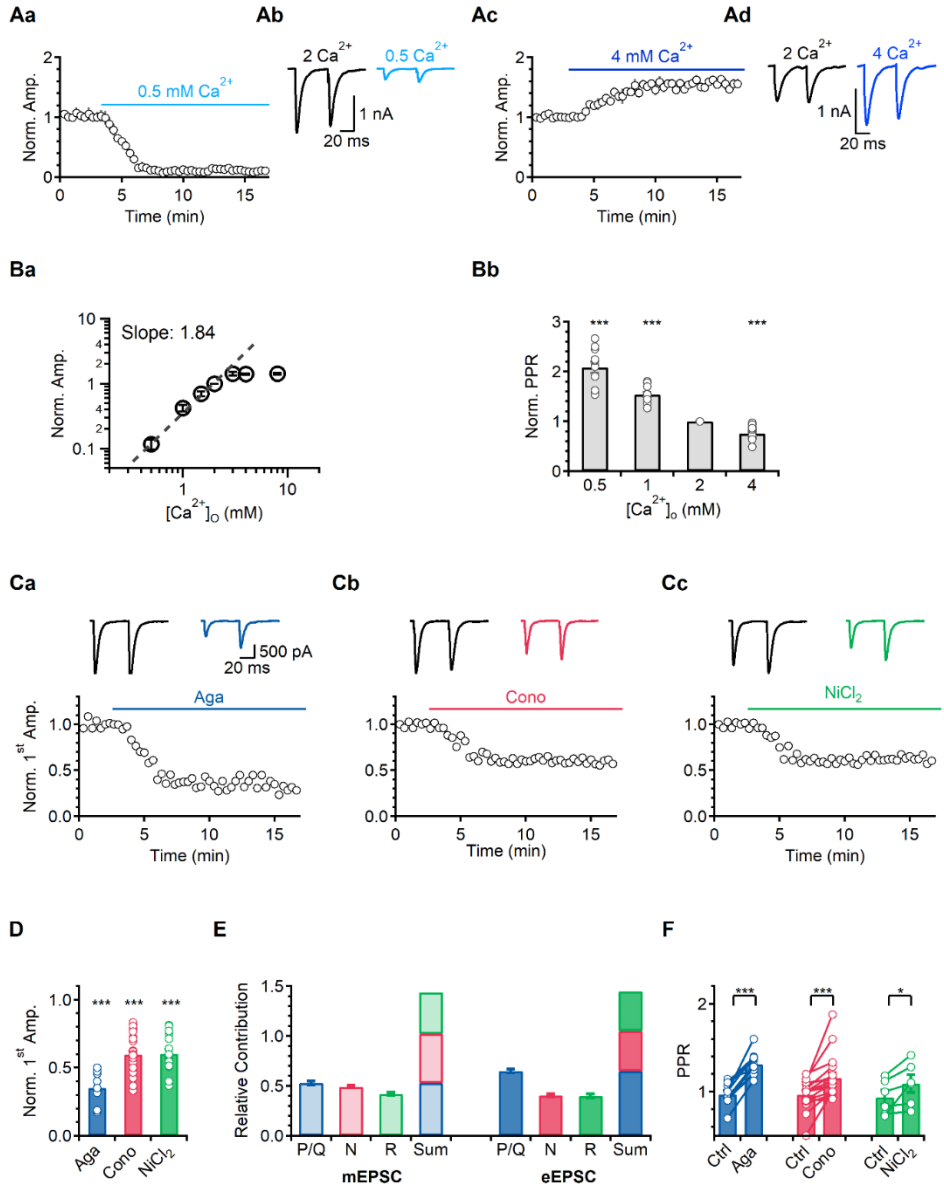

Figure 6. VGCCs contribute to evoked glutamate release.

(Aa, Ac) An average time course of eEPSC amplitude (0.5 *vs* 4 mM Ca^{2+}; 0.11 ± 0.02 *vs* 1.42 ± 0.04, compared to 2 mM Ca^{2+}, $N = 16$ *vs* 6, $P < 0.001$). The normalized values were calculated from the mean 1st amplitude of the control condition. (Ab,

Ad) Representative traces of eEPSC changing of $[Ca^{2+}]_o$. (Ba) A log-log plot for the eEPSC amplitude against $[Ca^{2+}]_o$. The slope of the eEPSC amplitude was 1.84 which was fitted from 2 mM to lower concentration (black circles and dash line). (Bb) A graph showing effects of $[Ca^{2+}]_o$ change on normalized paired-pulse ratio (PPR) at 2mM Ca^{2+} (0.5 Ca^{2+}, 2.08 ± 0.12, $N = 11$, $P < 0.001$; 1 Ca^{2+}, 1.54 ± 0.05, $N = 11$, $P < 0.001$; 4 Ca^{2+}, 0.75 ± 0.04, $N = 16$, $P < 0.001$). (Ca-c) Top. Representative traces of eEPSC amplitude in the presence of Aga, Cono, SNX, $NiCl_2$ or $CdCl_2$, respectively. Bottom. An average time course of 1st eEPSC amplitude. (D) A bar graph showing effects of individual blockers on the 1st eEPSC amplitude (Aga, 0.35 ± 0.03, $N = 12$; Cono, 0.6 ± 0.02, $N = 37$; $NiCl_2$, 0.6 ± 0.03, $N = 18$, compared to control). (E) A chart for the VGCC contribution to mEPSC (pale bar) or eEPSC (solid bar). The arithmetic sum of the contributions of each blocker exceeded 1 both in spontaneous and evoked release. All data are mean ± S.E.M., $*P < 0.05$, $**P < 0.01$, $***P < 0.001$, single group mean *t* test or paired *t*-test (F); n.s. = not significant.

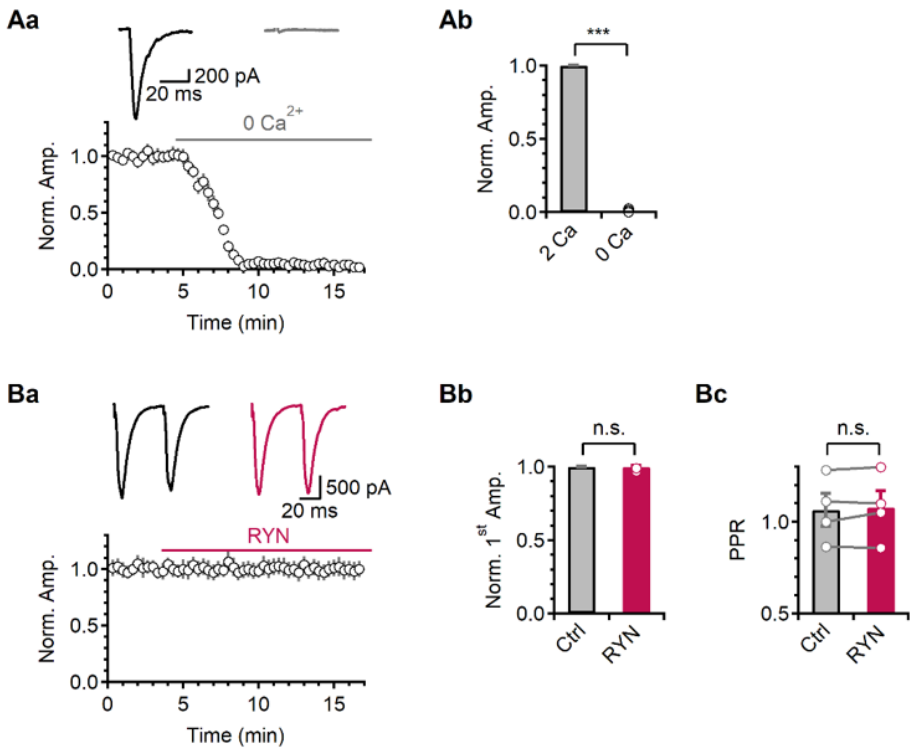

Figure 7. The effects of Ca^{2+} removal or RYN on eEPSC

(Aa) Top. Representative traces of eEPSC in Ca^{2+}-free extracellular solution. Bottom. An average time course of eEPSC amplitude. The normalized values were calculated from the mean 1st amplitude of the control condition. (Ab) A bar graph summarizing the effects of Ca^{2+}-free external solution on the eEPSC amplitude (0.008 ± 0.01, compared to control, $N = 7$). (Ba) Top. Representative eEPSC traces before (control) and 10 min after applying RYN. Bottom. An average time course of the 1st eEPSC amplitude applying RYN. (Ba, c) Bar graphs summarizing the effects of RYN on the 1st eEPSC amplitudes and PPR (0.99 ± 0.01, compared to control; control, 1.06 ± 0.09; RYN, 1.07 ± 0.1; $N = 4$). All data are mean ± S.E.M., ***$P < 0.001$, single group mean *t*-test; n.s. = not significant.

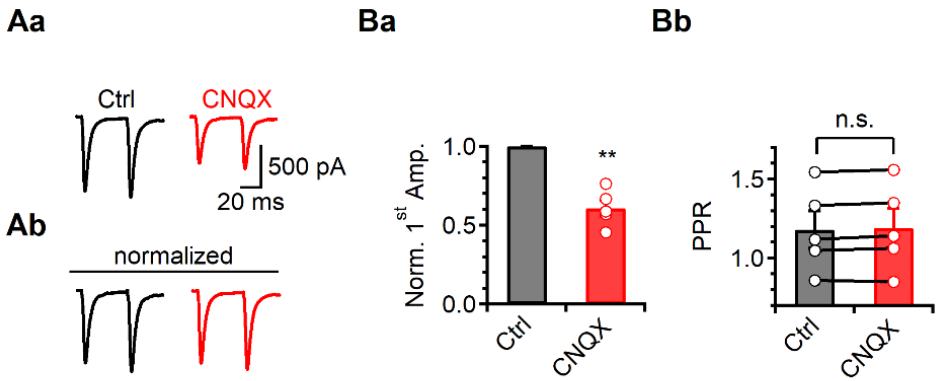

Figure 8. The effects of subsaturating concentration of CNQX on amplitudes and PPR

(Aa, b) Representative traces of eEPSC applying subsaturating doses of CNQX. (Aa) Raw traces. (Ab) Normalized traces. (Ba) A bar graph indicating normalized 1st EPSC amplitudes (CNQX, 0.61 ± 0.05, N = 7). (Bb) A bar graph showing PPR (control vs CNQX, 1.18 ± 0.12 vs 1.19 ± 0.12).

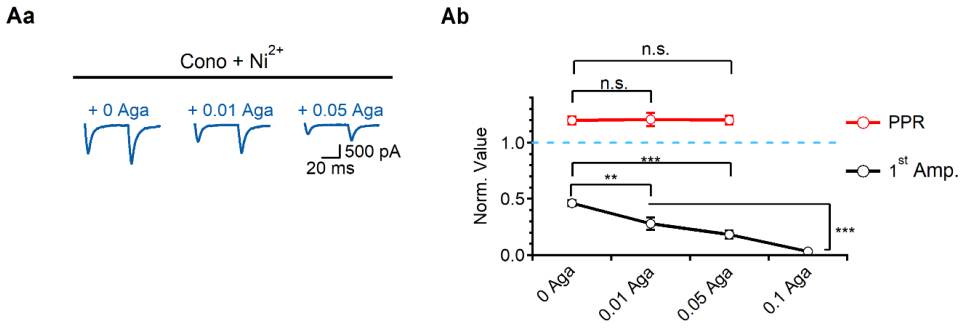

Figure 9. The effect of Aga on amplitudes and PPR in Cono + Ni^{2+} pre-treated cells

(Aa) Representative traces of eEPSC in Cono + Ni^{2+} pre-treated cells with dose-dependent application of Aga. (Ab) A graph showing the normalized 1^{st} amplitudes or normalized PPR, compared to control (1^{st} Amp.; Cono + Ni^{2+}, 0.46 ± 0.03; 0.01 μM Aga, 0.28 ± 0.05; 0.05 μM Aga, 0.18 ± 0.04; 0.1 μM Aga, 0.03 ± 0.01; PPR, Cono + Ni^{2+}, 1.2 ± 0.03; 0.01 μM Aga, 1.21 ± 0.06; 0.05 μM Aga, 1.2 ± 0.04, N = 6).

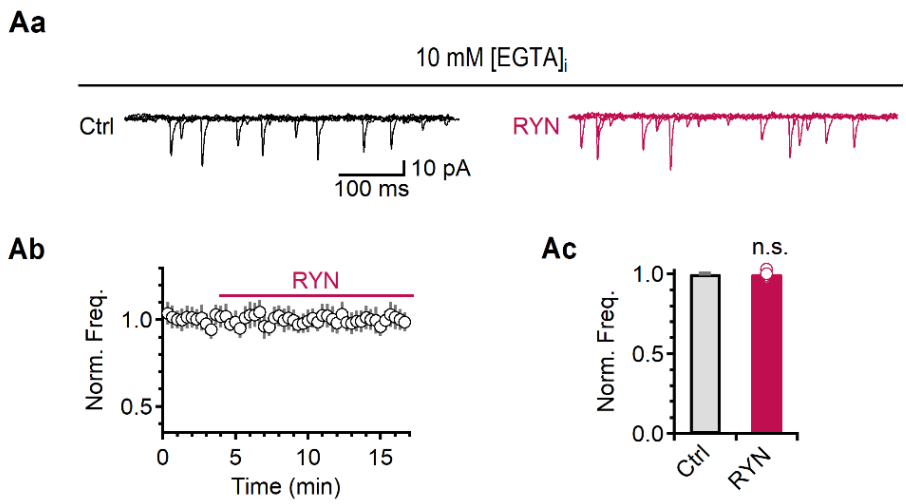

Figure 10. The effect of RYN on mEPSC frequency in the internal solution containing 10 mM EGTA

(Aa) Representative mEPSC traces before (control) and 10 min after applying RYN. (Ab) An average time course of mEPSC frequency applying RYN. The normalized values were calculated from the mean frequency of the control condition. (Ac) A bar graph of the effects of RYN on the mEPSC frequency (1.0 ± 0.01, compared to control, N = 4). All data are mean ± S.E.M., single group mean t test; n.s. = not significant.

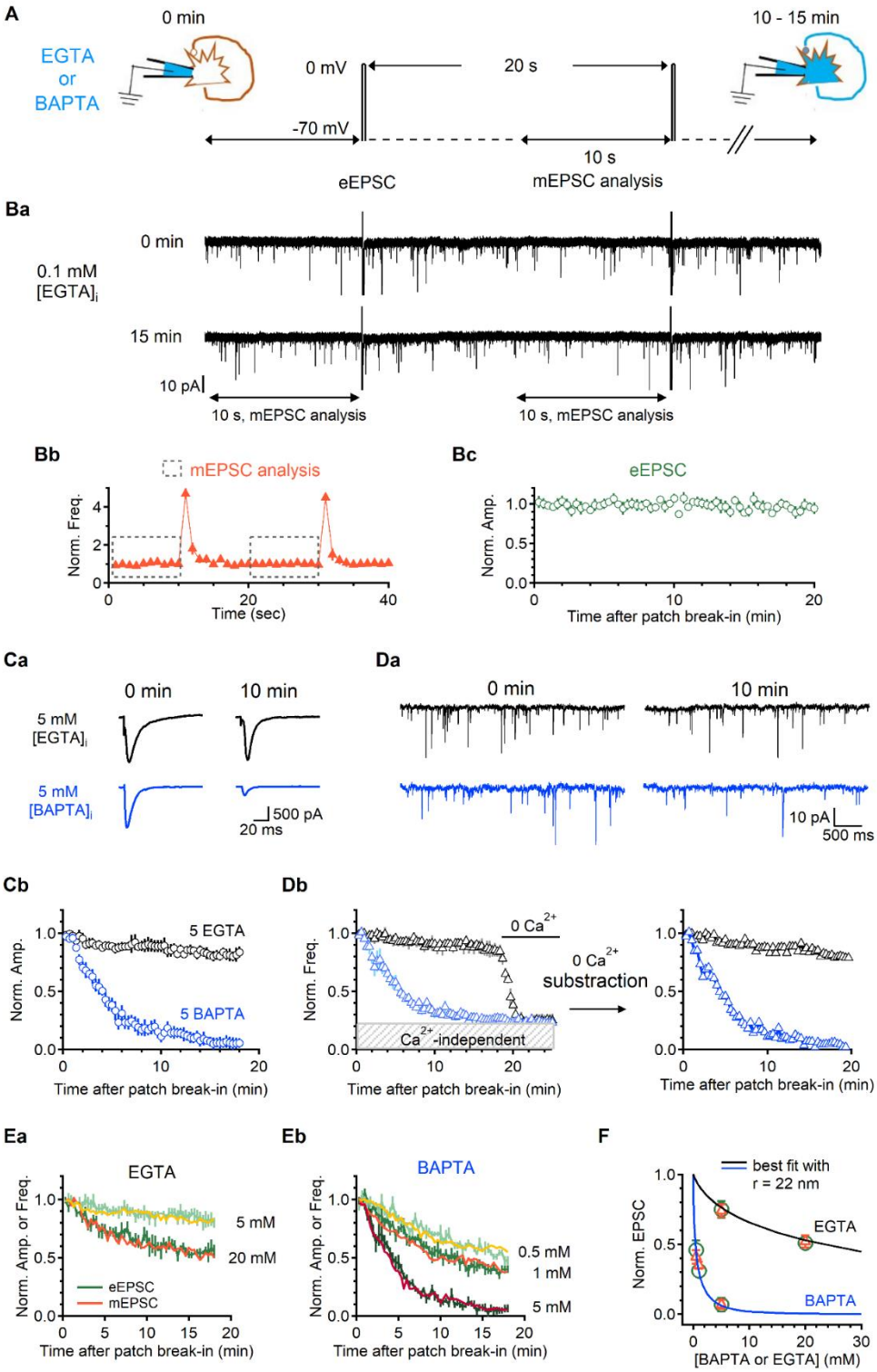
A
0 min
10 - 15 min
EGTA
or
BAPTA
0 mV
20 s
-70 mV
10 s
eEPSC
mEPSC analysis
Ba
0 min
0.1 mM
[EGTA]i
15 min
10 pA
10 s, mEPSC analysis
10 s, mEPSC analysis
Bb
mEPSC analysis
Norm. Freq.
Time (sec)
Bc
eEPSC
Norm. Amp.
Time after patch break-in (min)
Ca
0 min
10 min
5 mM
[EGTA]i
5 mM
[BAPTA]i
500 pA
20 ms
Da
0 min
10 min
10 pA
500 ms
Cb
5 EGTA
5 BAPTA
Norm. Amp.
Time after patch break-in (min)
Db
0 Ca2+
0 Ca2+
substraction
Ca2+-independent
Norm. Freq.
Time after patch break-in (min)
Ea
EGTA
5 mM
20 mM
eEPSC
mEPSC
Norm. Amp. or Freq.
Time after patch break-in (min)
Eb
BAPTA
0.5 mM
1 mM
5 mM
Norm. Amp. or Freq.
Time after patch break-in (min)
F
best fit with
r = 22 nm
EGTA
BAPTA
Norm. EPSC
[BAPTA or EGTA] (mM)

Figure 11. Nanodomain coupling between Ca^{2+} sources and Ca^{2+} sensors for both spontaneous and evoked glutamate release.

(A) An experimental scheme for sequential recordings of eEPSCs and mEPSCs from same cells. (Ba) Representative traces for the comparison of eEPSCs and mEPSC between immediately (top) after and 15 min (bottom) after patch break-in in presence of 0.1 mM EGTA. (Bb) An average time course of the mEPSC frequency normalized to the data acquired from initial 10s (orange triangle) with 1 s bin. Dashed-boxes indicate the mEPSC frequency analysis sections. (Bc) An average sequential time plot of the eEPSC amplitude normalized to the data acquired from initial 60s. (Ca, Da) Representative traces for the comparison of eEPSCs and mEPSC between immediately after (0 min) and 10 min after patch break-in in presence of 5 mM EGTA (black) or 5 mM BAPTA (blue) in intracellular solution. (Cb) An average time course of the normalized eEPSC amplitude. The normalized values were calculated from the mean amplitude of the first 3 eEPSCs after patch break-in. The magnitude of reduction at steady state and the time course (τ) were 0.75 ± 0.06 *vs* 0.07 ± 0.05 and 1146 ± 85 s *vs* 221 ± 9.2 s (5 EGTA *vs* 5 BAPTA; $N = 5$ *vs* 7). (Db) Left. Average time courses of normalized mEPSC frequency (triangles). The normalized values were calculated from the mean frequency of the initial 1 min after patch break-in. Once reached the steady state, extracellular solution was changed to Ca^{2+}-free medium to exclude Ca^{2+}-independent mechanism for mEPSC. Right. Extracellular Ca^{2+}-dependent mEPSC frequency was calculated by subtracting the Ca^{2+}-independent portion from the recorded mEPSC frequency. The magnitude of reduction at steady state and the time course (τ) were 0.74 ± 0.05 *vs* 0.07 ± 0.03 and 1004 ± 107 s *vs* 277 ± 12.3 s (5 EGTA *vs* 5 BAPTA). (Ea, Eb) Average sequential time plots for mEPSC frequency (lines) or eEPSC amplitude (symbols) in the presence of varying concentration of Ca^{2+} chelator in intracellular solution (20 EGTA, eEPSC vs mEPSC, 0.51 ± 0.03 *vs* 0.52 ± 0.04 and 307.7 ± 10.1 s *vs* 363.6 ± 13.4 s, steady state and τ, $N = 4$; 0.5 BAPTA, 0.46 ± 0.07 *vs* 0.41 ± 0.05 and 588.2 ± 37.6 s *vs* 625 ± 40 s, steady state and τ, $N = 5$; 1 BAPTA, 0.31 ± 0.04 *vs* 0.35 ± 0.03 and 357.1 ± 11.8 s *vs* 335.8 ± 14.3 s, steady state and τ, $N = 8$). (F) Concentration-effect curves for BAPTA (blue) and EGTA (black). The steady state values were normalized by the value of just after whole-cell patch break-in configuration. All data are represented as mean ± S.E.M.

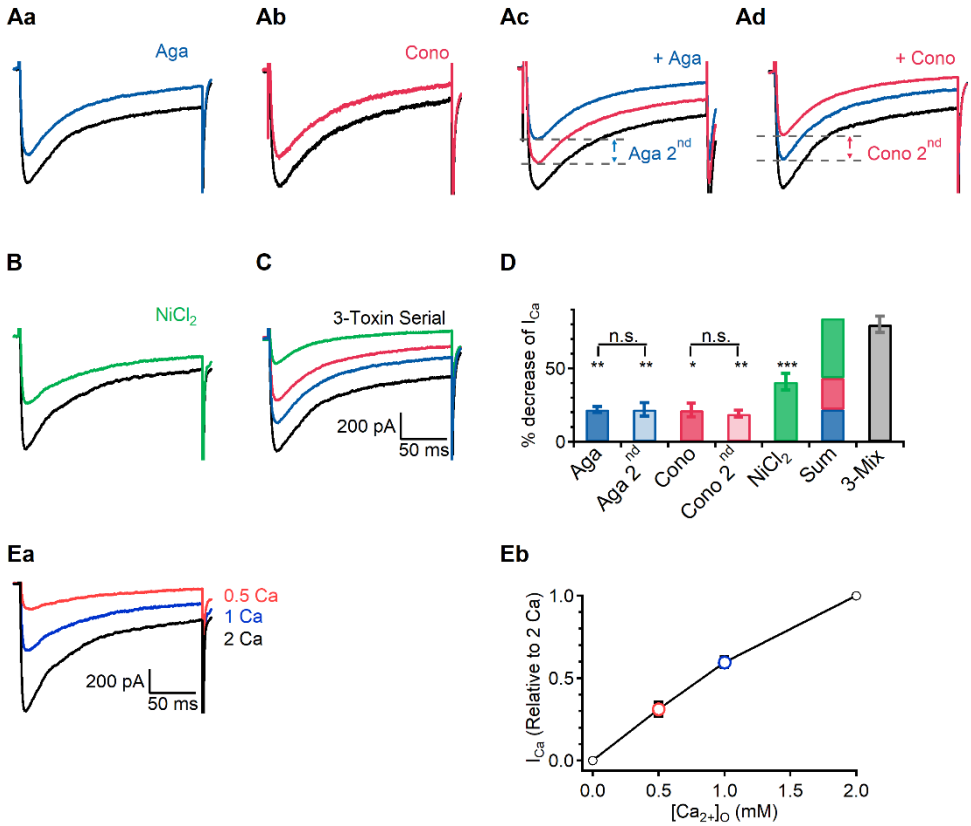

Figure 12. The effect of VGCC blockers to I_{Ca}

(A-C) Representative traces of I_{Ca} applying Aga (Aa), Cono (Ab), serial application of Aga and Cono (Ac, d), $NiCl_2$ (B), or serial application of all 3 VGCC blockers (C). (D) A bar graph summarizing % decrease of Ca^{2+} currents by VGCC blockers (25 ± 3.2%, 22 ± 4.5%, 42 ± 1.6%; Aga, Cono, $NiCl_2$, N = 5, 4, 3). (Ea) Representative traces of I_{Ca} changing external Ca^{2+} concentration. (Eb) A plot of $[Ca^{2+}]_O$ versus I_{Ca} (0.5 Ca, 0.31 ± 0.04; 1 Ca, 0.6 ± 0.03, compared to 2 Ca, N = 4). All data are mean ± S.E.M., *P < 0.05, **P < 0.01, ***P < 0.001, single group mean t test; n.s. = not significant.

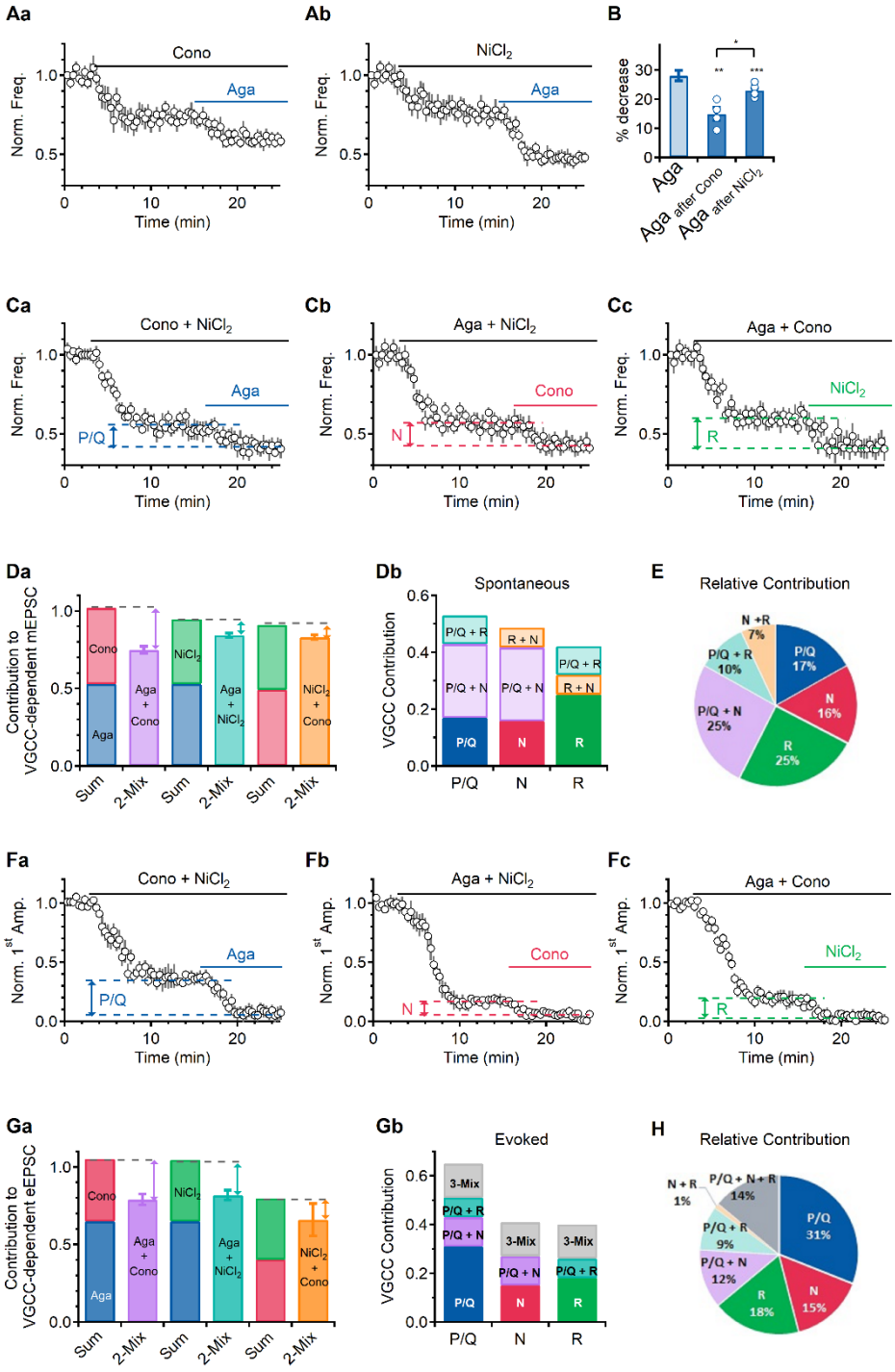
Aa
Cono
Aga
Norm. Freq.
Time (min)
Ab
NiCl2
Aga
Norm. Freq.
Time (min)
B
% decrease
Aga
Aga after Cono
Aga after NiCl2
Ca
Cono + NiCl2
Aga
P/Q
Norm. Freq.
Time (min)
Cb
Aga + NiCl2
Cono
N
Norm. Freq.
Time (min)
Cc
Aga + Cono
NiCl2
R
Norm. Freq.
Time (min)
Da
Contribution to VGCC-dependent mEPSC
Cono
Aga
Aga + Cono
NiCl2
Aga + NiCl2
NiCl2 + Cono
Sum
2-Mix
Db
Spontaneous
VGCC Contribution
P/Q + R
R + N
P/Q + N
P/Q
N
R
E
Relative Contribution
N +R 7%
P/Q + R 10%
P/Q 17%
P/Q + N 25%
N 16%
R 25%
Fa
Cono + NiCl2
Aga
P/Q
Norm. 1st Amp.
Time (min)
Fb
Aga + NiCl2
Cono
N
Norm. 1st Amp.
Time (min)
Fc
Aga + Cono
NiCl2
R
Norm. 1st Amp.
Time (min)
Ga
Contribution to VGCC-dependent eEPSC
Cono
Aga
Aga + Cono
NiCl2
Aga + NiCl2
NiCl2 + Cono
Sum
2-Mix
Gb
Evoked
VGCC Contribution
3-Mix
P/Q + R
P/Q + N
P/Q
N
R
H
Relative Contribution
N + R 1%
P/Q + N + R 14%
P/Q + R 9%
P/Q + N 12%
P/Q 31%
N 15%
R 18%

Figure 13. Coactivation of VGCCs contributes to spontaneous and evoked glutamate release

(Aa and b) Representative time courses of mEPSC frequency second applying Aga in the presence of Cono or $NiCl_2$, respectively. The normalized values were calculated from the mean frequency of the control condition. (B) The effect of Aga in the presence of Cono on mEPSC frequency was 14.8 ± 2.2% (N =4), and in the presence of $NiCl_2$ was 23 ± 0.8% (N = 6). The effect of Aga on mEPSC frequency decreased profoundly when Aga was applied in the presence of $NiCl_2$ (8.1%, compared to presence of Cono, unpaired t test). (Ca-c) Average time courses of mEPSC frequency reduction while applying the mixture of two blockers (Cono + $NiCl_2$, 0.55 ± 0.02, N = 8; Aga + $NiCl_2$, 0.55 ± 0.02, N = 8; Aga + Cono, 0.6 ± 0.03, N = 5) and secondary application of each remaining blocker (average of 3-mix, 0.47 ± 0.02). Each colored dashed line with an indicator arrow displays the sole contribution of each VGCC to spontaneous release (blue, P/Q-, 0.09 ± 0.01; red, N-, 0.08 ± 0.01; green, R-type VGCC, 0.13 ± 0.01). (Da) A bar graph for evaluating the contribution of a pair of VGCC blockers to mEPSC frequency. The contribution of each pair was compared with the arithmetic summation of two blockers or simultaneous application of two blockers. The summation data were calculated from (Fig. 3C) and 2-mix application from (C). Each colored arrow represents coactivation of two channels. (purple, Aga + Cono, 0.14; cyan blue, Aga + $NiCl_2$, 0.05; orange, Cono + $NiCl_2$, 0.04). (Db) A schematic chart of each VGCC contribution on spontaneous release subdivided by sole activation (solid) and coactivation with other channels (transparent). (E) A pie chart for the % VGCC contribution to spontaneous release. (Fa-c) Average time courses of the eEPSC amplitude reduction while applying the mixture of two blockers (Cono + $NiCl_2$, 0.34 ± 0.1, N = 4; Aga + $NiCl_2$, 0.18 ± 0.03, N = 4; or Aga + Cono, 0.21 ± 0.04, N = 4) and the secondary application of remaining each blocker (average of 3-mix, 0.03 ± 0.01). Each colored dashed line with an indicator arrow displays the sole contribution

of each VGCC to spontaneous release (blue, P/Q-, 0.31; red, N-, 0.15; green, R-type VGCC, 0.18). (Ga) bar graph for evaluating the contribution of a pair of VGCC blockers to eEPSC amplitude. The contribution of each pair was compared with the arithmetic sum of two blockers or simultaneous application of two blockers. The summation data were calculated from (Fig. 3F) and 2-mix application from (F). Each colored arrow represents coactivation of two channels. (Gb) A schematic chart of each VGCC contribution on evoked release subdivided by sole activation (solid) and coactivation with other channels (transparent). (H) Pie chart for % VGCC contribution to evoked release. All data are mean ± S.E.M., $*P < 0.05$, $**P < 0.01$, $***P < 0.001$, single group mean *t* test.

DISCUSSION

While Ca^{2+} influx through VGCCs in presynaptic axon terminals is critical for evoked synaptic transmitter release, the role of VGCCs in spontaneous glutamate release still remains controversial (Williams and Smith, 2018). In the present study, I found that spontaneous glutamate release is dependent on Ca^{2+} influx via P/Q-, N-, and R-type VGCCs in autaptic cultured hippocampal neurons. Moreover, estimation of the coupling distance between VGCCs and Ca^{2+} sensors by fitting the buffered Ca^{2+} diffusion model to the effects of two different Ca^{2+} chelators on mEPSCs and eEPSCs showed tight coupling configuration for both spontaneous and evoked release (~22 nm), suggesting general molecular machineries for VGCC-dependent exocytosis in both types of release. These data suggest that the coupling distance between Ca^{2+} sensors and Ca^{2+} sources is a critical factor in determining the contribution of VGCCs to spontaneous release. The present study highlights the role of coupling distance in regulating spontaneous neurotransmission.

It has been of a great interest whether molecular machineries of Ca^{2+}-dependent spontaneous release operate as those of evoked release do. Autaptic cultured neurons serve as ideal preparation to investigate this issue, since mEPSCs and eEPSCs are originated from the same set of presynaptic terminals, and thus, direct comparison of the two are allowed. These results obtained from autaptic hippocampal neurons showed remarkable similarities in VGCC-dependence as well as Ca^{2+} cooperativity between spontaneous and evoked release, suggesting that VGCCs could be the Ca^{2+} source for both of the two release, which is consistent with a previous study (Ermolyuk *et al.*, 2013). Likewise, Ca^{2+} sensors involved in the two release may not be different. A recent study showed that synaptic vesicles for miniature events are

originated from the recycling pool, which is also the source of evoked release (Hua *et al.*, 2010). The role of VGCCs in spontaneous glutamate release was, however, denied in many other studies (Courtney *et al.*, 2018; Dai *et al.*, 2015; Tsintsadze *et al.*, 2017; Vyleta and Smith, 2011), and a lack of VGCC contribution was regarded to represent fundamental differences in molecular machineries between spontaneous and evoked release (Williams and Smith, 2018). I showed that in autaptic cultured hippocampal neurons that have tight coupling between Ca^{2+} sources and sensors, spontaneous glutamate release is indeed mediated by VGCCs, with similar Ca^{2+} cooperativity to evoked release.

Unlike glutamatergic synapses, it is generally accepted that spontaneous release at GABAergic synapses is mediated mainly by VGCCs (Williams *et al.*, 2012; Williams and Smith, 2018). A low-affinity Ca^{2+} sensor synaptotagmin 1 (Syt1) was shown to mediate spontaneous as well as evoked release (Courtney *et al.*, 2018; Xu *et al.*, 2009) and VGCC blockers affected Syt1-dependent spontaneous release in GABAergic synapses, but not in glutamatergic synapses (Courtney *et al.*, 2018). These findings were regarded to represent divergence in the release machinery between GABAergic and glutamatergic neurons (Courtney *et al.*, 2018), but this study showed that VGCC-dependent spontaneous release occurred in certain glutamatergic synapses. It is interesting to note similar features underlying spontaneous GABA release reported previously (Williams *et al.*, 2012; Williams and Smith, 2018) and my results. Tight coupling regime was used both in VGCC-dependent GABAergic mini events in cultured neocortical neurons (Williams *et al.*, 2012) and glutamatergic mini events in autaptic cultured hippocampal neurons (Fig. 11). Thus, these results suggest that the tightness of coupling between VGCCs and Ca^{2+} sensors could be a universal mechanism underlying VGCC-dependence of spontaneous release regardless of the type of synapses. At GABAergic synapses where coupling is generally tight (Bucurenciu *et al.*, 2010; Hefft and Jonas, 2005),

VGCCs would play a critical role in spontaneous release, whereas at glutamatergic synapses, VGCCs could participate at certain synapses that have tight coupling configuration, but not at most synapses. mEPSCs in CA1 neurons did not show VGCC-dependence in the control conditions, but VGCC dependence emerged at high $[Ca^{2+}]_o$ (Courtney *et al.*, 2018), suggesting that loose coupling can be overcome when Ca^{2+} influx or intracellular $[Ca^{2+}]$ is increased. However, such interpretation may not be generalized to all synapses. In dentate gyrus granule cells, a major fraction of VGCC-dependent spontaneous GABA release is generated at the terminals of CCK-expressing interneurons (Goswami *et al.*, 2012), which are known to have loose coupling between VGCCs and sensors (Ali and Todorova, 2010; Daw *et al.*, 2009; Hefft and Jonas, 2005). In fact, mossy fiber-CA3 synapses are known as loose-coupling synapses with coupling distance 73 - 80 nm (Vyleta and Jonas, 2014). These results may suggest the presence of other factors that determine the contribution of VGCCs to spontaneous release than coupling distance. Possibly, the number of VGCCs at active zone may affect the VGCC contribution. To further understand the underlying mechanisms, information about the VGCCs-to-vesicle topography in the active zone of different synapses is required.

I did not identify the nature of $[Ca^{2+}]_o$-dependent mechanisms other than VGCCs in the present study. Activation of the Ca^{2+} sensing receptor (CaSR), a G-protein coupled receptor activated by extracellular Ca^{2+}, was proposed to stimulate spontaneous release in glutamatergic neurons (Vyleta and Smith, 2011). However, results obtained using CaSR knockout neurons revealed that CaSR activation mediates only ~30% of spontaneous release and CaSR-dependent release decreases, not increases, as $[Ca^{2+}]_o$ increases (Vyleta and Smith, 2011). Such response did not conform the typical response of spontaneous release upon changing $[Ca^{2+}]_o$. Possibly, multiple Ca^{2+} sources that are involved in regulating resting Ca^{2+} levels, such as internal Ca^{2+} source (Carter *et al.*, 2002; Sharma and Vijayaraghavan, 2003) or TRPC

(Peters *et al.*, 2010; Shoudai *et al.*, 2010), may contribute to spontaneous release by activating Doc2, a high-affinity Ca^{2+} sensor exclusively for spontaneous release (Groffen *et al.*, 2010), yet the relationship between these sources and Doc2 remains to be uncovered. Taken together, various Ca^{2+} sources would participate in spontaneous release at different cells and conditions.

CHAPTER 2

The mechanisms of L-type Ca^{2+} channels mediated glutamatergic synaptic transmission

INTRODUCTION

Voltage-gated calcium channels (VGCCs) are well known as key factors of evoked synaptic transmission, but this is less clear for spontaneous release where the probability of presynaptic VGCC activation is low because of the hyperpolarized resting membrane potential (Rodolfo R. *et al.*, 1989; Wheeler *et al.*, 1994). In Ca^{2+} dependent spontaneous release, the role of voltage-gated Ca^{2+} channels (VGCCs) is controversial. At inhibitory central synapses, the substantial part of spontaneous release is dependent on stochastic opening of presynaptic VGCCs with either tight (Ca^{2+} nanodomain) (Williams *et al.*, 2012) or loose (Ca^{2+} microdomain) coupling between VGCCs and vesicular Ca^{2+}-release sensors at resting membrane potentials (Courtney *et al.*, 2018; Goswami *et al.*, 2012; Tsintsadze *et al.*, 2017). These experiments suggest the notion that spontaneous and evoked release follow the Ca^{2+}-influx dependent exocytosis which is due to opening of presynaptic VGCCs (Xu *et al.*, 2009). Otherwise at excitatory synapses, researchers revealed that spontaneous release is independent on VGCCs at neocortical synapses and calyx of Held synapses (Tsintsadze *et al.*, 2017; Vyleta and Smith, 2011), as the inorganic nonselective VGCCs blocker Cd^{2+} (50−100 μM) did not reduced the frequency of spontaneous release. They proposed that spontaneous release is caused by activation of calcium-sensing receptor (CaSR) instead of VGCCs. As well as recent studies investigated that spontaneous is dependent on VGCCs at hippocampal and calyx of Held synapses (Dai *et al.*, 2015; Ermolyuk *et al.*, 2013), consistent with the similar mechanisms of inhibitory release likewise stochastic opening of presynaptic VGCCs at resting potential. These findings also propose the notion that evoked and spontaneous release were triggered by Ca^{2+}-influx through presynaptic VGCCs in excitatory synapses, nevertheless the effect of resting global Ca^{2+} concentration ($[Ca^{2+}]_i$) or the contribution of the L-type channels (LTCCs) on spontaneous release has

underestimated.

It is known that the subcellular localization of LTCCs in hippocampal neurons is abundant at soma and proximal dendrites, however, fewer at presynaptic terminals (Westenbroek *et al.*, 1990). The role of LTCC has been mediated in the activity-dependent regulation of neuronal development and thereby in mediating different forms of synaptic plasticity and in activity-induced regulation of gene expression. Calcium entering neurons through $Ca_V1.2$ and $Ca_V1.3$ calcium channels in response to membrane depolarization or synaptic activity contributes to synaptic plasticity (Moosmang *et al.*, 2005), synaptic scaling (Ibata *et al.*, 2008), heterosynaptic molecular dynamics (Rose *et al.*, 2009), and transcriptional regulation (Greer and Greenberg, 2008). LTCC is a low-voltage-activated and voltage-dependent Ca^{2+} current which is pharmacologically blocked by dihydropyridine (Avery and Johnston, 1996; Magee *et al.*, 1996). L-type $Ca2^{+}$ channel immunoreactivity is primarily found in dendrites (Westenbroek *et al.*, 1990), and recent immunogold labeling of L-type Ca^{2+} channels are demonstrated that both $Ca_V1.2$ and $Ca_V1.3$ channel subtypes are predominantly located in postsynaptic dendritic processes and somata in hippocampal slice, and relatively few presynaptic axonal terminals (~5%) though (Tippens *et al.*, 2008). Also LTCCs have been trigger spontaneous inhibitory release in synaptic terminals of CCK interneurons via microdomain coupling (Eggermann *et al.*, 2012). However, it has been poorly known whether LTCC can be involved in spontaneous glutamate release, moreover what is the presynaptic mechanism of LTCCs. Therefore, in present study I found that excitatory spontaneous release may occur Ca^{2+} influx via LTCCs by regulation of global resting Ca^{2+} concentration which might be involved in CaM-dependent vesicle exocytosis.

MATERIALS AND METHODS

1. Autaptic neuronal culture

All preparations were carried out under the animal welfare guideline of Seoul National University (SNU), and approved by IACUC of SNU. Primary cultures of rat hippocampal neurons were prepared as described previously with slight adaptations (Bekkers and Stevens, 1991). Briefly, hippocampal neurons and astrocytes were obtained from Sprague-Dawley (SD) rats according to the protocols approved by the Seoul National University Institutional Animal Care and Use Committee. Astrocyte cultures were prepared from the Sprague-Dawley rat cortices P0 - P1 and grown for 10 days in 100-mm culture dish in glial medium [minimum essential medium (MEM; Invitrogen) supplemented with 0.6 % glucose, 1 mM pyruvate, 2 mM GlutaMAX-I (Invitrogen), 10 % horse serum (HS; Invitrogen), and 1 % penicillin-streptomycin (PS; Invitrogen)] before plating on the sprayed microisland coverslips in 30-mm petri dishes. 2 - 3 days before neurons being added in sprayed microisland dishes, astrocytes were removed from the 100-mm culture dish using trypsin-EDTA (Invitrogen) and plated on the microisland coverslips at a density of 60,000 cells/dish. Hippocampi from P0 - P1 SD rats were dissected in Hank's balanced salt solution (Invitrogen), digested with papain (Worthington, Freehold, NJ, USA), and then triturated with a polished half-bore Pasteur pipette. Immediately after removing glia medium in 30-mm dishes of microisland-shaped astrocytes, hippocampal neurons were added at a density of 6,000 cells/dish and were grown in neurobasal medium supplemented with B27 and glutamax (Invitrogen).

2. Electrophysiology

For recordings in autaptic cultured neurons, cells were visualized with an Olympus IX70 inverted microscope. Whole-cell voltage- or current-clamp recordings from

hippocampal autaptic pyramidal neurons were performed at room temperature and continuously perfused with extracellular solution consisting of following composition (in mM): 135 NaCl, 2.5 KCl, 2 $CaCl_2$, 1 $MgCl_2$, 10 glucose, 10 HEPES, 0.1 EGTA, pH 7.3 adjusted with NaOH (295 - 300 mOsm), and maintained at 0.5 - 1 ml min-1. All recordings were done at least 23 days after neurons were plated on coverslips. The internal pipette solution for recording mEPSCs and resting membrane potential (RMP) was used K-gluconate based solution.

Whole-cell voltage- or current-clamp recordings were performed at 32 ± 1°C and the rate of aCSF perfusion was maintained at 1 - 1.5 ml min-1. For high $[K^+]_o$ experiments, NaCl was reduced to maintain osmolarity. Recordings were made in somata with an EPC-10 amplifier (HEKA Electonik, Lambrecht/Pfalz, Germany). Signals were low-pass filtered at 5 kHz (low-pass Bessel filter) and sampled at 10 kHz. Series resistance (Rs) was monitored, and only recordings with Rs remained constant (<30% change during a recording) were used. Rs was compensated to 50 - 70 %. The data were analyzed using IGOR software (Wavemetrics, Lake Oswego, OR, USA). Patch electrodes were pulled from borosilicate glass capillaries to a resistance between 3 and 4 MΩ when filled with pipette solution. The internal pipette solution for recording miniature excitatory postsynaptic currents (mEPSCs) contained the following composition (in mM): 130 Cs-methanesulfate, 8 NaCl, 4 MgATP, 0.3 NaGTP, 10 HEPES, 0.1 EGTA, pH 7.3 adjusted with CsOH (295 - 300 mOsm). For RMP recording, K-gluconate was substituted for Cs-methanesulfate, and pH was adjusted with KOH.

The mEPSCs of hippocampal autapses were recorded at holding potential of -70 mV. 0.5 μM TTX and 0.1 mM picrotoxin (PTX) was added during recordings in acute slices. Events exceeding 6 - 7 pA within a specified interval of three to four digitized

points (0.5 - 0.8 ms) that showed a single exponential decay time course were identified as mEPSC. The rise time of mEPSC indicated the 20 - 80 % rise time. mEPSC frequency esd measured within 20 s bins. Synaptic activities were recorded at a holding potential of -70 mV. eEPSCs were recorded every 20 s after applying depolarization pulses from -70 to 0 mV for 2 ms. From the continuous recordings at -70 mV without stimulations, toxins and chemicals were typically applied for 5 - 20 min until a constant effect was observed.

3. Drugs

Nimodipine and Bay K 8644 were purchased from Tocris. All other chemicals were purchased from Sigma (St. Louis, MO, USA). Toxin stock solutions were made at 1000-fold concentration with DMSO and stored at -20°C.

4. Statistical analysis

Data were expressed as the mean ± SEM, where *N* represents the number of cells studied. Statistical analysis was performed using IgorPro (version 6.1, WaveMetrics, Lake Oswego, OR, USA) and OriginPro (version 9.0, OriginLab Corp., Northampton, MA, USA). Significant differences between the experimental groups were analyzed using independent or paired Student's *t*-tests. $P<0.05$ was considered statistically significant.

RESULTS

1. LTCCs contribute to spontaneous glutamate

I showed previously that P/Q-, N-, and R-type VGCCs triggered spontaneous glutamate release at synapses of hippocampus of both in cultures and brain slices and calyx of Held (Lee *et al.*, 2020). I investigated contribution of LTCCs to glutamate release using autaptic cultured hippocampal neurons. Blockade of LTCC with 10 μM nimodipine (Nimo) decreased the mEPSC frequency significantly (Figs. 14Aa; 0.81 ± 0.01, $N = 17$, compared to noramalized control value), without affecting mEPSC amplitudes (Fig. 14Ad). Moreover, application of 10 μM Bay K 8644 (Bay K), an LTCC activator, induced a huge increase in mEPSC frequency (Figs 14Ab: 1.79 ± 0.11, $N = 7$, compared to control), suggesting that Ca^{2+} influx via LTCC contributes to spontaneous glutamate release. T-type VGCC blockade with 40 μM $NiCl_2$ had no effect on the mEPSC frequency (1.01 ± 0.003, $N = 4$, Fig. 15).

VGCCs may contribute to spontaneous glutamate release by two possible mechanisms. Ca^{2+} influx upon stochastic openings of VGCCs directly triggers exocytosis via increasing local [Ca^{2+}] near primed vesicles at active zone with nanodomain coupling (Ermolyuk *et al.*, 2013) and/or indirectly increases the probability of vesicle release triggered by local Ca^{2+} increase via increasing presynaptic global [Ca^{2+}] levels. To examine these two possibilities, I examined the effect of Nimo and Bay K while P/Q-, N-, and R-type VGCCs which were shown to directly trigger mEPSCs were inhibited by the mixture of 0.1 μM Aga, 0.1 μM Cono, and 100 μM $NiCl_2$. The mixture significantly decreased the spontaneous release by ~ 0.6 fold ($N = 11$) and additional treatment of Nimo or Bay K did not show further change (Fig. 14B). These results suggest that Ca^{2+} influx via LTCC is not able to directly activate Ca^{2+} sensors involved in spontaneous release, but facilitate spontaneous release triggered by other VGCCs, possibly via increasing resting Ca^{2+} levels. To further test this idea, I examined effects of Nimo and Bay K on mEPSC

frequency in the presence of 10 mM EGTA in the pipette solution where resting [Ca^{2+}] was kept low. Under this condition, the effects of Nimo and Bay K on mEPSC frequency were completely abolished (Fig. 14Ca, Cb). In contrast, effects of Aga, Cono, and 100 μM $NiCl_2$ on mEPSC frequency (Fig. 16B) were not significantly different from their effects obtained in the presence of 0.1 mM EGTA shown in the previous data (Fig. 16C).

2. Regulation of spontaneous release by RMP change is mediated by LTCCs

Enhancement of AP-triggered glutamate release by subthreshold somatic depolarization was noted in many neurons, but it is controversial whether underlying mechanisms involve increased resting Ca^{2+} level (Alle and Geiger, 2006) or increased frequency of VGCC openings (Christie *et al.*, 2011). I investigated whether the subthreshold depolarization can enhance the spontaneous release and if it is the case which mechanism is involved. To determine the relationship between subthreshold RMP change and spontaneous release, mEPSCs frequency was recorded at different holding potentials (HP). Hyperpolarization of HP from -70 mV to -80 mV caused a significant reduction in mEPSC frequency (Figs. 17Aa, B, 0.82 ± 0.02, N = 12, compared to normalized -70 mV), while depolarization of HP from -70 mV to -60 mV caused a significant increase in mEPSC frequency (Figs. 17Aa and B, 1.49 ± 0.06, compared to normalized -70 mV. N = 11). The amplitude of mEPSCs were decreased by depolarization (-80 mV, 17.66 ± 0.68; -70 mV, 15.98 ± 0.54; -60 mV, 14.2 ± 0.56 pA), which may reflect the decrease in driving force for non-selective cation currents. Effects of RMP on mEPSC frequency were similarly observed when RMP was changed by changing external K^+ concentration (Figs. 17Ab, B; RMP, mEPSC frequency;1 mM $[K^+]_o$, -85.33 ± 1.9 mV, 0.72 ± 0.03, N =

6; 2.5 mM $[K^+]_o$, -73.4 ± 1.37 mV, 0.93 ± 0.04, N = 7; 5 mM $[K^+]_o$, -54.67 ± 2.72 mV, 1.43 ± 0.16, N = 7). The effects of HP changes on mEPSC frequency were abolished in the presence of 10 mM EGTA in pipette solutions (Figs. 17Ca, Cb). Interestingly, HP changes did not affect mEPSC frequency in the presence of nimodipine or Bay K (Figs. 17Da, Db). Nimodipine significantly decreased mEPSCs frequency by 0.19-fold at -70 mV and did not show significantly change by depolarization or hypepolarization, while Bay K increased the frequency by 1.8-fold at -70 mV, but did not show further changes at depolarized or hyperpolarized potential. These results suggest that the effects of HP changes in this range on mEPSC frequency are mediated not by the increased frequency of local Ca^{2+} increase, but by the changes in global Ca^{2+} concentrations, and that membrane potential-dependent changes in global Ca^{2+} concentrations are mainly attributable LTCCs. To examine this idea, I measured effects of HP on global Ca^{2+} concentrations ($[Ca^{2+}]_c$) and how they are affected by VGCC blockers (Fig. 17E). I used the fluorescent Ca^{2+} indicator Fura-2 for a ratiometric fluorescent dye. The normalized F1/F2 ratio was significantly enhanced by depolarizing HP (Fig. 15E, -80 mV, 0.97 ± 0.01; -60 mV, 1.08 ± 0.02, N = 6), however, Nimo or Bay K did not change the fluorescent ratio (Fig. 17E). Taken together, LTCCs is newly identified in RMP-dependent analogue modulation of spontaneous glutamatergic synaptic transmission in hippocampal autaptic neurons, and Ca^{2+} influx via LTCCs may contribute to spontaneous release not by direct triggering but by regulating presynaptic global Ca^{2+} concentrations.

3. Calmodulin mediates LTCC dependent modulation of spontaneous glutamate release

Modulation of VGCC-dependent transmitter release by $[Ca^{2+}]_c$ may be attributable to two mechanisms. Changes in $[Ca^{2+}]_c$ affect local Ca^{2+} increase by buffer saturation effects (Jackson and Redman, 2003; Rusakov, 2006), and/or regulate exocytosis by

Ca^{2+}-dependent signaling mechanism. Calmodulin (CaM) is known as a potential Ca^{2+} regulator in neurotransmitter release(DeLorenzo, 1981; Steinhardt and Alderton, 1982). In addition, CaM has a plethora of functions at synapses, making it difficult to pinpoint a single molecular target of CaM in neurotransmission (Di Giovanni *et al.*, 2010; Lipstein *et al.*, 2013; Pang *et al.*, 2010). Moreover, previous study has shown that CaM also can modulate the spontaneous neurotransmitter release by control of SNARE complex assembly via regulation of V100 (Wang *et al.*, 2014). Therefore, I examined whether the LTCCs-dependent spontaneous release might be affected by CaM-dependent synaptic vesicle exocytosis pathway using calmodulin inhibition peptide (CaM-iP) containing internal patch pipette solution. Fig. 18Aa shows a schematic image for the diffusion of CaM-iP through the autaptic pyramidal neuron. The frequency of mEPSC were recorded immediately after patch break-in. Sequential recordings for mEPSCs continued until the effects of CaM-iP perfusion reached steady state (Figs. 18Ab, Ac). At steady state, CaM-iP reduced the mEPSC frequency by 0.77 ± 0.04 (Fig. 18Ad, $N = 11$). I performed these experiments in the presence of Nimo or Bay K to elucidate the effects of CaM on LTCCs-dependent spontaneous glutamate release. The effect of CaM-iP on mEPSC frequency did not change in LTCCs inhibition or activation condition (Figs. 18Ba-Bd). Moreover, the effect of HP on spontaneous release did not appear at CaM inhibition condition (Figs. 18Ca, Cb). Therefore, these data suggested that the LTCCs-dependent modulation of spontaneous glutamate release might be mediated the CaM-dependent vesicle exocytosis pathway.

4. Contribution of LTCCs to spontaneous release is developmentally regulated

Previous study reported that local Ca^{2+} increase mediated by stochastic opening of P/Q-, N-, R-type VGCCs can explain Ca^{2+}-dependent spontaneous glutamate release

in hippocampal cultured neurons (Ermolyuk *et al.*, 2013). However, they did not notice the effect of LTCC on spontaneous release. Since neurons that they used were younger than ours (8 ~ 11 days *vs* more than 3 weeks after plating), it is likely that contribution of LTCC may be developmentally regulated, so that the effect of LTCC did not appear at young neurons. I therefore examined contribution of each VGCC to mEPSCs frequency in hippocampal neurons at DIV 8 to 11 in an autaptic culture system. I found that Nimo and Bay K did not affect mEPSC frequency (N = 6, 4), while Aga, Cono, or 100 μM $NiCl_2$ significantly decreased the frequency by 0.4 ± 0.06 (N = 4), 0.36 ± 0.04 (N = 7), or 0.3 ± 0.03-fold (N = 4), respectively (Figs. 19A, B). The Ca^{2+} influx-dependent spontaneous release was 0.6 ± 0.01-fold (N = 7), which is equivalent to the value obtained from neurons at DIV 21 or more (0.42 ± 0.03, Fig. 2Ba). To examine whether the lack of LTCCs contribution to spontaneous release in young neurons is due to the low level of LTCCs expression in young neurons, I tested the effect of Nimo on Ca^{2+} currents elicited by depolarization from -70 mV to 0 mV (200 ms duration). Nimo decreased the amplitude of inward Ca^{2+} current significantly in young neurons, which was not significantly different from the inhibitory effects of Nimo on Ca^{2+} current in adult neurons (Fig. 19C). These results suggest that LTCCs are already present in young neurons, but localization of LTCC to presynaptic terminals may occur later.

I showed the relationship between LTCCs contribution and effect of HP changes on spontaneous release (Fig. 17). I examined whether lack of L-type contribution in young neurons leads to the lack of HP effects on spontaneous release. Changing HP between -80 and -60 mV did not affect mEPSC frequency (Figs. 19Da, Db), further confirming that the effect of HP changes on spontaneous release is mediated by LTCCs.

5. Contribution of LTCCs to evoked glutamate release

To explore whether the LTCCs affect evoked glutamate release, the eEPSC was recorded in presence of Nimo or Bay K. The 1st EPSC amplitude was significantly reduced by Nimo (Fig. 20Ac, 0.7 ± 0.05, $N = 13$) and significantly enhanced by Bay K (Fig. 20Ac, 1.82 ± 0.18, $N = 6$). which was associated with an increase in PPR by Nimo or decrease in Bay K (Fig. 20Ad). Next, I tested the effect of CaM on evoked glutamate release. As shown in Fig. 16, CaM-iP was applied in internal patch pipette solution. At steady state, the 1st EPSC amplitude was significantly decreased by CaM inhibition (Fig. 20Bc, 0.77 ± 0.07, $N = 11$). To examine whether the effect of LTCCs on evoked release which might be mediated by CaM-dependent exocytosis pathway. The inhibition or activation of LTCCs did not change the 1st EPSC amplitude in presence of CaM-iP (Fig. 20C). Therefore, LTCCs also contribute to evoked glutamate release which might be mediated the CaM-dependent vesicle exocytosis pathway.

6. Contribution of calmodulin to the size of readily releasable pool

The release probability and the size of synaptic vesicle pool are the key determinants of the presynaptic mechanism which can regulate the neurotransmitter release. The inhibition of CaM decreased the frequency of spontaneous release and increase the PPR (Figs. 18A, 20B), so I considered that CaM -mediated synaptic vesicle exocytosis might be regulated by presynaptic mechanism. To explore how the CaM affect the both types of synaptic transmission, I recorded the size of readily releasable pool (RRP) by extracellular application of hypertonic sucrose solution. Previous study showed the pivotal role of Ca^{2+}-Calmodulin-Munc13-1 complex on short-term synaptic plasticity (Lipstein *et al.*, 2013). They suggested that Ca^{2+}-Calmodulin-Munc13-1 complex can regulate the recovery rate of the releasable synaptic vesicle pool, moreover the Ca^{2+}-CaM effect on releasable SV pool refilling is mediated by

Munc13-1. However, the Ca^{2+}-Calmodulin-Munc13-1 complex did not change the size of RRP testing in Munc13-1 knockin mouse lines. In present study, I examine the effect of CaM inhibition on RRP size via hypertonic sucrose solution (500 mM) application. Changes in RRP size by experimental conditions were monitored by measuring the area of current trace under the baseline (Fig. 21). Immediately after patch-break in, the hypertonic sucrose solution was applied approximately every 2.5 mins until the ends of experiment. Under the control condition, RRP size measured at the the 2nd and 3rd application of sucrose solution was smaller than that measured at the 1st application (0.68 ± 0.06, $N = 9$, Fig. 21A). In the presence of CaM-iP in the pipette solution, the decrease in RRP size at the 2 or 3 times of sucrose application after 8 mins of patch-break in was significantly smaller (0.47 ± 0.06, $N = 5$, Fig. 21B) than that under control condition ($P = 0.0014$), suggesting the contribution of CaM to RRP size. Next, I tested whether the LTCCs also affected the RRP size. The blockade of LTCCs decreases the RRP size by 0.7 ± 0.05 and the activation of LTCCs increases the RRP size by 1.16 ± 0.02 (Figs. 21C and D). However, the P/Q channel blocker Aga did not significantly change the RRP size (Fig. 21E, 0.97 ± 0.04). These results support the idea that CaM regulates synaptic transmission, at least in part, by regulating the size of releasable pool, and that LTCCs contribute to CaM activation. Taken together, I suggested that the LTCCs did not directly trigger the spontaneous release like Ca_V2 families which locate in the vicinity of synaptic vesicles. Possibly, LTCCs may control the spontaneous release at peri-synaptic regions via regulating the global $[Ca^{2+}]_i$ and the global $[Ca^{2+}]_i$ modulate the spontaneous release by CaM-mediated exocytosis pathway via regulating RRP size.

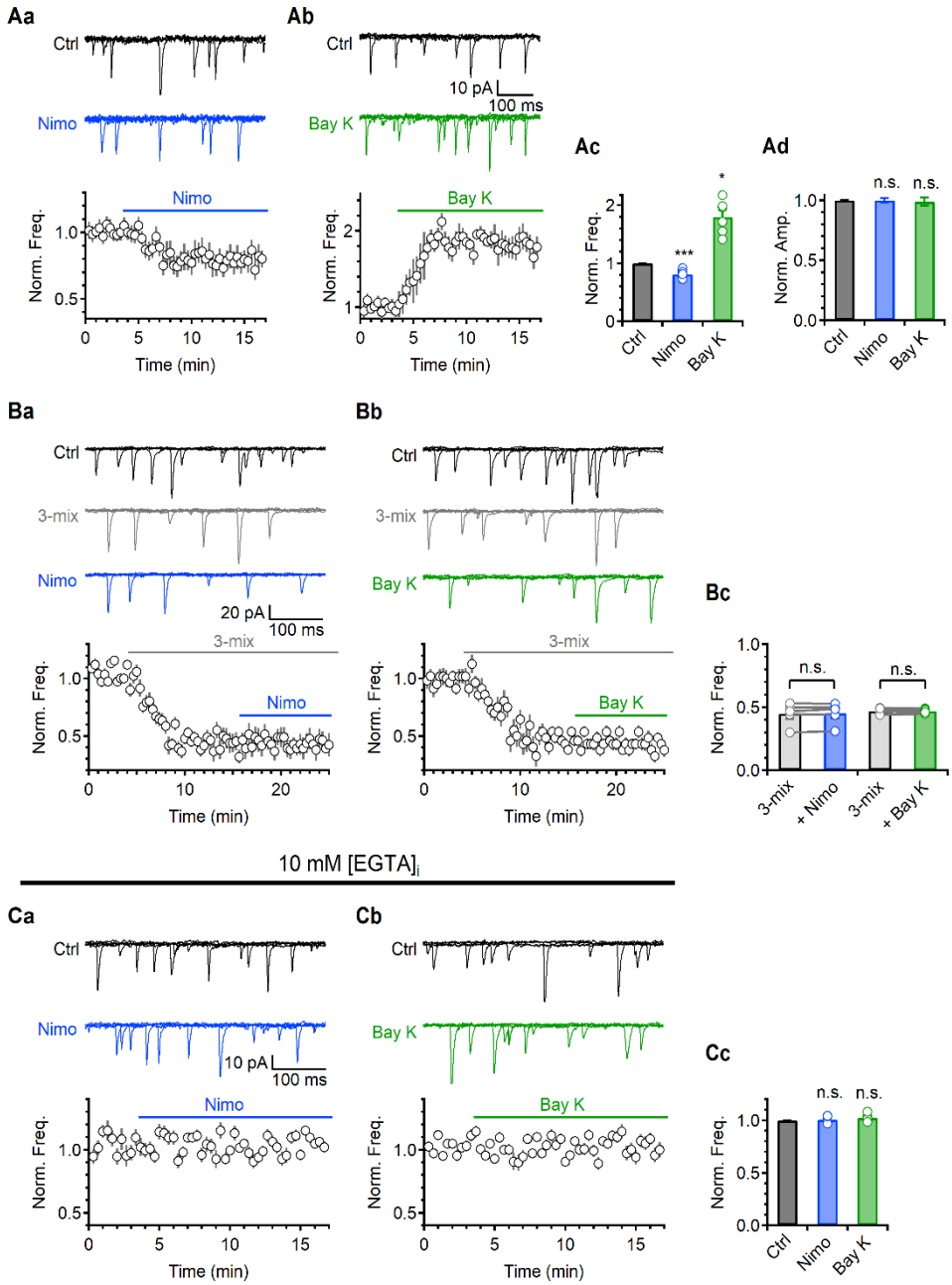

Figure 14. LTCCs contribute to spontaneous glutamate release

(Aa, Ab) Top. Representative traces of mEPSC frequency in the presence of Nimo

or Bay K, respectively. Bottom. An average time course of mEPSC frequency. The normalized values were calculated from the mean frequency of the control condition. The top solid line indicates an application point for each VGCC blocker or activator. (Ac, Ad) Bar graphs showing normalized mEPSC frequency (Nimo, blue, 0.81 ± 0.01, $N = 17$; Bay K, green, 1.8 ± 0.12, $N = 7$, compared to control; Ac) and amplitude (Ad). (Ba, Bb) Top. Representative traces of mEPSC frequency in the presence of 3-mix blockers with Nimo or Bay K, respectively. Bottom. An average time course of mEPSC frequency. The top solid line indicates an application point for each VGCC blocker or activator. (Bc) A bar graph showing normalized mEPSC frequency (3-mix *vs* Nimo, 0.45 ± 0.05 *vs* 0.45 ± 0.04, $N = 10$; 3-mix *vs* Bay K, 0.47 ± 0.01 *vs* 0.47 ± 0.06, $N = 12$). (Ca, Cb) Top. Representative traces of mEPSC frequency in the presence of Nimo or Bay K in 10 mM EGTA containing patch pipette solution, respectively. Bottom. An average time course of mEPSC frequency. (Cc) A bar graph showing normalized mEPSC frequency (Nimo, 1.0 ± 0.01, $N = 5$; Bay K, 1.02 ± 0.02, $N = 5$, compared to control). All data are mean ± S.E.M., $*P < 0.05$, $***P < 0.001$, single group mean *t*-test or paired *t*-test (Bc); n.s. = not significant.

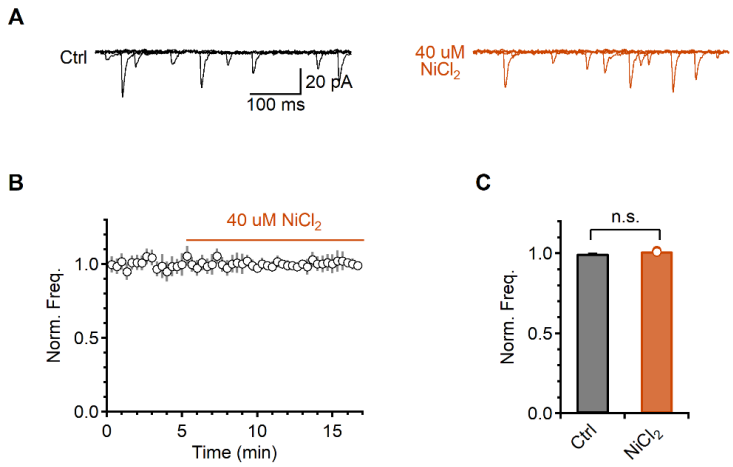

Figure 15. T-type VGCCs do not contribute to spontaneous glutamate release

(A) Representative traces of mEPSC frequency in the presence of 40 μM $NiCl_2$. (B) An average time course of mEPSC frequency. The normalized values were calculated from the mean frequency of the control condition. The top solid line indicates an application point for VGCC blocker. (C) A bar graph showing normalized mEPSC frequency ($NiCl_2$, 1.01 ± 0.01, N = 5). All data are mean ± S.E.M., Single group mean *t*-test; n.s. = not significant.

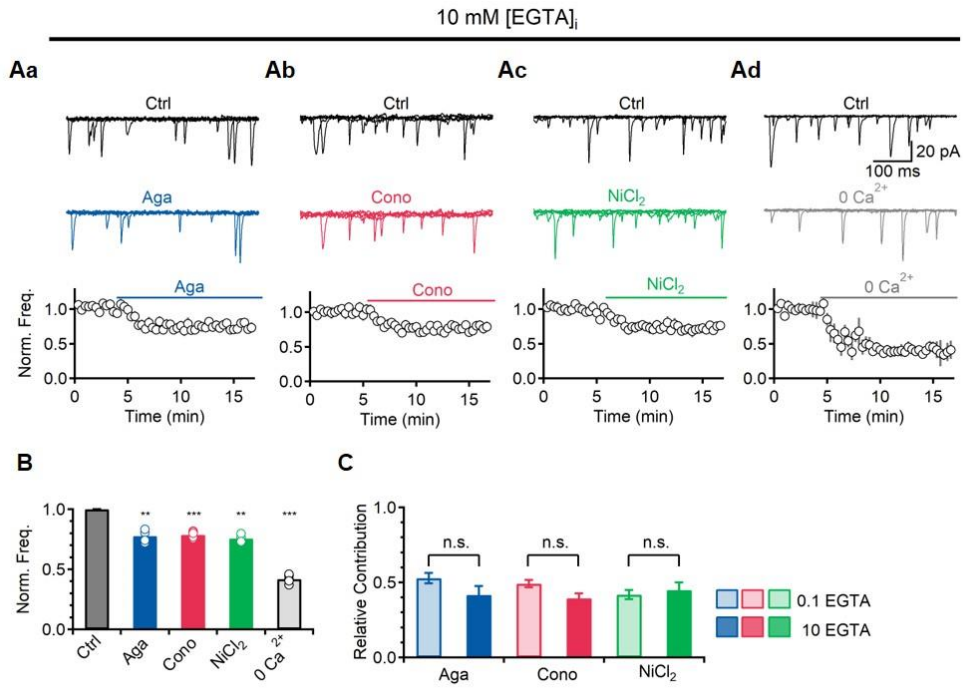

Figure 16. VGCCs contribute to spontaneous glutamate release in 10 mM $[EGTA]_i$

(A) Top. Representative traces of mEPSC frequency in the presence of Aga, Cono, SNX, $NiCl_2$ or Ca^{2+}-free condition in 10 mM EGTA containing patch pipette solution, respectively. Bottom. An average time course of mEPSC frequency. The normalized values were calculated from the mean frequency of the control condition. (B) A bar graph showing normalized mEPSC frequency (Aga, 0.77 ± 0.03, $N = 5$, $P < 0.001$; Cono, 0.78 ± 0.02, $N = 6$; $NiCl_2$, 0.76 ± 0.03, $N = 5$; 0 Ca^{2+}, 0.42 ± 0.02 $N = 5$, compared to control). (C) A bar graph showing the comparison of relative contribution of each VGCCs to mEPSC frequency in 0.1 mM $[EGTA]_i$ and 10 mM $[EGTA]_i$ (0.1 mM $[EGTA]_i$ *vs* 10 mM $[EGTA]_i$; Aga, 0.53 ± 0.03 *vs* 0.42 ± 0.06; Cono, 0.49 ± 0.02 *vs* 0.39 ± 0.03; $NiCl_2$, 0.42 ± 0.03 *vs* 0.45 ± 0.05). The contribution of each VCGG to spontaneous release was calculated from the reduction of mEPSC frequency in each VGCC blocker, and then adjusted by the proportion of VGCC-dependent spontaneous release (divided by 0.53 of 0.1 mM $[EGTA]_i$ or 0.58 of 10 mM $[EGTA]_i$). All data are mean ± S.E.M., $*P < 0.05$, $**P<0.005$, $***P < 0.001$, single group mean *t*-test or paired *t*-test (C); n.s. = not significant.

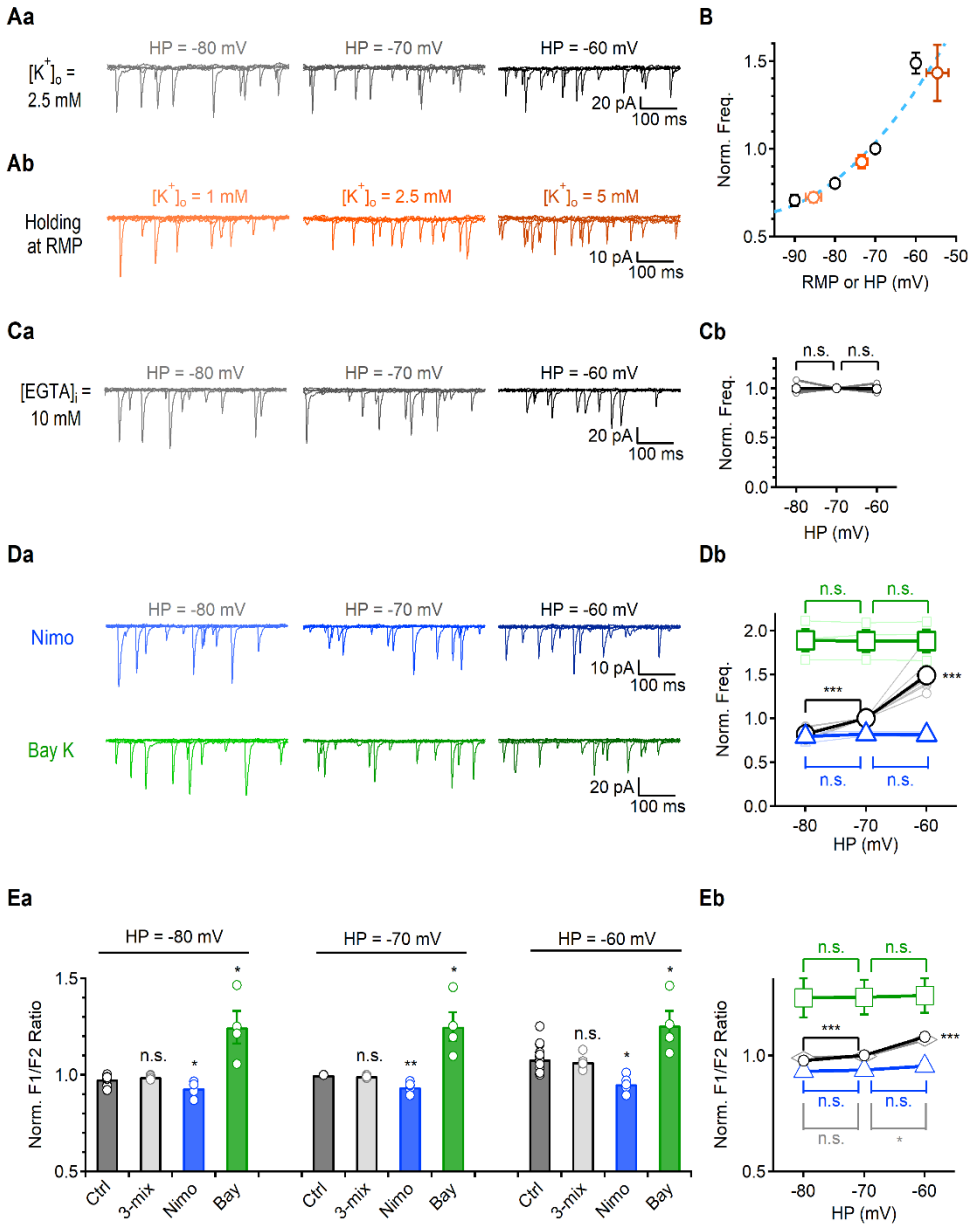

Figure 17. Regulation of spontaneous release by RMP change is mediated by LTCCs

(Aa) Representative traces of mEPSC frequency in each holding potential at 2.5 mM $[K^+]_o$. (Ab) Representative traces of mEPSC frequency in various $[K^+]_o$ at -70 mV

holding potential. (B) A graph indicating the relationship between HP (black circles) or RMP (orange circles) and the normalized mini frequency, compared to control -70 mV or 2.5 K^+ value (HP; black circles; -80 mV, 0.8 ± 0.02, *N* =10; -60 mV, 1.49 ± 0.06, *N* =13), (RMP *vs* frequency; orange circles; 1 K^+, -85.33 ± 1.9 mV *vs* 0.72 ± 0.03; 2.5 K^+, -73.4 ± 1.37 mV *vs* 0.93 ± 0.04; 5 K^+, -54.67 ± 2.72 mV *vs* 1.43 ± 0.16, *N* = 8). (Ca) Representative traces of mEPSC frequency in each holding potential at 2.5 mM $[K^+]_o$. The patch pipette contained 10 mM EGTA. (Cb) A graph indicating the normalized mEPSC frequency in various HP, compared to -70 mV value (-80 mV, 0.99 ± 0.02; -60 mV, 0.99 ± 0.03, *N* =7). (Da) Representative traces of mEPSC frequency in each holding potential at 2.5 mM $[K^+]_o$ applying Nimo or Bay K. (Db) A graph indicating the normalized mEPSC frequency in various HP with Nimo or Bay K treatment, compared to control at -70 mV value (-80 mV, -70 mV, -60 mV; Nimo, 0.79 ± 0.03, 0.82 ± 0.01, 0.81 ± 0.03; Bay K, 1.89 ± 0.13, 1.88 ± 0.12, 1.88 ± 0.13, *N* =4). (Ea, Eb) A bar graph (Ea) and a line graph (Eb) showing the normalized F1/F2 ratio at various HP, compared to control at -70 mV value (-80 mV, -70 mV, -60 mV; control, 0.98 ± 0.02, 1.0 ± 0.0, 1.08 ± 0.02, *N* = 8; Nimo, 0.93 ± 0.02, 0.94 ± 0.01, 0.95 ± 0.02, *N* = 6; Bay K, 1.25 ± 0.08, 1.25 ± 0.08, 1.26 ± 0.07, *N* = 7; 3-mix, 0.99 ± 0.01, 0.99 ± 0.01, 1.07 ± 0.02, *N* = 4). All data are mean ± S.E.M., ***$P < 0.001$, single group mean *t*-test or paired *t*-test (Db, Eb); n.s. = not significant.

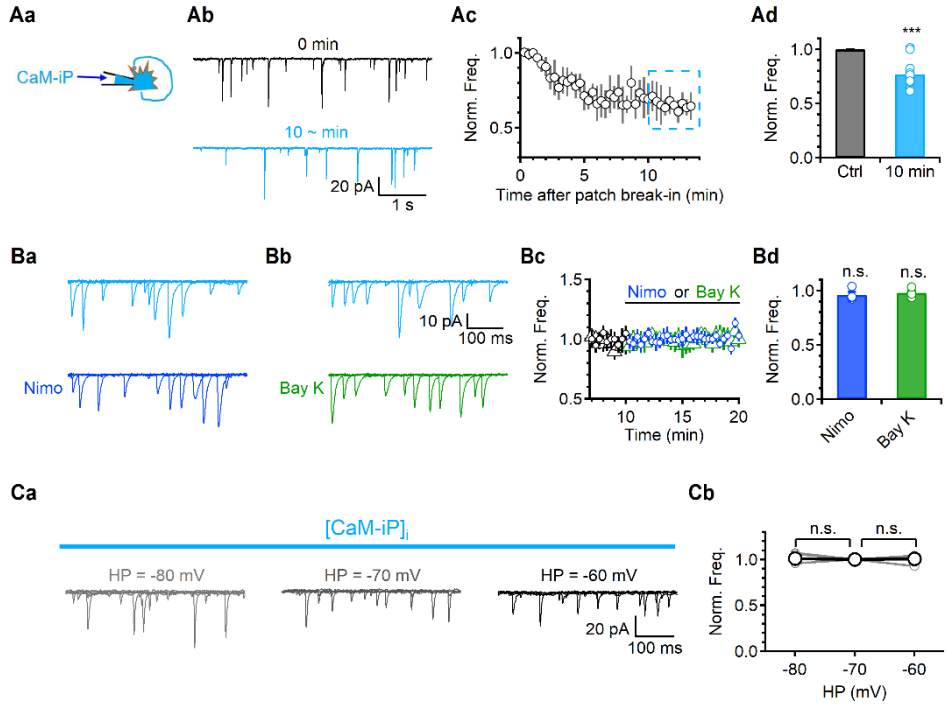

Figure 18. Calmodulin mediates LTCCs dependent modulation of spontaneous glutamate release

(Aa) A schematic image of CaM-iP diffusion through autaptic cell body to synaptic terminal. (Ab) Representative traces for the comparison of mEPSC between immediately patch break-in and 10 min after patch in presence of 10 μM CaM-iP (blue). (Ac) An average time course of mEPSC frequency. The normalized values were calculated from the mean frequency of the control condition. (Ad) A bar graph showing the normalized mEPSC frequency 10 min after patch in presence of CaM-iP (0.77 ± 0.07, N = 11). (Ba, Bb) Representative traces of mEPSC 10 min after patch in presence of CaM-iP (blue) applying Nimo or Bay K, respectively. (Bc) An average time course of mEPSC frequency with Nimo or Bay K. (Bd) A bar graph showing the effect of Nimo or Bay K on normalized mEPSC frequency 10 min after patch in presence of CaM-iP (Nimo, 0.96 ± 0.03, N = 6; Bay K, 0.98 ± 0.02, N = 4). (Ca) Representative traces of mEPSC 10 min after patch in presence of CaM-iP with changing HP. (Cb) A graph showing the HP effect on mEPSC frequency in presence of CaM-iP, compared to -70 mV (-80 mV, -60 mV; 1.01 ± 0.03, 1.0 ± 0.03, N = 5). All data are mean ± S.E.M., ***P < 0.001, single group mean t-test or paired t-test (Cb); n.s. = not significant.

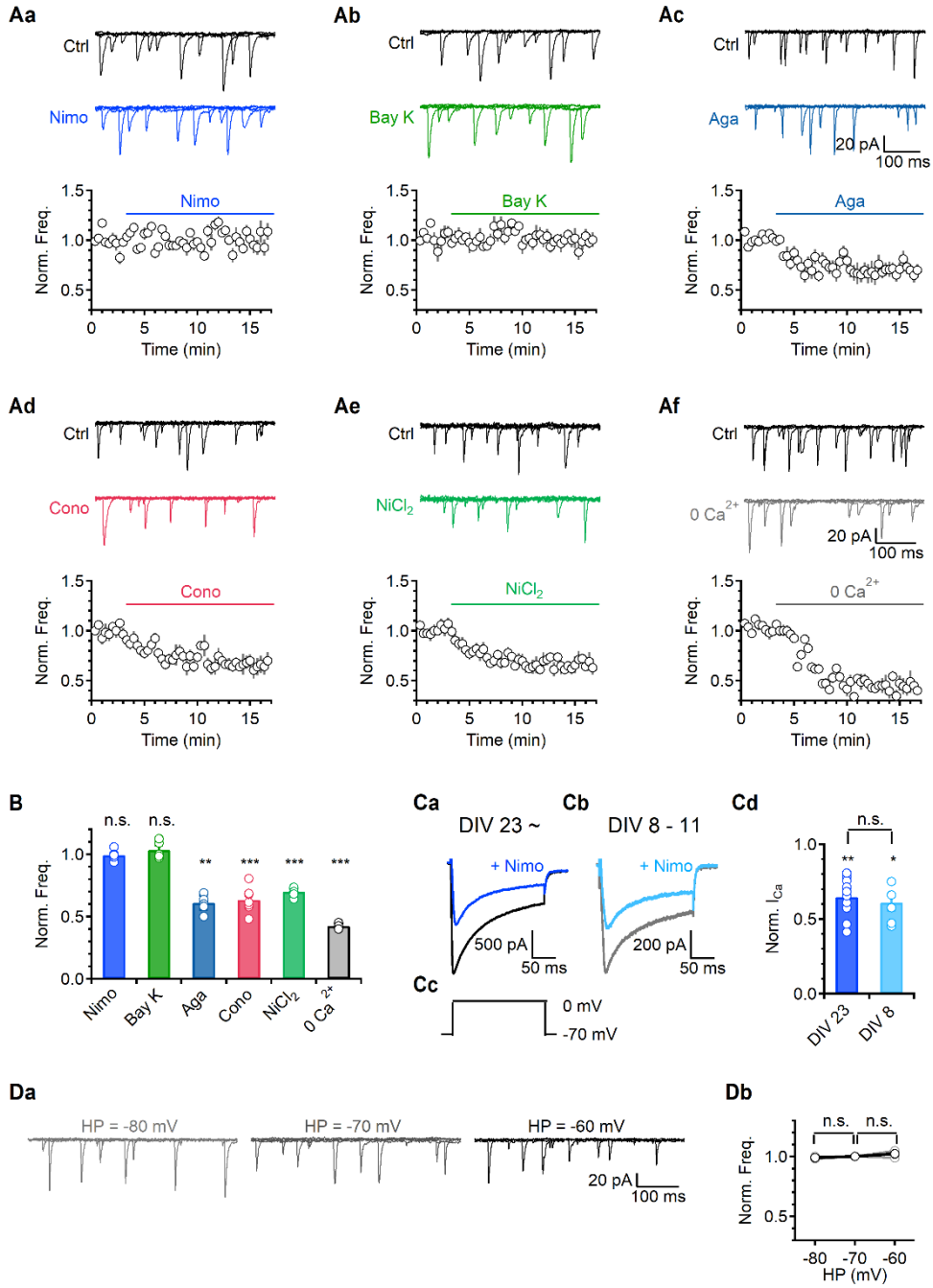

Figure 19. Contribution of LTCCs to spontaneous release is developmentally regulated

(Aa-Af) Top. Representative traces of mEPSC frequency in the presence of Nimo, Bay K, Aga, Cono, $NiCl_2$ or Ca^{2+}-free condition, respectively. Bottom. An average time course of mEPSC frequency. The normalized values were calculated from the mean frequency of the control condition. The top solid line indicates an application point for each drug application. (B) A bar graph showing normalized mEPSC frequency (Nimo, 0.99 ± 0.02, $N = 6$; Bay K, 1.03 ± 0.04, $N = 5$; Aga, 0.61 ± 0.06, $N = 6$; Cono, 0.63 ± 0.04, $N = 8$; $NiCl_2$, 0.7 ± 0.03, $N = 6$; 0 Ca^{2+}, 0.43 ± 0.01, $N = 6$, compared to control). (Ca, Cb) Representative traces of I_{Ca} applying Nimo comparison between DIV 23 ~ and DIV 8 - 11. (Cc) A pulse protocol for recording VGCC currents. The VGCC currents were activated by steps from -70 to -10 mV in bath solution containing 25 mM tetraethylammonium (TEA), 5 mM 4-AP, 1 μM TTX, 10 μM CNQX and 100 μM PTX. (B) A bar graph of normalized I_{Ca} in Nimo (DIV 23 *vs* 8; 0.64 ± 0.04, $N = 12$; 0.61 ± 0.06, $N = 6$). All data are mean ± S.E.M., $*P < 0.05$, $**P < 0.005$, $***P < 0.001$, single group mean *t*-test or paired *t*-test (Cd); n.s. = not significant.

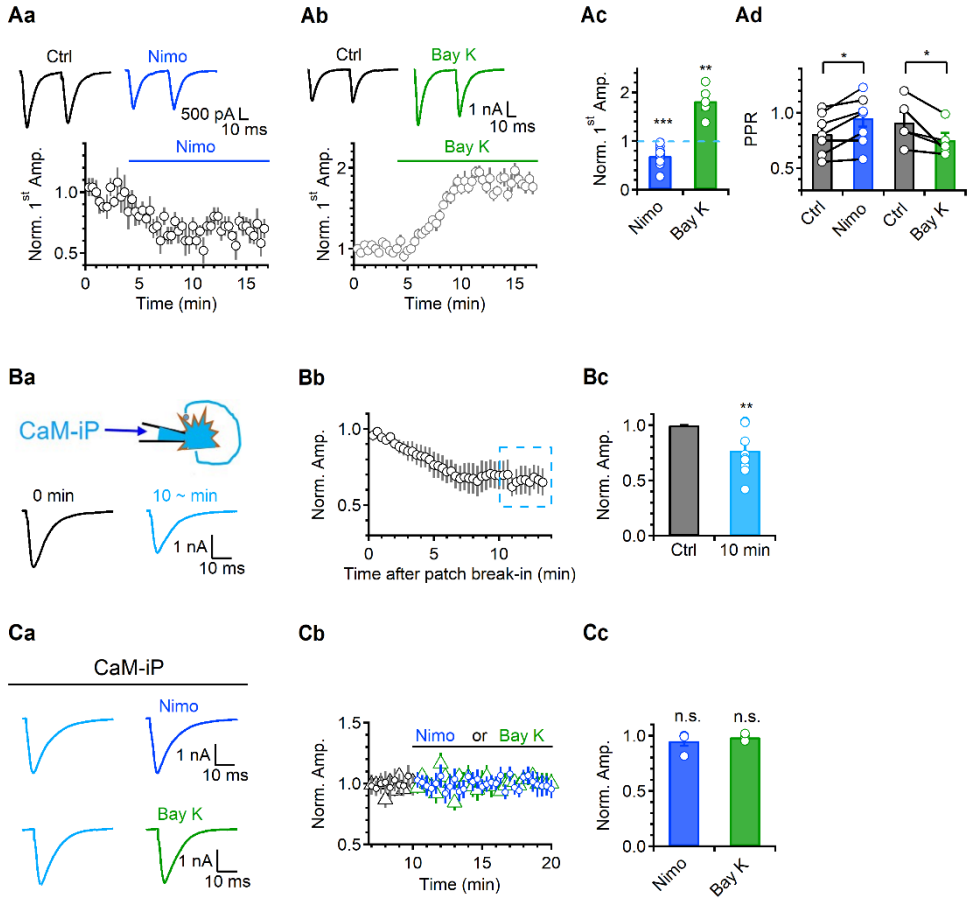

Figure 20. Contribution of LTCCS to evoked glutamate release

(Aa, Ab) Top. Representative traces of 1st eEPSC amplitude in the presence of Nimo or Bay K, respectively. Bottom. An average time course of 1st eEPSC amplitude. (Ac) A bar graph showing effects of individual blockers on the 1st eEPSC amplitude (Nimo, 0.7 ± 0.05, $N = 13$; Bay K, 1.82 ± 0.18, $N = 6$, compared to control). (Ad) A bar graph showing effects of individual blockers on paired-pulse ratio (PPR) (Nimo, 0.81 ± 0.07 *vs* 0.95 ± 0.08; Bay K, 0.91 ± 0.09 *vs* 0.75 ± 0.06, compared to control, paired *t* test). (Ba) Top. A schematic image of CaM-iP diffusion through autaptic cell body to synaptic terminal. Bottom. Representative traces for the comparison of

eEPSC between immediately patch break-in and 10 min after patch in presence of 10 μM CaM-iP (blue). (Bb) An average time course of 1st eEPSC amplitude. (Bc) A bar graph showing the normalized 1st eEPSC amplitude 10 min after patch in presence of CaM-iP (0.77 ± 0.08, $N = 12$). (Ca) Representative traces of eEPSC 10 min after patch in presence of CaM-iP (blue) applying Nimo or Bay K, respectively. (Cb) An average time course of 1st eEPSC amplitude with Nimo or Bay K. (Cc) A bar graph showing the effect of Nimo or Bay K on normalized 1st eEPSC amplitude 10 min after patch in presence of CaM-iP (Nimo, 0.95 ± 0.05, $N = 4$; Bay K, 0.99 ± 0.01, $N = 4$). All data are mean ± S.E.M., $^{**}P < 0.005$, $^{***}P < 0.001$, single group mean *t*-test or paired *t*-test (Ad); n.s. = not significant.

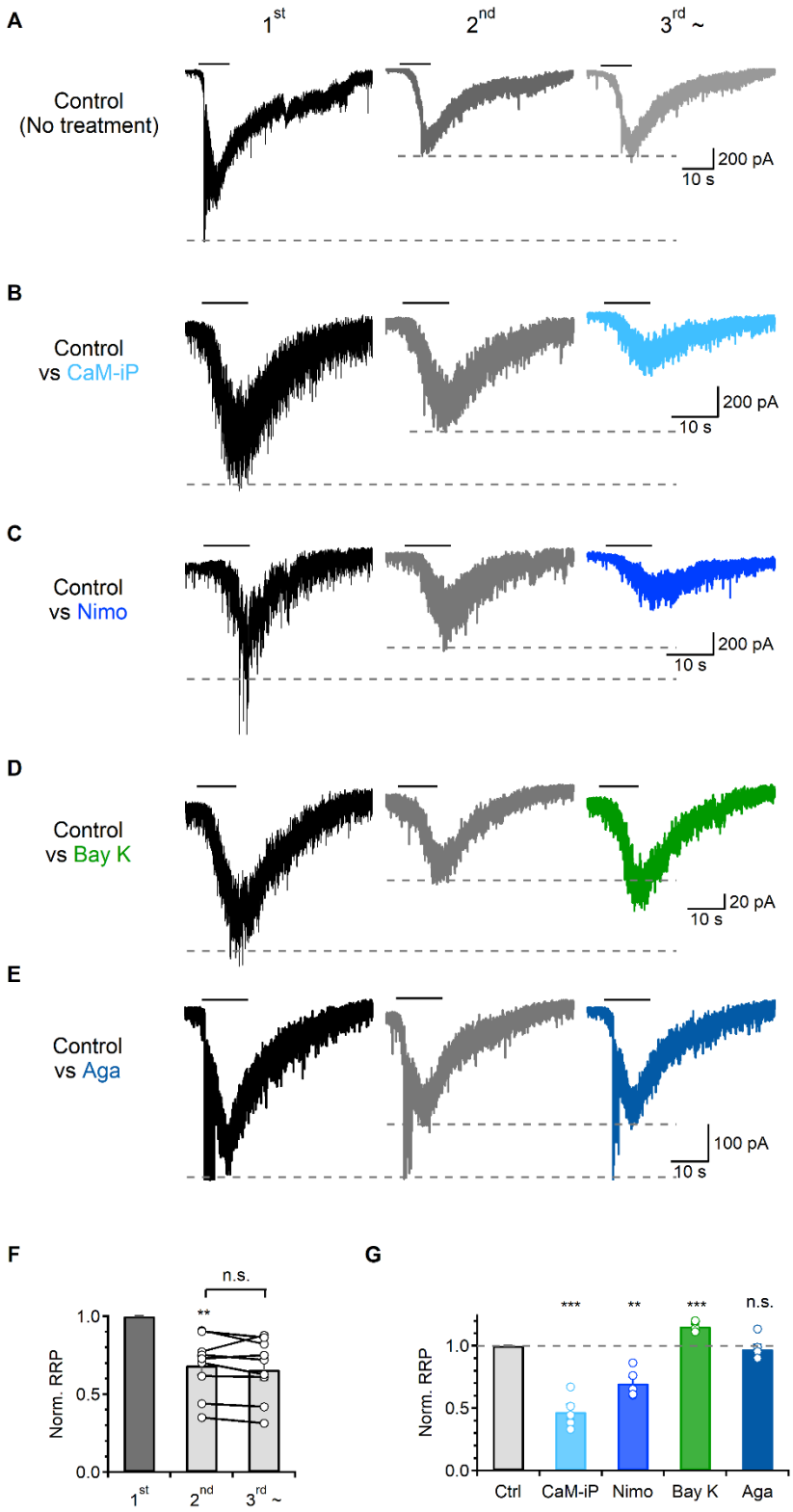
A
1st
2nd
3rd ~
Control
(No treatment)
200 pA
10 s
B
Control
vs CaM-iP
200 pA
10 s
C
Control
vs Nimo
200 pA
10 s
D
Control
vs Bay K
20 pA
10 s
E
Control
vs Aga
100 pA
10 s
F
n.s.
**
Norm. RRP
1.0
0.5
0.0
1st
2nd
3rd ~
G
***
**
***
n.s.
Norm. RRP
1.0
0.5
0.0
Ctrl
CaM-iP
Nimo
Bay K
Aga

Figure 21. The effect of calmodulin inhibition or blockade of Ca^{2+} channels on the size of readily releasable pool

(A-E) Representative traces of the application of hypertonic sucrose solution in the control condition or in the presence of CaM-iP, Nimo, Bay K or Aga, respectively. (F) A bar graph showing the normalized RRP size in 1st to 3rd challenge of sucrose application in control condition (2nd, 0.68 ± 0.06 *vs* 3rd, 0.67 ± 0.09, $N = 9$). (G) A bar graph showing the normalized RRP size patch in presence of CaM-iP (0.47 ± 0.06, $N = 5$), Nimo (0.7 ± 0.05, $N = 5$), Bay K (1.16 ± 0.02, $N = 5$), Aga (0.97 ± 0.04, $N = 6$), respectively.

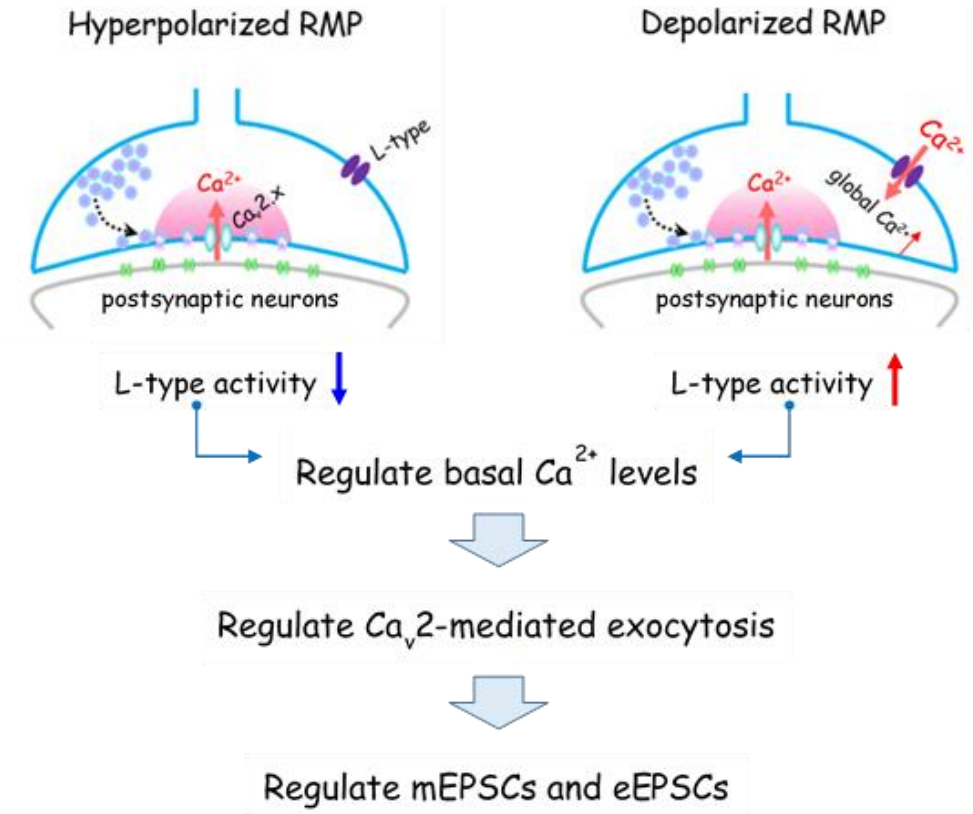

Figure 22. Summarized schematic image for VGCCs-dependent spontaneous glutamate release

The VGCCs-dependent spontaneous glutamate release is triggered by two different ways in hippocampal autapse. If the VGCCs, such as P/Q-, N-, and R-type channels, are extremely localized in synaptic vesicles, the VGCCs can directly trigger the exocytosis via their stochastic opening due to local $[Ca^{2+}]_i$ increase. Otherwise, if the VGCCs are localized in far from the vesicles (such as L-type channels), they could be regulated the spontaneous release by regulating global $[Ca^{2+}]$, not be directly triggered the exocytosis through high affinity Ca^{2+} sensors. Therefore, regulation of basal Ca^{2+} level via LTCC can regulate the activity of Ca_V2-mediated exocytosis.

DISCUSSION

It is well-known that enhancement of intracellular Ca^{2+} concentration through extracellular Ca^{2+} influx or Ca^{2+} release from intracellular Ca^{2+} store can facilitate spontaneous transmitter release (Emptage *et al.*, 2001; Vyleta and Smith, 2011; Xu *et al.*, 2009). Autapses which form self-synapses can regulate intracellular Ca^{2+} concentration by adjusting the holding potential in whole-cell patch clamping condition (Fig. 1). Because axons are not electrotonically isolated from the somatodendritic compartment, but instead support the electrotonic spread of subthreshold somatic (Alle and Geiger, 2006; Christie *et al.*, 2011; Kole *et al.*, 2007; Mejia-Gervacio *et al.*, 2007; Shu *et al.*, 2007). As a result, the open probability of voltage-sensitive ion channels in axons can be modified by somatic depolarization. Although I did not directly determine the presynaptic terminal potential in autapse, the frequency of spontaneous release recorded at the fixed holding potential did not change under various concentration of extracellular K^{+}, indicating that somatic voltage clamping could maintain the membrane potential even in axon. Subthreshold depolarization can induce enhancement of $[Ca^{2+}]_i$ via Ca^{2+} influx through VGCCs which can enhance evoked synaptic transmitter release and asynchronous release in Calyx of Held and cerebella circuit (Awatramani *et al.*, 2005; Christie *et al.*, 2011). Our finding is that spontaneous glutamate release is facilitated according to holding potential depolarization which is due to contribution of LTCCs on global $[Ca^{2+}]_i$ (Fig. 17).

LTCC is a low-voltage-activated and voltage-dependent Ca^{2+} current which is pharmacologically blocked by dihydropyridine (Avery and Johnston, 1996; Magee *et al.*, 1996). LTCC immunoreactivity is primarily found in dendrites (Westenbroek

et al., 1990), and recent immunogold labeling of LTCCs are demonstrated that both $Ca_V1.2$ and $Ca_V1.3$ channel subtypes are predominantly located in postsynaptic dendritic processes and somata in hippocampal slice, and relatively few presynaptic axonal terminals (~5%) though (Tippens *et al.*, 2008). Thus, it can be expected that presynaptic LTCCs may be involved in spontaneous glutamate release (Fig. 14). Also LTCCs have been trigger spontaneous inhibitory release in synaptic terminals of CCK interneurons via microdomain coupling (Goswami *et al.*, 2012). However, it is different from our model which is suggested that Ca^{2+} influx via LTCCs may not directly trigger, but contribute to spontaneous release via regulating global Ca^{2+} concentrations. The effect of LTCCs on spontaneous release is occluded in high concentration of EGTA (Fig. 14). Furthermore, the effect of 10 EGTA, Nimo or BayK on holding potential change in spontaneous release also disappeared (Fig. 17C), so these results can support the contribution of LTCCs on spontaneous release by global Ca^{2+} concentration. However, in accordance with previous report, resting Ca^{2+} concentration did not directly affect the spontaneous release instead of transient Ca^{2+} spark from intracellular Ca^{2+} store or Ca^{2+} influx (Emptage *et al.*, 2001). Our study also showed that ryanodine which blocks Ca^{2+} release from internal Ca^{2+} store (Sharma and Vijayaraghavan, 2003) significantly reduces mEPSC frequency, but do not change the amplitude. RYN further decrease the frequency of Nimo or BayK treatment cells. Moreover, bath application of EGTA-AM on Ca^{2+}-free solution also further reduce the frequency, so the effect of Ca^{2+} influx by LTCCs and Ca^{2+} release from RyR on spontaneous glutamate release is independent event, at least. Our data suggest that presynaptic LTCCs may modulate global Ca^{2+} concentration, therefore it may increase the probability of stochastic opening of presynaptic P/Q-, N- and R-type VGCCs. When the patch pipette containing 10 mM EGTA, the individual VGCCs blockers or Ca^{2+}-free solution significantly reduced spontaneous release similar to the Figs. 4C and 16B. However, contribution of LTCCs to spontaneous release was abolished in 10 mM $[EGTA]_i$ (Fig. 15C), indicating that LTCCs may be

located far from the vesicle Ca^{2+} sensors so that they may regulate global resting Ca^{2+} concentration rather than stochastic channel opening (Kaeser *et al.*, 2011). Figure 21 summarized the mechanisms for different types of VGCCs-dependent spontaneous release in hippocampal autapses. The VGCCs-dependent spontaneous glutamate release is triggered by two different ways in hippocampal autapse. If the VGCCs, such as P/Q-, N-, and R-type channels, are extremely localized in synaptic vesicles, the VGCCs can directly trigger the exocytosis via their stochastic opening due to local $[Ca^{2+}]_i$ increase. Otherwise, if the VGCCs are localized in far from the vesicles (such as L-type channels), they could be regulated the spontaneous release by regulating global $[Ca^{2+}]$, not be directly triggered the exocytosis through high affinity Ca^{2+} sensors. Therefore, regulation of basal Ca^{2+} level via LTCC can regulate the activity of Ca_V2-mediated exocytosis

There are two kinds of the possible mechanisms for LTCCs-dependent spontaneous release. The first is that changes in $[Ca^{2+}]_c$ affect local Ca^{2+} increase by buffer saturation effects (Jackson and Redman, 2003; Rusakov, 2006), and/or regulate exocytosis by Ca^{2+}-dependent signaling mechanism. Moreover, it has been well-known that CaM plays a potential Ca^{2+} regulator in neurotransmitter release(DeLorenzo, 1981; Steinhardt and Alderton, 1982), and also can modulate the spontaneous neurotransmitter release by control of SNARE complex assembly via regulation of V100 (Wang *et al.*, 2014). Therefore, I explored the effect of LTCCs on spontaneous release which might be mediated by CaM-dependent vesicle exocytosis (Fig. 18A), and found out LTCCs-dependent modulation of spontaneous glutamate release might be mediated the CaM-dependent vesicle exocytosis pathway. CaM can regulate calcium channel activity, and play a role in synaptic vesicle release and recycling (Ben-Johny and Yue, 2014; Liang *et al.*, 2021; Sakaba and Neher, 2001). The role of CaM in spontaneous release has not been reported in mammalian central synapses, but, CaM has been reported to participate in spontaneous release at

various synapses such as Drosophila neuromuscular junction and rat retinal ribbon synapses, through v-ATPase subunit and myosin light chain kinase, respectively (Liang *et al.*, 2021; Wang *et al.*, 2014). The involvement of CaM implies that spontaneous release is not a passive phenomenon determined by physical location of VGCCs and synaptic vesicles, but can be modulated by physiological conditions that change the activity of CaM. In present study, I also showed that CaM control the synaptic transmission via regulation of the release probability as well as the size of the releasable pool (Figs. 18A, 20B and 21A). Taken together, this study indicates that the LTCCs did not directly trigger the spontaneous release such as Ca_V2 families which locate in the vicinity of synaptic vesicles. Meanwhile the LTCCs also control the spontaneous release at peri-synaptic regions via regulating the global $[Ca^{2+}]_i$, and the global $[Ca^{2+}]_i$ modulate the spontaneous release by CaM-mediated exocytosis pathway via regulating RRP size.

CHAPTER 3

A specific association of presynaptic K^+ channels with Ca^{2+} channels underlies K^+ channel-mediated regulation of glutamate release

INTRODUCTION

Neuronal voltage-gated potassium channels (VGKCs) have been shown to contribute to resting membrane potentials, postsynaptic potentials, propagated action potentials, action potential firing patterns, and neurotransmitter release (Hille, 1978; Rudy, 1988). Recent studies have shown that control of the presynaptic resting potential via resting K^+ channels conductance (e.g. $K_V7.2/3$ at hippocampus or $K_V7.5$ at Calyx of Held) can modulate the post synaptic signals in mammalian nerve terminals (Huang and Trussell, 2011; Sun and Kapur, 2012), and they also known to be located at presynaptic terminals (Chung *et al.*, 2006). In addition, these channels are also known as slow activation, non-inactivation channels and activated at subthreshold potentials, so that they may be able to control the presynaptic potentials (Brown and Adams, 1980; Brown and Passmore, 2009). It is known that KCNQ2/KCNQ3 subunits are preferentially located in the surface of axons both at the axonal initial segment and more distally in hippocampus (Chung *et al.*, 2006). Recent studies reveal that K_V7 families are involved in the regulation of neurotransmitter release (Shah *et al.*, 2011; Vervaeke *et al.*, 2006). In addition, several studies insist that K_V1 families are preferentially located at axons and axon terminals in hippocampal pyramidal neurons (Cooper *et al.*, 1998; Wang *et al.*, 1993). Previous study explore that Kv1 channels are also able to regulate spontaneous release in inhibitory synapses (He *et al.*, 2012).

The other VGKCs, K_V1 families, have been reported in several studies that they are low-threshold activated K^+ currents localized at axons and axon terminals (Cooper *et al.*, 1998; Wang *et al.*, 1993), which are blocked by low dose of 4-AP or α-dendrotoxin, and can determine the action potential waveform and activity-

dependent spike broadening in hippocampal mossy fiber synapses and prefrontal cortical pyramidal neurons, therefore it is possible to modulate the post synaptic signals which are consequences for presynaptic Ca^{2+} entry (Geiger and Jonas, 2000b; Shu *et al.*, 2007). Besides, recent study investigated that the subthreshold somatic depolarization in hippocampal pyramidal neurons by blockade of $K_V1.1$ can affect the shape of presynaptic action potentials, Ca^{2+} influx, and consequently occur the neurotransmitter release (Vivekananda *et al.*, 2017). However, little has been known about the relationship between subthreshold RMP depolarization which is regulated by various types of VGKCs and spontaneous neurotransmitter release which is depended on Ca^{2+} influx through the multiple types of VGCCs. In present study reveals that excitatory spontaneous release may occur Ca^{2+} influx via multiple types of VGCCs with their stochastic opening or regulation of global resting Ca^{2+} concentration, in addition, a specific association between K^+ and Ca^{2+} channels in the presynaptic terminals, which allows K^+ channels to control Ca^{2+} channel activity strongly with a high specificity.

MATERIALS AND METHODS

1. Autaptic neuronal culture

All preparations were carried out under the animal welfare guideline of Seoul National University (SNU), and approved by IACUC of SNU. Primary cultures of rat hippocampal neurons were prepared as described previously with slight adaptations (Bekkers and Stevens, 1991). Briefly, hippocampal neurons and astrocytes were obtained from Sprague-Dawley (SD) rats according to the protocols approved by the Seoul National University Institutional Animal Care and Use Committee. Astrocyte cultures were prepared from the Sprague-Dawley rat cortices

P0 - P1 and grown for 10 days in 100-mm culture dish in glial medium [minimum essential medium (MEM; Invitrogen) supplemented with 0.6 % glucose, 1 mM pyruvate, 2 mM GlutaMAX-I (Invitrogen), 10 % horse serum (HS; Invitrogen), and 1 % penicillin-streptomycin (PS; Invitrogen)] before plating on the sprayed microisland coverslips in 30-mm petri dishes. 2 - 3 days before neurons being added in sprayed microisland dishes, astrocytes were removed from the 100-mm culture dish using trypsin-EDTA (Invitrogen) and plated on the microisland coverslips at a density of 60,000 cells/dish. Hippocampi from P0 - P1 SD rats were dissected in Hank's balanced salt solution (Invitrogen), digested with papain (Worthington, Freehold, NJ, USA), and then triturated with a polished half-bore Pasteur pipette. Immediately after removing glia medium in 30-mm dishes of microisland-shaped astrocytes, hippocampal neurons were added at a density of 6,000 cells/dish and were grown in neurobasal medium supplemented with B27 and glutamax (Invitrogen).

2. Hippocampal slice preparation

Hippocampal slices were prepared from 3-week-old (P17 - 21) or 4-week-old (P23 - 30) Sprague-Dawley rats. After anaesthetized by inhalation with 5% isoflurane, rats were decapitated and the brain was quickly removed and chilled in an ice-cold high-magnesium cutting solution containing the following (in mM): 110 choline chloride, 25 $NaHCO_3$, 20 glucose, 2.5 KCl, 1.25 NaH_2PO_4, 1 sodium pyruvate, 0.5 $CaCl_2$, 7 $MgCl_2$, 0.57 ascorbate (pH 7.3 bubbled with 95 % O_2 - 5 % CO_2; osmolarity ~300 mOsm. The isolated brain was glued onto the stage of a vibrating blade microtome (VT1200S, Leica Microsystems) and 300 μm-thick transverse hippocampal slices were cut. The slices were incubated at 34°C for 30 min in artificial cerebrospinal fluid (aCSF) containing the following (in mM): 125 NaCl, 25 NaHCO3, 20 glucose, 2.5 KCl, 1.25 NaH_2PO_4, 1 sodium pyruvate, 2 $CaCl_2$, 1 $MgCl_2$, 0.57 ascorbate, bubbled with 95 % O_2 - 5 % CO_2, and thereafter maintained at room temperature

until required.

3. Electrophysiology

For recordings in autaptic cultured neurons, cells were visualized with an Olympus IX70 inverted microscope. Whole-cell voltage- or current-clamp recordings from hippocampal autaptic pyramidal neurons were performed at room temperature and continuously perfused with extracellular solution consisting of following composition (in mM): 135 NaCl, 2.5 KCl, 2 $CaCl_2$, 1 $MgCl_2$, 10 glucose, 10 HEPES, 0.1 EGTA, pH 7.3 adjusted with NaOH (295 - 300 mOsm), and maintained at 0.5 - 1 ml min-1. All recordings were done at least 23 days after neurons were plated on coverslips. The internal pipette solution for recording mEPSCs and resting membrane potential (RMP) was used K-gluconate based solution.

For recordings in hippocampal slices, slices were transferred to an immersed recording chamber continuously perfused with oxygenated aCSF using a peristaltic pump (Gilson). CA3 or CA1 pyramidal cells were visualized using an upright microscope equipped with differential interference contrast optics (BX51WI, Olympus). Whole-cell voltage- or current-clamp recordings were performed at 32 ± 1°C and the rate of aCSF perfusion was maintained at 1 - 1.5 ml min-1. For high $[K^+]_o$ experiments, NaCl was reduced to maintain osmolarity. Recordings were made in somata with an EPC-10 amplifier (HEKA Electonik, Lambrecht/Pfalz, Germany). Signals were low-pass filtered at 5 kHz (low-pass Bessel filter) and sampled at 10 kHz. Series resistance (Rs) was monitored, and only recordings with Rs remained constant (<30% change during a recording) were used. Rs was compensated to 50 - 70 %. The data were analyzed using IGOR software (Wavemetrics, Lake Oswego, OR, USA). Patch electrodes were pulled from borosilicate glass capillaries to a

resistance between 3 and 4 MΩ when filled with pipette solution. The internal pipette solution for recording miniature excitatory postsynaptic currents (mEPSCs) contained the following composition (in mM): 130 Cs-methanesulfate, 8 NaCl, 4 MgATP, 0.3 NaGTP, 10 HEPES, 0.1 EGTA, pH 7.3 adjusted with CsOH (295 - 300 mOsm). For RMP recording, K-gluconate was substituted for Cs-methanesulfate, and pH was adjusted with KOH.

The mEPSCs of hippocampal slices or hippocampal autapses were recorded at holding potential of -70 mV. 0.5 μM TTX and 0.1 mM picrotoxin (PTX) was added during recordings in acute slices. Events exceeding 6 - 7 pA within a specified interval of three to four digitized points (0.5 - 0.8 ms) that showed a single exponential decay time course were identified as mEPSC. The rise time of mEPSC indicated the 20 - 80 % rise time. The mEPSC frequency was measured within 20 s bins. Synaptic activities were recorded at a holding potential of -70 mV. The eEPSCs were recorded every 20 s after applying depolarization pulses from -70 to 0 mV for 2 ms. From the continuous recordings at -70 mV without stimulations, toxins and chemicals were typically applied for 5 - 20 min until a constant effect was observed.

4. Drugs

Linopirdine, XE991, and dendrotoxin were purchased from Alomone Labs (Jerusalem, Israel). All other chemicals were purchased from Sigma (St. Louis, MO, USA). Toxin stock solutions were made at 1000-fold concentration with distilled water and stored at -20°C.

5. Statistical analysis

Data were expressed as the mean ± SEM, where *N* represents the number of cells studied. Statistical analysis was performed using IgorPro (version 6.1, WaveMetrics, Lake Oswego, OR, USA) and OriginPro (version 9.0, OriginLab Corp., Northampton, MA, USA). Significant differences between the experimental groups were analyzed using independent or paired Student's *t*-tests. $P<0.05$ was considered statistically significant.

RESULTS

1. RMP depolarization is not sufficient to explain enhancement of spontaneous release by M-type K^+ channel blocker

It is known that KCNQ2/KCNQ3 subunits are preferentially located in the surface of axons both at the axonal initial segment and more distally in hippocampus (Chung *et al.*, 2006). In addition, recent studies showed that M-channels are involved in the regulation of neurotransmitter release (Vervaeke *et al.*, 2006). In the SC synapses, the blockade of M-type K^+ channels increased the miniature EPSCs frequency. The previous study suggested that the mechanisms of this enhancement should be due to presynaptic RMP depolarization by M-channel blocker (Huang and Trussell, 2011; Sun and Kapur, 2012). However, I thought that it is not enough to explain the enhancement of glutamate release by linopirdine (Lino) or XE991 (XE). The present study suggested that there could be another mechanism existed.

To examine the mechanisms between the enhancement of the spontaneous glutamate

release and the blockade of K^+ channels, I measure the effects of K^+ channels blockers on somatic RMP from CA3 pyramidal cells which are presynaptic partner for CA1 pyramidal cells and mEPSCs frequency from CA1 pyramidal neurons in acute hippocampal slices under whole-cell patch clamp configuration in standard extracellular K^+ concentration, $[K^+]_o$ (2.5 mM). Application of Lino on hippocampal acute slice increased miniature frequency by 2.1 ± 0.6-fold (Fig. 23Ba, N = 7, P= 0.006), normalized to control value, but these blockers did not change their amplitudes (Fig. 23Bb, 30 ± 4.4 pA *vs.* 29.7 ± 3.8 pA). In addition, the kinetics of mEPSCs were not changed by Lino. In the CA3 PCs, Lino depolarized the somatic RMP from -68.7 ± 1.11 mV to -65.9 ± 1.21 mV (Fig. 24B, N = 24, P = 0.009).

2. Enhancement of spontaneous release by K^+ channel blocker in hippocampal autaptic cultured neurons

I investigated the effects of Lino or other K^+ channel blocker 100 μM 4-AP, which blocks K_V1, on somatic RMP and spontaneous EPSCs frequency from hippocampal autaptic neurons. Under the CC condition, the somatic RMP was slightly depolarized by 3.1 ± 0.35 mV via Lino (Figs. 25Aa, Ab, -74.5 ± 2.84 vs. -71.7 ± 2.78 mV, N = 19, P = 0.0001). In addition, 4-AP slightly depolarized somatic RMP by 2.34 mV (Figs 25Ba, Bb, N = 12).

Under the VC condition recorded at -70 mV, the bath application of Lino enhanced the mEPSCs frequency by 1.7 ± 0.08 folds (N = 16) and XE991 (analogue for Lino) increased the frequency by 1.74 ± 0.09 folds (N = 8) of control value, respectively (Figs. 24Ba, C). Moreover, 4-AP increased the frequency by 1.47 ± 0.08 folds (Figs. 26Bb, C, N = 8). However, the amplitudes, rise time, and decay time of mEPSCs were not changed. These results indicated that even in voltage clamping condition,

the enhancement of the mEPSCs frequency by Lino or 4-AP could not be completely depended on the depolarization (Fig. 26D). Additionally, Lino or 4-AP can change RMP slightly and, otherwise, enhance the spontaneous release tremendously.

3. XE991 effect is dependent on Ca^{2+} and K^{+}

Calcium is an important element for neurotransmitter release. I tested that the enhancement of spontaneous glutamate releases by Lino might be depended on external Ca^{2+} influx through variable Ca^{2+} channels on cell membrane (Ermolyuk *et al.*, 2013; Schneggenburger and Rosenmund, 2015; Xu *et al.*, 2009). At calcium-free external recording solutions, the enhancement of mEPSCs frequency by XE disappeared by 0.41 ± 0.07 folds in 0 mM Ca^{2+} with XE (0.42 ± 0.05 folds), normalized to control value (Fig. 27Ab, $N = 4$). Moreover, 4-AP did not change the mEPSC frequency at Ca^{2+}-free condition (Fig. 27Bb, 0.99 ± 0.02, $N = 5$). These data indicated that the enhancement of spontaneous frequency by Lino or depolarization could be depended on extracellular calcium influx.

Furthermore, to support the effect of XE991 on K^{+}-fluxes which influence the Ca^{2+} influx I used the Cs^{+}-contained internal solutions. In this circumstance, the spontaneous frequency was not changed by XE991 treatment (Fig. 27Cb, 1.0 ± 0.02 folds, $N = 6$), indicating that the effect of XE991 on autaptic mEPSCs frequency depends on K^{+} flux through the cell membrane. Taken together, these results implied that the enhancement of glutamate release by XE991 could be regulated by K^{+} efflux through the cell membranes along with external calcium influx.

4. Enhancement of spontaneous glutamate release by Lino or

XE991 is mediated via L-type Ca^{2+} channels

To further determine which types of Ca^{2+} channels had been involved in Lino-induced enhancement of spontaneous release at autaptic excitatory synapse, I tested the effects of several specific Ca^{2+} channel blockers (Ermolyuk *et al.*, 2013). The P/Q-type Ca^{2+} channel blocker, N-type Ca^{2+} channel blocker, R-type Ca^{2+} channel blocker, and L-type Ca^{2+} channel blocker significantly reduced mEPSCs, respectively, normalized to control value (Figs. 4, 14). Furthermore, additional bath application of XE991 significantly increased in spontaneous release at Aga or Cono presented cells by 1.58 ± 0.03 folds and 1.34 ± 0.04 folds, respectively, normalized to control value (Fig. 28B). However in Nimo presented cells, the mEPSCs frequency were not significantly changed by XE991 to 0.98 ± 0.08 folds of control value (Fig. 28B). Taken together, these results suggested that the M-type K^+ channels might be involved in the spontaneous neurotransmitter releases through the coupling of Ca^{2+} channels especially LTCCs.

5. Effects of K^+ channel blockade by 4-AP (D-type) on spontaneous release is specific to P/Q-type calcium channels

In other case, additional bath application of 4-AP significantly increased in spontaneous release at Nimo or Cono presented cells by 1.6 ± 0.28 folds and 1.59 ± 0.25 folds, respectively, normalized to control value (Fig. 28B). However in Aga presented cells, the mEPSCs frequency were not significantly changed by 4-AP to 1.06± 0.06 folds of control value (Fig. 28B). Therefore, these results suggested that the D-type K^+ channels might be involved in the spontaneous neurotransmitter releases through the coupling of Ca^{2+} channels especially P/Q-type Ca^{2+} channels.

Increased spontaneous release by K^+ channel block is generally believed to be attributable to the depolarization-induced increase in presynaptic Ca^{2+} levels. Above results appeared to be compatible with this idea, but the increases in mEPSC frequency by IK_M or IK_D block were far greater than the increases expected by somatic RMP depolarization. Furthermore, the effects of IK_M or IK_D block on mEPSCs occur even under the voltage clamp condition. These results suggest that presynaptic membrane potential changes induced by blocking IK_M or IK_D may be larger than somatic RMP changes and are not completely controlled via somatic patch pipettes under voltage clamp mode. Therefore, above results could not give a clear answer to the contribution of presynaptic RMP changes to the increased spontaneous release by IK_M or IK_D block. To address this issue, I examined the effects of IK_M or IK_D block on mEPSCs in the presence of 10 mM EGTA and in the presence of nimodipine, since effects of RMP changes on spontaneous release are abolished under these conditions (Figs. 29A, C). Surprisingly, XE and 4-AP showed distinct results. Effects of XE on mEPSCs were abolished in the presence of 10 mM EGTA (Figs. 29A, C left) and in the presence of nimodipine (Fig. 28B), which is consistent with the idea that presynaptic RMP depolarization by IK_M block increases resting Ca^{2+} levels by increasing L-type VGCC activity. In contrast, effects of 4-AP on mEPSCs were unaffected in the presence of 10 mM EGTA (Fig. 29C middle) and in the presence of nimodipine (Fig. 28B). Moreover, the effect of 4-AP on mEPSC still, but slightly, appeared in the presence of 10 mM BAPTA (Fig. 29C right). It might be due to incomplete chelation by BAPTA. These results implied that IK_D block induces the increase in activities of presynaptic VGCCs that directly trigger glutamate release by local Ca^{2+} increases. These results may suggest that K^+ channels that mediate IK_M and those mediate IK_D are differentially compartmentalized in the presynaptic terminals with different type of VGCCS.

6. Variable types of K^+ channel blockers do not change the size of the readily releasable pool

Next, I recorded the size of readily releasable pool (RRP) to determine whether the enhancement of spontaneous glutamate release by K^+ channel blockers would be due to the increase in the RRP size by the K^+ channel blockers. XE or 4-AP did not significantly change the RRP size (Fig. 30B, XE, 4.02 ± 1.38 *vs* 3.74 ± 1.4 nC, N = 4; 4-AP, 5.7± 1.9 *vs* 5.9 ± 1.8 nC, N = 3). Therefore, the enhancement of spontaneous glutamate release by blockade of VGKCs was not mediated by change of RRP size by K^+ channels.

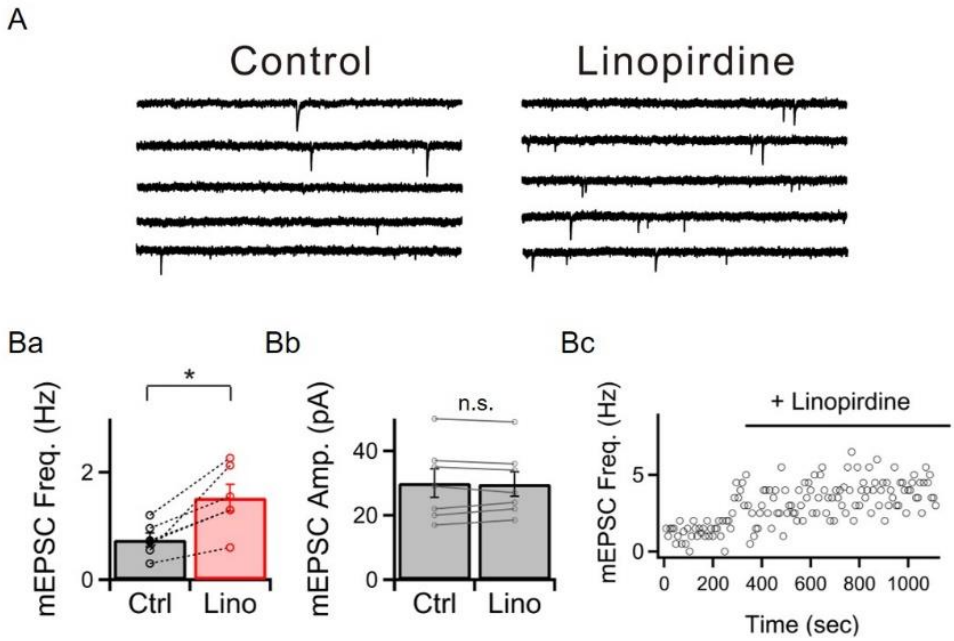

Figure 23. The effect of M-type K^+ channel blocker on spontaneous glutamate release in hippocampal CA1 pyramidal neurons

(A) Representative traces of mEPSC in the presence of Lino. (Ba) A bar graph showing effects of Lino on mEPSC frequency (1.05 ± 0.32. *vs* 2.09 ± 0.61, $N = 7$). (Bb) A bar graph showing effects of Lino on mEPSC amplitude (30 ± 4.4 pA *vs.* 29.7 ± 3.8 pA). (Bc) An average time course of mEPSC frequency. All data are mean ± S.E.M., *$P < 0.01$, single group mean *t*-test or paired *t*-test (Ba); n.s. = not significant.

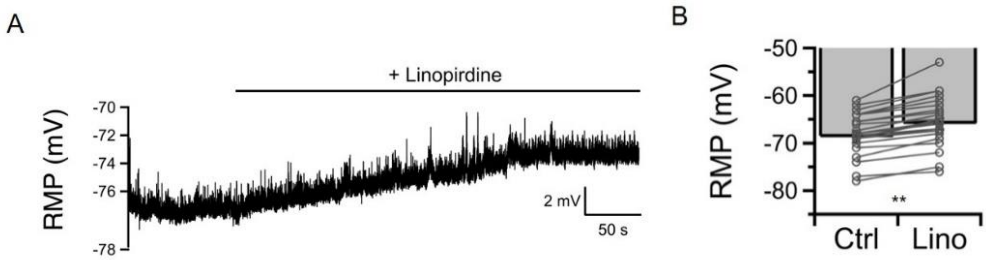

Figure 24. The effect of M-type K^+ channel blocker on RMP in hippocampal CA3 pyramidal neurons

(A) Representative traces of somatic RMP in the presence of Lino. (B) A bar graph showing the effect of Lino on RMP (-68.7 ± 1.11 mV *vs* -65.9 ± 1.21 mV, $N = 24$). All data are mean ± S.E.M., $^{**}P < 0.005$, paired *t*-test (B).

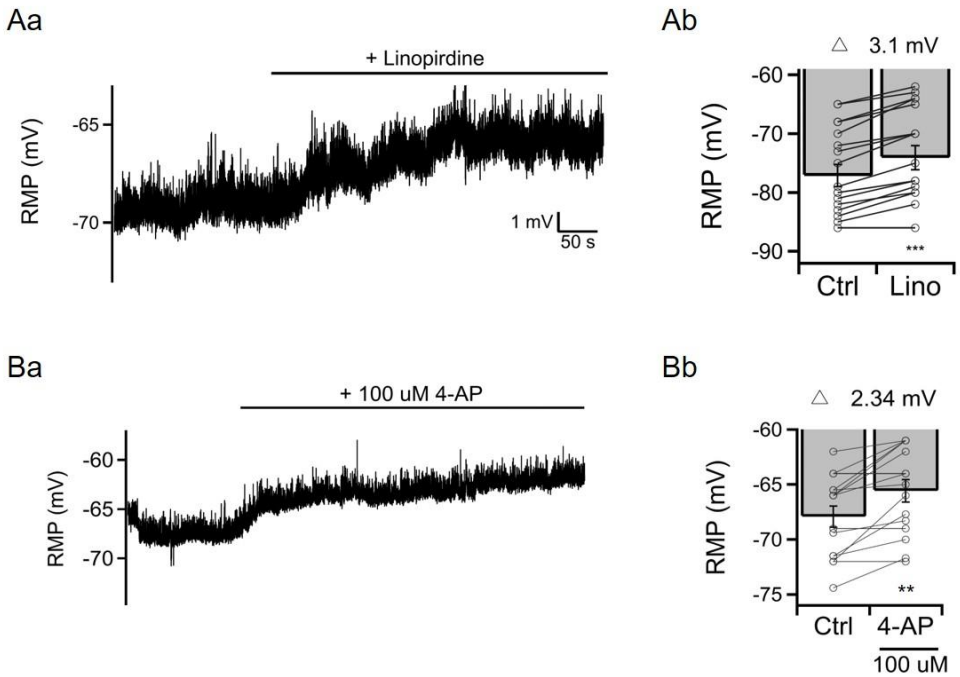

Figure 25. The effects of K^+ channel blockers on RMP in hippocampal autaptic hippocampal pyramidal neurons

(Aa, Ba) Representative traces of RMP in the presence of Lino or 4-AP. (Ab, Bb) Bar graphs showing the effects of Lino (Ab, -74.5 ± 2.84 vs. -71.7 ± 2.78 mV, N = 19) or 4-AP (Bb) on RMP (-67.4 ± 1.8 mV *vs* -65.1 ± 1.73 mV, N = 12). All data are mean ± S.E.M., $^{**}P < 0.005$, $^{***}P < 0.001$, paired *t*-test (B).

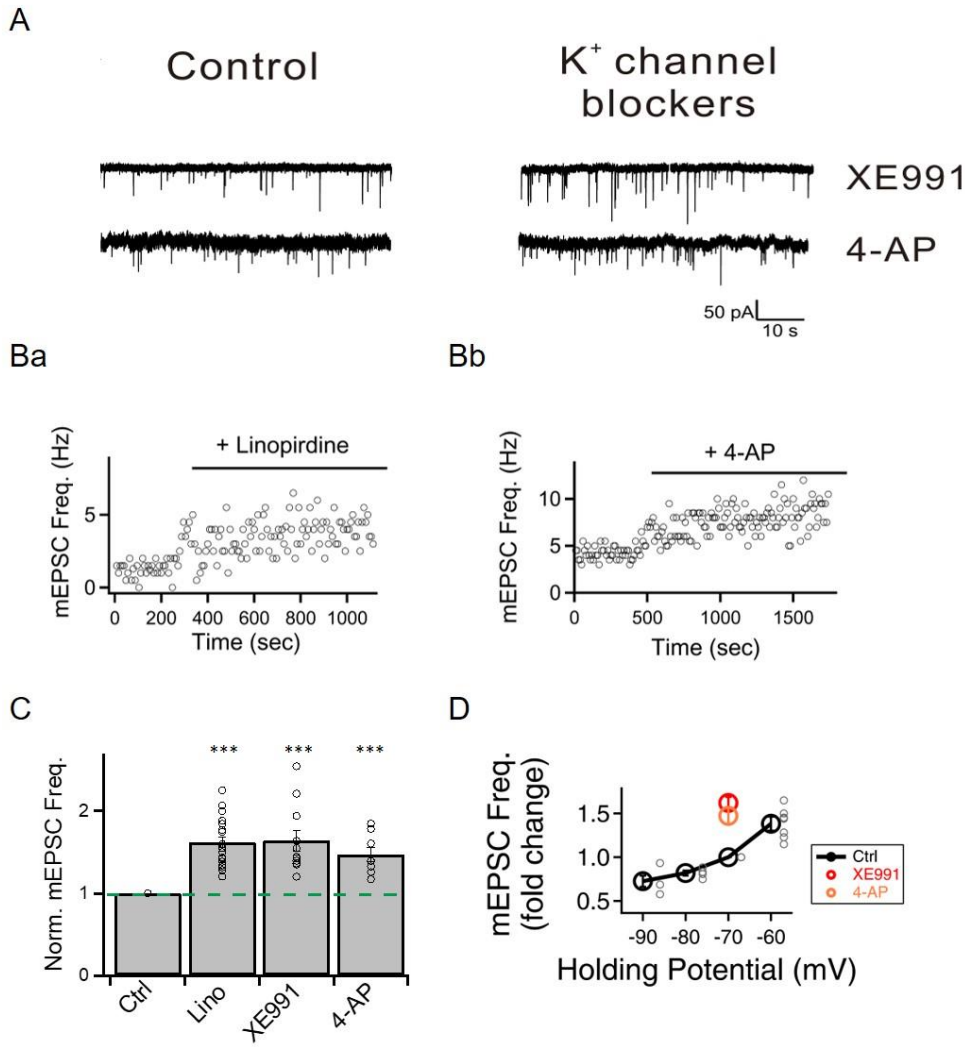

Figure 26. The effects of K^+ channel blockers on mEPSC frequency in hippocampal pyramidal autaptic neurons

(A) Representative traces of mEPSC in the presence of Lino or 4-AP. (Ba, Bb) Average time courses of mEPSC frequency of Lino (Ba) or 4-AP (Bb). (C) A bar graph showing effects of Lino, XE991 or 4-AP on normalized mEPSC frequency, compared to control value (Lino, 1.62 ± 0.07, N = 23; XE, 1.64 ± 0.13, N = 11; 4-AP, 1.47 ± 0.09, N = 8). (D) A bar graph showing effects of XE or 4-AP on mEPSC frequency at -70 mV holding potential. The effects of K+ channel blockers were overlaid with the graph of holding potential effect on mEPSC frequency (data from Fig. 17Db). All data are mean ± S.E.M., ***$P < 0.001$, single group mean t-test.

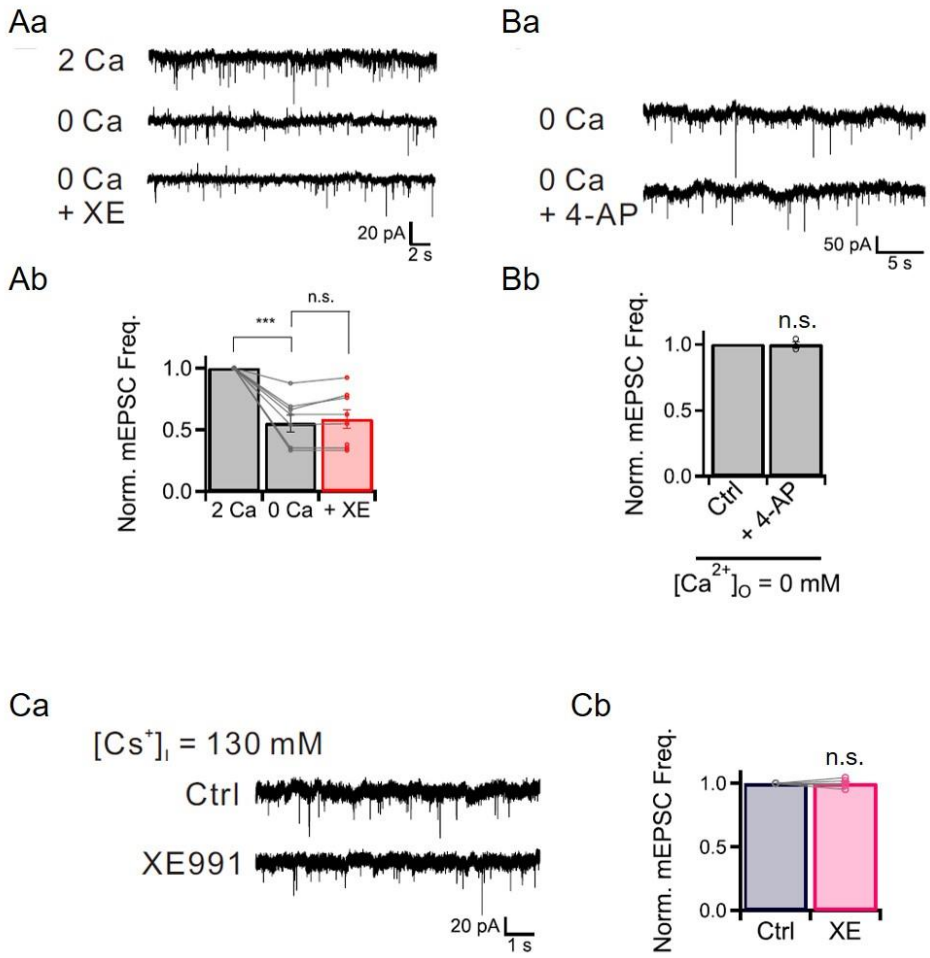

Figure 27. The dependency of the effect of K^+ channel blockers on mEPSC frequency on extracellular Ca^{2+} influx and K^+ flux

(Aa, Ba) Representative traces of mEPSC in the presence of XE or 4-AP in Ca^{2+}-free condition. (Ab, Bb) Bar graphs showing effects of XE991 (Ab, 0.55 ± 0.07 vs 0.59 ± 0.08, N = 8) or 4-AP (Bb, 0.99 ± 0.02, N = 4) on normalized mEPSC frequency in Ca^{2+}-free condition. (Ca) Representative traces of mEPSC in the presence of XE in 130 mM Cs^+ containing patch pipette solution. (Cb) A bar graph showing effects of XE991 on normalized mEPSC frequency (1.0 ± 0.02, N = 6). All data are mean ± S.E.M., ***P < 0.001, single group mean t-test or paired t-test (Ab); n.s. = not significant.

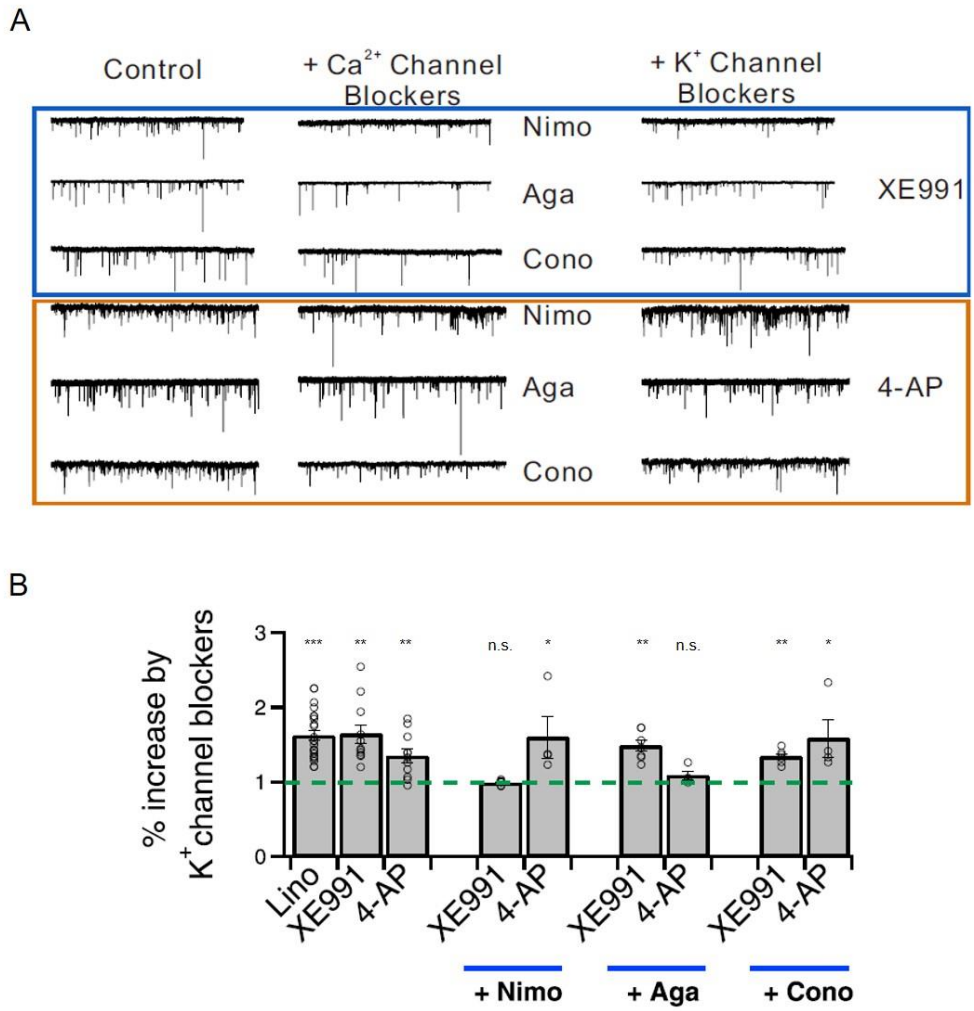

Figure 28. The specific coupling of K^+ channels with Ca^{2+} channels

(A) Representative traces of mEPSC in the presence of XE or 4-AP with Ca^{2+} channel blockers. (B) A bar graph showing effects of XE991 or 4-AP presence in Ca^{2+} channel blockers (XE *vs* 4-AP; Nimo, 0.99 ± 0.01 *vs* 1.6 ± 0.28, $N = 8$ *vs* 5; Aga, 1.49 ± 0.07 *vs* 1.09 ± 0.06, $N = 8$ *vs* 5; Cono, 1.34 ± 0.04 *vs* 1.59 ± 0.25, $N = 7$ *vs* 5) on normalized mEPSC frequency, compared to control. All data are mean ± S.E.M., $^{**}P < 0.005$, $^{***}P < 0.001$, single group mean *t*-test; n.s. = not significant.

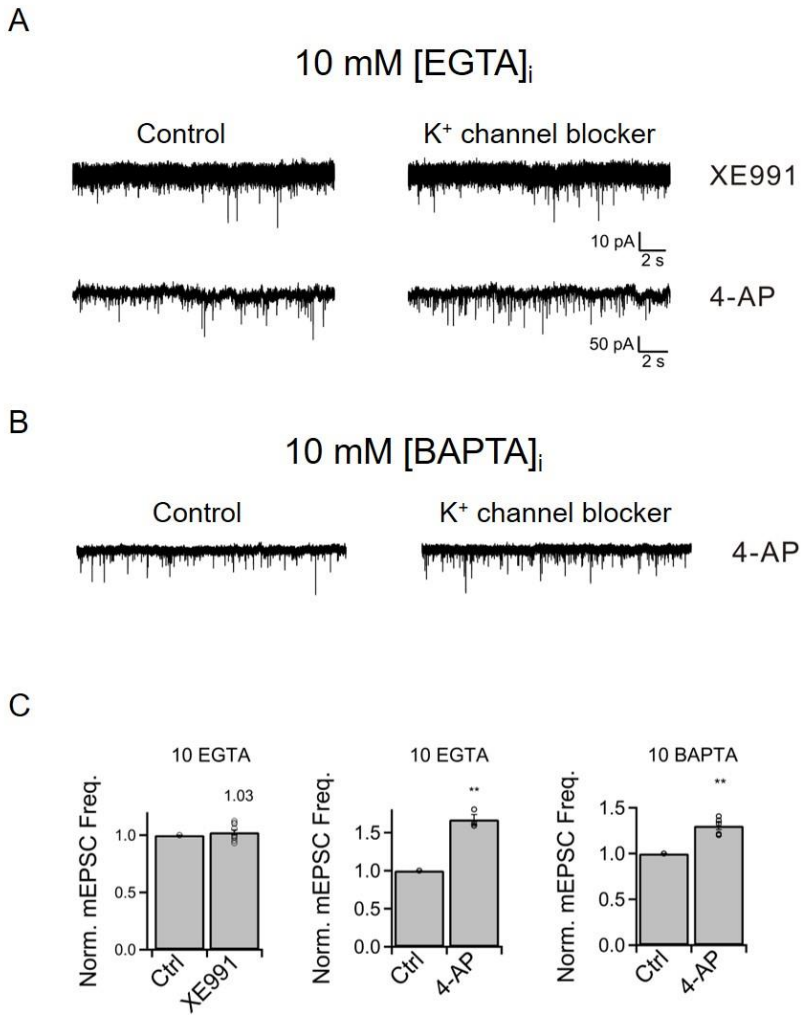

Figure 29. The effects of K^+ channel blockers on spontaneous glutamate release in EGTA or BAPTA containing internal patch pipette solution

(A, B) Representative traces of mEPSC in the presence of XE or 4-AP in 10 mM EGTA or 10 mM BAPTA containing internal solution. (C) Bar graphs showing effects of XE991 or 4-AP on normalized mEPSC frequency in 10 EGTA or 10 BAPTA condition. Left. XE, 1.03 ± 0.02, $N = 5$. Middle. 4-AP, 1.67 ± 0.07, $N = 4$. Right. 4-AP, 1.31 ± 0.04, $N = 5$. All data are mean ± S.E.M., $^{**}P < 0.005$, single group mean *t*-test; n.s. = not significant.

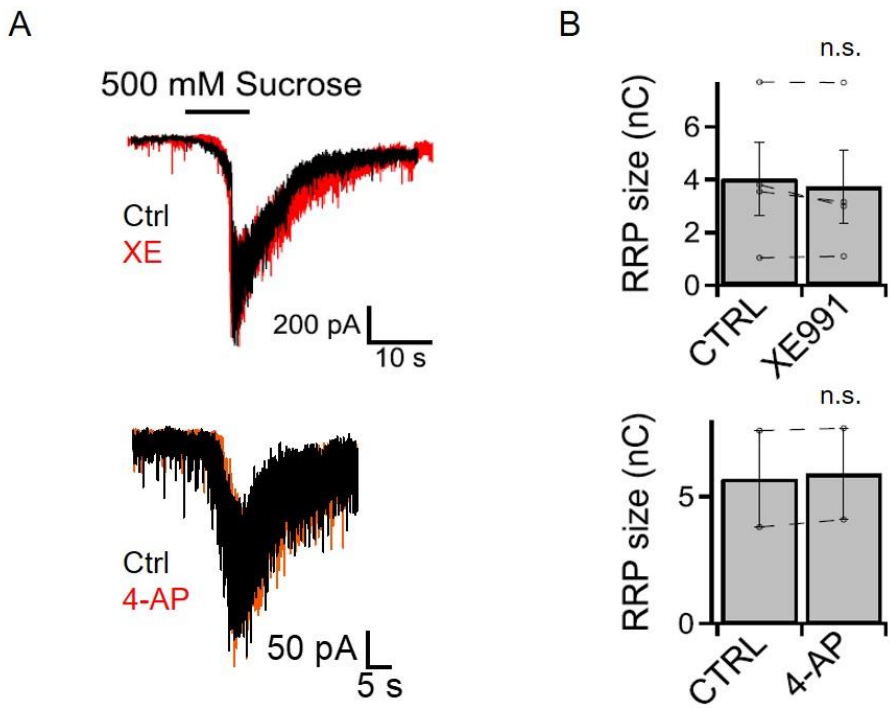

Figure 30. The effects of K+ channel blockers on the size of readily releasable pool

(A) Representative traces of the effect of hypertonic sucrose solution on resting state in the presence of XE (Top) or 4-AP (Bottom). (B) Bar graph indicating the RRP size. Top. XE, 4.03 ± 1.38 vs 3.74 ± 1.4 nC, N = 5. Bottom. 4-AP, 5.7 ± 1.9 vs 5.9 ± 1.8 nC, N = 2. All data are mean ± S.E.M., n.s. = not significant.

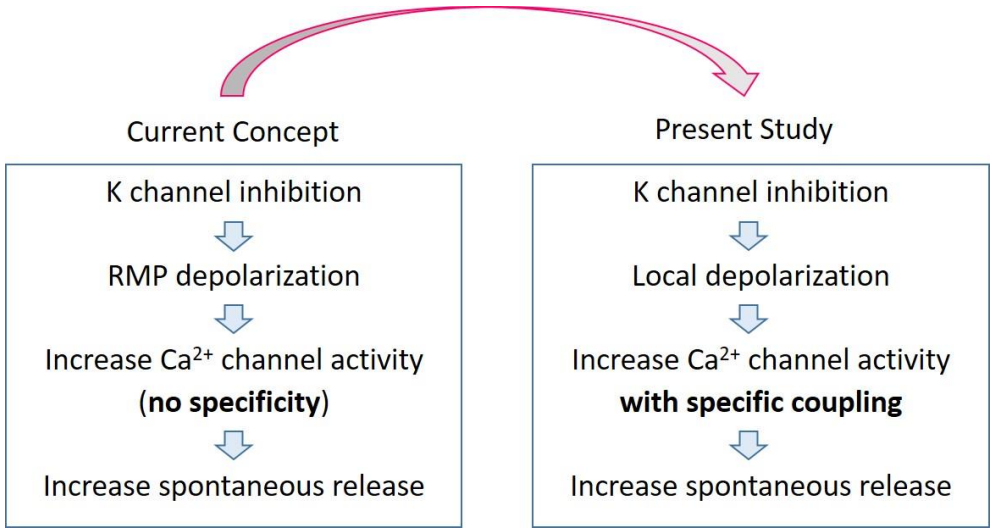

Figure 31. The summarized mechanism for VGKCs-dependent spontaneous release.

The previous study suggested that the effect of VGKCs on spontaneous release was induced by regulation of presynaptic I_{Ca} or RMP depolarization. If the K^+ channels are inhibited, presynaptic depolarization should be occurred. According to this depolarization, the postsynaptic response could be enhanced due to the Ca^{2+} channel activity with no specificity, However, the present study demonstrates that the local presynaptic depolarization controlled by VGKCs might modulate the of Ca^{2+} channels activity with specific coupling of VGKCs. This configuration may allow K^+ channels to control Ca^{2+} channel activity strongly with a high specificity.

DISCUSSION

VGKCs are key factor for regulation of membrane potential in various types of cells in diverse species, and some kinds of VGKCs are also distributed in neuronal axon terminal (Huang and Trussell, 2011; Kole *et al.*, 2007; Shah *et al.*, 2011; Vervaeke *et al.*, 2006; Vivekananda *et al.*, 2017). Thus, blockade of VGKCs can be expected to promote synaptic transmitter release by presynaptic depolarization, which may be mediated by Ca^{2+} influx through VGCCs (Huang and Trussell, 2011; Sun and Kapur, 2012). Surprisingly, our study found that blockade of K_V1 or K_V7 significantly increased spontaneous release even under voltage-clamping condition. The increment of frequency was far greater than what I expected from voltage depolarization (Fig. 24D).

Lots of studies implied that blockade of presynaptic K^+ channels can enhance the post synaptic responses due to the presynaptic terminal depolarization or elongation of presynaptic AP durations. At squid giant synapse, the blockade of presynaptic delayed rectifier K^+ currents by TEA induced presynaptic AP broadening and caused an enhancement and increase in the time-to-peak of resultant postsynaptic responses (Augustine, 1990). In hippocampal mossy fiber boutons, the blockade of fast-inactivating K^+ channels by TEA or dendrotoxin induced presynaptic AP broadening which increased presynaptic Ca^{2+} inflow, so presynaptic AP broadening might potentiate transmitter release (Geiger and Jonas, 2000a). The previous studies did not consider the particular relationship between K^+ currents and Ca^{2+} influx. I wondered if the dramatic enhancement of postsynaptic responses by inhibition of presynaptic K^+ channels could be specifically coupled with presynaptic Ca^{2+} channels. Fig. 31 shows the summarized the notion of the present study.

In this study, I found that presynaptic P/Q-, N- and R-type VGCCs are directly involved in spontaneous glutamate release machinery at hippocampal glutamatergic autaptic neurons triggered by local Ca^{2+} (Ca^{2+}-nano/microdomains) increase which is consistent with previous report (Ermolyuk *et al.*, 2013). Furthermore, present study found that presynaptic LTCCs are also mediated in spontaneous glutamate release indirectly via regulating resting Ca^{2+} concentration. It has been well-known that VGKCs can control the resting membrane potentials, then they would regulate an influx of Ca^{2+} through presynaptic VGCCs. I found that either K_V7 blocker (XE991 or Lino) or K_V1 blocker (100 μM 4-AP) depolarize the RMP around 3~5 mV at hippocampal glutamatergic autapses. Interestingly, these blockers also significantly enhance the frequency of spontaneous release under voltage clamping condition though. However, high-voltage-activated K^+ channels which are blocked by TEA do not change the RMP nor the frequency of spontaneous release. These results could predict that far greater enhancement of spontaneous glutamate release by blockade of VGKCs might be occurred by high compartmentalization between VGCCs and VGKCs in presynaptic terminals. I also found that the effect of XE991 in presence of high concentration of EGTA is abolished and the effect of 4-AP in presence of high concentration of BAPTA is still somewhat remained. To investigate whether the specific relationship between VGKCs and VGCCs in presynaptic terminal may occur, I performed the pharmacological experiments that individual VGCCs blockers are combined with individual VGKCs blockers on spontaneous glutamate release. Finally, I suggested that increased spontaneous release by blockade of K_V7 may specifically associate with LTCCs, while K_V1 may specifically associate with P/Q-type VGCCs.

GENERAL DISCUSSION

In the present study, I found that spontaneous glutamate release is dependent on Ca^{2+} influx via P/Q-, N-, and R-type VGCCs in autaptic cultured hippocampal neurons. Moreover, estimation of the coupling distance between VGCCs and Ca^{2+} sensors by fitting the buffered Ca^{2+} diffusion model to the effects of two different Ca^{2+} chelators on mEPSCs and eEPSCs showed tight coupling configuration for both spontaneous and evoked release (~22 nm), suggesting general molecular machineries for VGCC-dependent exocytosis in both types of release. These data suggest that the coupling distance between Ca^{2+} sensors and Ca^{2+} sources is a critical factor in determining the contribution of VGCCs to spontaneous release. The physical distance between presynaptic VGCCs and Ca^{2+} sensors, which may vary depending on cell types and developmental states (Baur *et al.*, 2015; Bornschein *et al.*, 2019; Taschenberger *et al.*, 2002; Wang *et al.*, 2008), has been considered as an important feature of the synapses that determines the characteristics of AP-triggered neurotransmission (Eggermann *et al.*, 2012; Rebola *et al.*, 2019). This study highlights the role of coupling distance in regulating spontaneous neurotransmission. Moreover, the present study suggests that the contribution of LTCCs on spontaneous release by global Ca^{2+} concentration and individual stochastic opening of other VGCCs. The previous study did not mention the contribution of L-type VGCC on spontaneous release, because they used cultured hippocampal neurons 14-19 day after plating which was relatively younger than I have used. At young stage 8-10 DIV, the contribution of LTCCs on spontaneous glutamate release was not shown (Fig. 19) while Nimo decreased the amplitude of inward Ca^{2+} current significantly in young neurons which was not significantly different from the inhibitory effects of Nimo on Ca^{2+} current in adult neurons.

At last, I found the relation between K^+ channels and Ca^{2+} channels which can affect the spontaneous glutamate release. The role of K^+ channels on presynaptic Ca^{2+} at basal state is thought to be attributable to the changes in resting membrane potential (RMP), but direct experimental evidence is lacking. In the present study, I found a significant disparity between the effect of K^+ channels on RMP and that on spontaneous glutamate release, and presented evidence for a novel mechanism that enables a specific K^+ channel to regulate a specific Ca^{2+} channel in presynaptic terminals. To investigate whether the specific relationship between VGKCs and VGCCs in presynaptic terminal may occur, I performed the pharmacological experiments that individual VGCCs blockers are combined with individual VGKCs blockers on spontaneous glutamate release. Finally, I suggested that increased spontaneous release by blockade of K_V7 may specifically associate with LTCCs, while K_V1 may specifically associate with P/Q-type VGCCs.

REFERENCES

Adler, E.M., Augustine, G.J., Duffy, S.N., Charlton, M.P., 1991. Alien intracellular calcium chelators attenuate neurotransmitter release at the squid giant synapse. *J. Neurosci.*, 1496–1507

Ali, A.B., Todorova, M., 2010. Asynchronous release of GABA via tonic cannabinoid receptor activation at identified interneuron synapses in rat CA1. *Eur. J. Neurosci.* 31, 1196-1207.

Alle, H., Geiger, J.R., 2006. Combined analog and action potential coding in hippocampal mossy fibers. *Science* 311, 1290-1293.

Augustin, I., Rosenmund, C., Südhof, T.C., Brose, N., 1999. Munc13-1 is essential for fusion competence of glutamatergic synaptic vesicles *Nature* 400, 457-461.

Augustine, G., 1990. Regulation of transmitter release at the squid giant synapse by presynaptic delayed rectifier potassium current. *J. Physiol.* 431, 343-364.

Avery, R.B., Johnston, D., 1996. Multiple channel types contribute to the low-voltage-activated calcium current in hippocampal CA3 pyramidal neurons. *J. Neurosci.* 16, 5567-5582.

Awatramani, G.B., Price, G.D., Trussell, L.O., 2005. Modulation of transmitter release by presynaptic resting potential and background calcium levels. *Neuron* 48, 109-121.

Baur, D., Bornschein, G., Althof, D., Watanabe, M., Kulik, A., Eilers, J., Schmidt, H., 2015. Developmental tightening of cerebellar cortical synaptic influx-release coupling. *J. Neurosci.* 35, 1858-1871.

Bekkers, J.M., Stevens, C.F., 1991. Excitatory and inhibitory autaptic currents in isolated hippocampal neurons maintained in cell cultur. *Proc. Nati. Acad. Sci. U.S.A.* 88, 7834-7838.

Ben-Johny, M., Yue, D.T., 2014. Calmodulin regulation (calmodulation) of voltage-gated calcium channels. *J Gen Physiol* 143, 679-692.

Bornschein, G., Eilers, J., Schmidt, H., 2019. Neocortical high probability release sites are formed by distinct Ca^{2+} channel-to-release sensor topographies during development. *Cell. Rep.* 28, 1410-1418 e1414.

Brown, D.A., Adams, P.R., 1980. Muscarinic suppression of a novel voltage-sensitive K^+ current in a vertebrate neurone. *Nature* 283, 673-676.

Brown, D.A., Passmore, G.M., 2009. Neural KCNQ (Kv7) channels. *Br. J. Pharmacol.* 156,

1185-1195.

Bucurenciu, I., Bischofberger, J., Jonas, P., 2010. A small number of open Ca^{2+} channels trigger transmitter release at a central GABAergic synapse. *Nat. Neurosci.* 13**,** 19-21.

Carter, A.G., Vogt, K.E., Foster, K.A., Regehr, W.G., 2002. Assessing the role of calcium-induced calcium release in short-term presynaptic plasticity at excitatory central synapses. *J. Neurosci.* 22**,** 21–28.

Christie, J.M., Chiu, D.N., Jahr, C.E., 2011. Ca^{2+}-dependent enhancement of release by subthreshold somatic depolarization. *Nat. Neurosci.* 14**,** 62-68.

Chung, H.J., Jan, Y.N., Jan, L.Y., 2006. Polarized axonal surface expression of neuronal KCNQ channels is mediated by multiple signals in the KCNQ2 and KCNQ3 C-terminal domains. *PNAS* 103**,** 8870-8875.

Cooper, E.C., Milroy, A., Jan, Y.N., Jan, L.Y., Lowenstein, D.H., 1998. Presynaptic localization of Kv1.4-containing A-Type potassium channels near excitatory synapses in the hippocampus. *J. Neurosci.* 18**,** 965-974.

Courtney, N.A., Briguglio, J.S., Bradberry, M.M., Greer, C., Chapman, E.R., 2018. Excitatory and inhibitory neurons utilize different Ca^{2+} sensors and sources to regulate spontaneous release. *Neuron* 98**,** 977-991.

Dai, J., Chen, P., Tian, H., Sun, J., 2015. Spontaneous vesicle release Is not tightly coupled to voltage-gated calcium channel-mediated Ca^{2+} influx and is triggered by a Ca^{2+} sensor other than synaptotagmin-2 at the juvenile mice calyx of Held synapses. *J. Neurosci.* 35**,** 9632-9637.

Daw, M.I., Tricoire, L., Erdelyi, F., Szabo, G., McBain, C.J., 2009. Asynchronous transmitter release from cholecystokinin-containing inhibitory interneurons is widespread and target-cell independent. *J. Neurosci.* 29**,** 11112-11122.

DeLorenzo, R.J., 1981. The calmodulin hypothesis of neurotransmission. *Cell Calcium* 2**,** 365-385.

Di Giovanni, J., Iborra, C., Maulet, Y., Leveque, C., El Far, O., Seagar, M., 2010. Calcium-dependent regulation of SNARE-mediated membrane fusion by calmodulin. *J. Biol. Chem.* 285**,** 23665-23675.

Dodge, F.A.J., Rahamimoff, R., 1967. Co-operative action of calcium ions in transmitter release at the neuromuscular junction. *J. Physiol.* 193**,** 419-432.

Eggermann, E., Bucurenciu, I., Goswami, S.P., Jonas, P., 2012. Nanodomain coupling between Ca^{2+} channels and sensors of exocytosis at fast mammalian synapses. *Nat. Rev. Neurosci.* 13**,** 7-21.

Emptage, N.J., Reid, C.A., Fine, A., 2001. Calcium Stores in hippocampal synaptic boutons mediate short-term plasticity, store-operated Ca^{2+} entry, and spontaneous transmitter release. *Neuron* 29**,** 197-208.

Ermolyuk, Y.S., Alder, F.G., Surges, R., Pavlov, I.Y., Timofeeva, Y., Kullmann, D.M., Volynski, K.E., 2013. Differential triggering of spontaneous glutamate release by P/Q-, N- and R-type Ca^{2+} channels. *Nat. Neurosci.* 16**,** 1754-1763.

Geiger, J.R.P., Jonas, P., 2000a. Dynamic control of presynaptic Ca^{2+} inflow by fast-inactivating K^+ channels in mossy fiber boutons. *Neuron* 28**,** 927-939.

Geiger, R.P., Jonas, P., 2000b. Dynamic control of presynaptic Ca^{2+} inflow by fast-inactivating K^+ channels in hippocampal mossy fiber boutons. *Neuron* 28**,** 927-939.

Goswami, S.P., Bucurenciu, I., Jonas, P., 2012. Miniature IPSCs in hippocampal granule cells are triggered by voltage-gated Ca^{2+} channels via microdomain coupling. *J. Neurosci.* 32**,** 14294-14304.

Greer, P.L., Greenberg, M.E., 2008. From synapse to nucleus: calcium-dependent gene transcription in the control of synapse development and function. *Neuron* 59**,** 846-860.

Groffen, A.J., Martens, S., Arazola, R.D., Cornelisse, L., Lozovaya, N., Jong, A.P.H., Goriounova, N.A., Habets, R.L.P., Takai, Y., Borst, J.G., Brose, N., McMahon, H.T., Verhage, M., 2010. Doc2b is a high-affinity Ca^{2+} sensor for spontaneous neurotransmitter release. *Science* 327**,** 1614-1618.

He, S., Shao, L.-R., Rittase, W.B., Bausch, S.B., 2012. Increased Kv1 Channel Expression May Contribute to Decreased sIPSC Frequency Following Chronic Inhibition of NR2B-Containing NMDAR. *Neuropsychopharmacology* 37**,** 1338-1356.

Hefft, S., Jonas, P., 2005. Asynchronous GABA release generates long-lasting inhibition at a hippocampal interneuron-principal neuron synapse. *Nat. Neurosci.* 8**,** 1319-1328.

Hille, B., 1978. Ionic channels in excitable membranes. Current problems and biophysical approaches. *Biophys. J.* 22**,** 283-294.

Hua, Y., Sinha, R., Martineau, M., Kahms, M., Klingauf, J., 2010. A common origin of synaptic vesicles undergoing evoked and spontaneous fusion. *Nat. Neurosci.* 13**,** 1451-1453.

Huang, H., Trussell, L.O., 2011. KCNQ5 channels control resting properties and release probability of a synapse. *Nat. Neurosci.* 14**,** 840-847.

Ibata, K., Sun, Q., Turrigiano, G.G., 2008. Rapid synaptic scaling induced by changes in postsynaptic firing. *Neuron* 57**,** 819-826.

Jackson, M.B., Redman, S.J., 2003. Calcium dynamics, buffering, and buffer saturation in

the boutons of dentate granule-cell axons in the hilus. *J. Neurosci.* 23**,** 1612-1621.

Kaeser, P.S., Deng, L., Wang, Y., Dulubova, I., Liu, X., Rizo, J., Sudhof, T.C., 2011. RIM proteins tether Ca^{2+} channels to presynaptic active zones via a direct PDZ-domain interaction. *Cell* 144**,** 282-295.

Kavalali, E.T., 2015. The mechanisms and functions of spontaneous neurotransmitter release. *Nat. Rev. Neurosci.* 16**,** 5-16.

Kole, M.H., Letzkus, J.J., Stuart, G.J., 2007. Axon initial segment Kv1 channels control axonal action potential waveform and synaptic efficacy. *Neuron* 55**,** 633-647.

Lee, B.J., Yang, C.H., Lee, S.Y., Lee, S.H., Kim, Y., Ho, W.K., 2020. Voltage-gated calcium channels trigger spontaneous glutamate release via nanodomain coupling.

Liang, C.Q., Zhang, G., Zhang, L., Chen, S.Y., Wang, J.N., Zhang, T.T., Singer, J.H., Ke, J.B., 2021. Calmodulin Bidirectionally Regulates Evoked and Spontaneous Neurotransmitter Release at Retinal Ribbon Synapses. *eNeuro* 8.

Lipstein, N., Sakaba, T., Cooper, B.H., Lin, K.H., Strenzke, N., Ashery, U., Rhee, J.S., Taschenberger, H., Neher, E., Brose, N., 2013. Dynamic control of synaptic vesicle replenishment and short-term plasticity by Ca^{2+}-calmodulin-Munc13-1 signaling. *Neuron* 79**,** 82-96.

Lipstein, N., Verhoeven-Duif, N.M., Michelassi, F.E., Calloway, N., van Hasselt, P.M., Pienkowska, K., van Haaften, G., van Haelst, M.M., van Empelen, R., Cuppen, I., van Teeseling, H.C., Evelein, A.M., Vorstman, J.A., Thoms, S., Jahn, O., Duran, K.J., Monroe, G.R., Ryan, T.A., Taschenberger, H., Dittman, J.S., Rhee, J.S., Visser, G., Jans, J.J., Brose, N., 2017. Synaptic UNC13A protein variant causes increased neurotransmission and dyskinetic movement disorder. *J. Clin. Invest.* 127**,** 1005-1018.

Magee, J.C., Avery, R.B., Christie, B.R., Johnston, D., 1996. Dihydropyridine-sensitive, voltage-gated Ca^{2+} channels contribute to the resting intracellular Ca^{2+} concentration of hippocampal CA1 pyramidal neurons *J. Neurophysiol.* 76**,** 3460-3470.

Mejia-Gervacio, S., Collin, T., Pouzat, C., Tan, Y.P., Llano, I., Marty, A., 2007. Axonal speeding: shaping synaptic potentials in small neurons by the axonal membrane compartment. *Neuron* 53**,** 843-855.

Moosmang, S., Haider, N., Klugbauer, N., Adelsberger, H., Langwieser, N., Muller, J., Stiess, M., Marais, E., Schulla, V., Lacinova, L., Goebbels, S., Nave, K.A., Storm, D.R., Hofmann, F., Kleppisch, T., 2005. Role of hippocampal $Ca_V1.2$ Ca^{2+} channels in NMDA receptor-independent synaptic plasticity and spatial memory. *J. Neurosci.*

25, 9883-9892.

Murthy, V.N., Stevens, C.F., 1999. Reversal of synaptic vesicle docking at central synapses. *Nat. Neurosci.* 2, 503-507.

Neher, E., 1998. Usefulness and limitations of linear approximations to the understanding of Ca^{2+} signals. *Cell Calcium* 24, 345-357.

Neher, E., Sakaba, T., 2008. Multiple roles of calcium ions in the regulation of neurotransmitter release. *Neuron* 59, 861-872.

Pang, Z.P., Cao, P., Xu, W., Sudhof, T.C., 2010. Calmodulin controls synaptic strength via presynaptic activation of calmodulin kinase II. *J. Neurosci.* 30, 4132-4142.

Peters, J.H., McDougall, S.J., Fawley, J.A., Smith, S.M., Andresen, M.C., 2010. Primary afferent activation of thermosensitive TRPV1 triggers asynchronous glutamate release at central neurons. *Neuron* 65, 657-669.

Rebola, N., Reva, M., Kirizs, T., Szoboszlay, M., Lorincz, A., Moneron, G., Nusser, Z., DiGregorio, D.A., 2019. Distinct nanoscale calcium channel and synaptic vesicle topographies contribute to the diversity of synaptic function. *Neuron* 104, 693-710 e699.

Rhee, J.S., Betz, A., Pyott, S., Reim, K., Varoqueaux, F., Augustin, I., Hesse, D., Südhof, T.C., Takahashi, M., Rosenmund, C., Brose, N., 2002. Beta phorbol ester- and diacylglycerol-induced augmentation of transmitter release is mediated by Munc13s and not by PKCs *Cell* 108, 121-133.

Rodolfo R., L., Mutsuyuki, S., Bruce, C., 1989. Voltage-dependent calcium conductances in mammalian neurons. *Ann. N. Y. Acad. Sci.* 560, 103-111.

Rose, J., Jin, S.X., Craig, A.M., 2009. Heterosynaptic molecular dynamics: locally induced propagating synaptic accumulation of CaM kinase II. *Neuron* 61, 351-358.

Rosenmund, C., Sigler, A., Augustin, I., Reim, K., Brose, N., Rhee, J.S., 2002. Differential control of vesicle priming and short-term plasticity by Munc13 isoforms *Neuron* 33, 411-424.

Rudy, B., 1988. Diversity and ubiquity of K channels. *Neuroscience* 25, 729-749.

Rusakov, D.A., 2006. Ca^{2+}-dependent mechanisms of presynaptic control at central synapses. *Neuroscientist* 12, 317-326.

Sakaba, T., Neher, E., 2001. Calmodulin mediates rapid recruitment of fast-releasing synaptic vesicles at a calyx-type synapse. *Neuron* 32, 1119-1131.

Sara, Y., Virmani, T., Deak, F., Liu, X., Kavalali, E.T., 2005. An isolated pool of vesicles recycles at rest and drives spontaneous neurotransmission. *Neuron* 45, 563-573.

Schmidt, H., Brachtendorf, S., Arendt, O., Hallermann, S., Ishiyama, S., Bornschein, G., Gall,

D., Schiffmann, S.N., Heckmann, M., Eilers, J., 2013. Nanodomain coupling at an excitatory cortical synapse. *Curr. Biol.* 23**,** 244-249.

Schneggenburger, R., Rosenmund, C., 2015. Molecular mechanisms governing Ca^{2+} regulation of evoked and spontaneous release. *Nat. Neurosci.* 18**,** 935-941.

Scimemi, A., Diamond, J.S., 2012. The number and organization of Ca^{2+} channels in the active zone shapes neurotransmitter release from Schaffer collateral synapses. *J Neurosci.* 32**,** 18157-18176.

Shah, M.M., Migliore, M., Brown, D.A., 2011. Differential effects of Kv7 (M-) channels on synaptic integration in distinct subcellular compartments of rat hippocampal pyramidal neurons. *J. Physiol.* 589**,** 6029-6038.

Sharma, G., Vijayaraghavan, S., 2003. Modulation of presynaptic store calcium induces release of glutamate and postsynaptic firing. *Neuron* 38**,** 929-939.

Shoudai, K., Peters, J.H., McDougall, S.J., Fawley, J.A., Andresen, M.C., 2010. Thermally active TRPV1 tonically drives central spontaneous glutamate release. *J. Neurosci.* 30**,** 14470-14475.

Shu, Y., Yu, Y., Yang, J., McCormick, D.A., 2007. Selective control of cortical axonal spikes by a slowly inactivating K^+ current. *PNAS* 104**,** 11453-11458.

Steinhardt, R.A., Alderton, J.M., 1982. Calmodulin confers calcium sensitivity on secretory exocytosis. *Nature* 295**,** 154-155.

Sun, J., Kapur, J., 2012. M-type potassium channels modulate Schaffer collateral-CA1 glutamatergic synaptic transmission. *J. Physiol.* 590**,** 3953-3964.

Swandulla, D., Armstrong, C.M., 1989. Calcium channel block by cadmium in chicken sensory neurons. *Proc. Nati. Acad. Sci. U.S.A.* 86**,** 1736-1740.

Taschenberger, H., Leão, R.M., Rowland, K.C., Spirou, G.A., von Gersdorff, H., 2002. Optimizing synaptic architecture and efficiency for high-frequency transmission *Neuron* 36**,** 1127-1143.

Tippens, A.L., Pare, J.F., Langwieser, N., Moosmang, S., Milner, T.A., Smith, Y., Lee, A., 2008. Ultrastructural evidence for pre- and postsynaptic localization of $Ca_v1.2$ L-type Ca^{2+} channels in the rat hippocampus. *J. Comp. Neurol.* 506**,** 569-583.

Tsintsadze, T., Williams, C.L., Weingarten, D.J., von Gersdorff, H., Smith, S.M., 2017. Distinct actions of voltage-activated Ca^{2+} channel block on spontaneous release at excitatory and inhibitory central synapses. *J. Neurosci.* 37**,** 4301-4310.

Vervaeke, K., Gu, N., Agdestein, C., Hu, H., Storm, J.F., 2006. Kv7/KCNQ/M-channels in rat glutamatergic hippocampal axons and their role in regulation of excitability and transmitter release. *J. Physiol.* 576**,** 235-256.

Vivekananda, U., Novak, P., Bello, O.D., Korchev, Y.E., Krishnakumar, S.S., Volynski, K.E., Kullmann, D.M., 2017. Kv1.1 channelopathy abolishes presynaptic spike width modulation by subthreshold somatic depolarization. *PNAS* 114**,** 2395-2400.

Vyleta, N.P., Jonas, P., 2014. Loose coupling between Ca^{2+} channels and release sensors at a plastic hippocampal synapse. *Science* 343**,** 665-670.

Vyleta, N.P., Smith, S.M., 2011. Spontaneous glutamate release is independent of calcium influx and tonically activated by the calcium-sensing receptor. *J. Neurosci.* 31**,** 4593-4606.

Wang, D., Epstein, D., Khalaf, O., Srinivasan, S., Williamson, W.R., Fayyazuddin, A., Quiocho, F.A., Hiesinger, P.R., 2014. Ca^{2+}-Calmodulin regulates SNARE assembly and spontaneous neurotransmitter release via v-ATPase subunit V0a1. *J. Cell. Biol.* 205**,** 21-31.

Wang, H., Kunkel, D.D., Martin, T.M., Schwartzkroin, P.A., Tempel, B.L., 1993. Heteromultimeric K^+ channels in terminal and juxtaparanodal regions of neurons *Nature* 365**,** 75-79.

Wang, L.Y., Neher, E., Taschenberger, H., 2008. Synaptic vesicles in mature calyx of Held synapses sense higher nanodomain calcium concentrations during action potential-evoked glutamate release. *J. Neurosci.* 28**,** 14450-14458.

Westenbroek, R.E., Ahlijanian, M.K., Catterall, W.A., 1990. Clustering of L-type Ca^{2+} channels at the base of major dendrites in hippocampal pyramidal. *Nature* 347**,** 281-284.

Wheeler, D.B., Randall, A., Tsien, R.W., 1994. Roles of N-type and Q-type Ca^{2+} channels in supporting hippocampal synaptic transmission *Science* 264**,** 107-111.

Williams, C., Chen, W., Lee, C.H., Yaeger, D., Vyleta, N.P., Smith, S.M., 2012. Coactivation of multiple tightly coupled calcium channels triggers spontaneous release of GABA. *Nat. Neurosci.* 15**,** 1195-1197.

Williams, C.L., Smith, S.M., 2018. Calcium dependence of spontaneous neurotransmitter release. *J. Neurosci. Res.* 96**,** 335-347.

Xu, J., Mashimo, T., Sudhof, T.C., 2007. Synaptotagmin-1, -2, and -9: Ca^{2+} sensors for fast release that specify distinct presynaptic properties in subsets of neurons. *Neuron* 54**,** 567-581.

Xu, J., Pang, Z.P., Shin, O.H., Sudhof, T.C., 2009. Synaptotagmin-1 functions as a Ca^{2+} sensor for spontaneous release. *Nat. Neurosci.* 12**,** 759-766.

ABSTRACT in KOREAN

시냅스 말단에 도달한 활동 전위에 의해 유발되는 신경 전달 물질의 방출은 신경 세포 사이의 신호 전달의 핵심 과정이다. 또한 휴지기 상태에서도 자발적으로 신경 전달 물질이 방출되며, 이 자발적 방출은 시냅스의 성숙 및 유지, 항상성 및 가소성에서 중추적인 역할을 한다. 자발적 방출의 기본이 되는 분자 기전은 활동 전위에 의해 유발된 신경 전달 물질의 방출과 동일한지 여부는 아직 많은 것이 밝혀지지 않았다. 이번 연구는 단일 신경세포가 스스로 시냅스를 이룰 수 있게 배양 된 해마의 흥분성 신경 세포 (autaptic hippocampal excitatory neuron)에서 전압 클램프를 이용하여 -70 mV에서 측정 된 미니어쳐 흥분성 후시냅스 전류 (mEPSC)의 유발 빈도를 분석하여 자발적 글루탐산 방출에 대한 전압 의존적 칼슘 이온 통로 (voltage-gated Ca^{2+} channel)의 기여를 관찰하였다. ω-Agatoxin-IVA, ω-Conotoxin GVIA 및 SNX-482 또는 100 μM $NiCl_2$를 사용한 P/Q-, N- 및 R- 형 칼슘 이온 통로의 차단은 mEPSC 유발 빈도를 29%, 27% 및 23%로 크게 감소 시켰다. 또한 세 가지 칼슘 이온 통로 차단제의 동시 적용 또는 세포 외용액의 칼슘 이온 제거는 mEPSC 유발 빈도를 60% 감소 시켰으며, 이는 자발적 방출의 60 %가 칼슘 이온 통로를 통한 칼슘이온의 유입에 의해 매개됨을 시사한다. 세포 외부 칼슘 이온 농도에 대한 칼슘 이온 통로 의존성 mEPSC 유발 빈도의 log-log 그래프에서 기울기는 1.24였으며, 이는 자발적 방출에 대한 칼슘 이온의 cooperativity를 시사한다. mEPSC의 방출 빈도는 5mM EGTA에 의해 크게 영향을 받지 않았지만, BAPTA에 의해 감소했다. BAPTA 농도가 0.5mM에서 1mM 및 5mM으로 증가함에 따라 감소 속도가 더

빨라짐을 관찰하였다. BAPTA에 의한 mEPSC 방출 빈도의 농도 의존적 감소로부터 추정 된 시냅스 소포체의 칼슘 감지 단백질과 칼슘 이온 통로 사이의 거리는 약 20 nm로 관찰되었다. 종합하면, 칼슘 이온 통로의 확률적 개방은 전압 의존적 칼슘 이온 통로와 시냅스 소포체의 칼슘 감지 단백질 사이의 나노 도메인 결합에 의해 자발적 글루탐산 방출을 유발한다. 다음으로, 자발적 방출에 대한 글로벌 칼슘 이온 농도의 영향을 알아보기 위해 전압 클램프의 막전압을 조절하여 다양한 막전압에서 mEPSC 유발 빈도를 기록하였다. 탈분극 된 막전압은 mEPSC 유발을 증가시키지만, L-형 칼슘 이온 통로의 차단 또는 항진을 하게 되면 탈분극에 의한 mEPSC 유발 빈도의 증가가 사라짐을 발견하였다. 더욱이, 칼모듈린 억제 펩티드를 처리하여 칼모듈린 의존적 시냅스 소포의 세포외방출을 억제하면, L-형 칼슘 이온 통로에 의한 mEPSC 유발빈도가 나타나지 않음을 관찰하였다. 따라서, L-형 칼슘 이온 통로는 글로벌 칼슘 이온 농도를 조절하여 칼모듈린 의존적 시냅스 소포 세포외방출 경로를 통해 자발적 글루탐산 방출을 일으킬 수 있음을 제시한다. 마지막으로 자발적 글루탐산 방출에 대한 칼륨 이온 통로와 칼슘 이온 통로 사이의 관계를 관찰하였다. 전시냅스 말단에서 전압 의존적 칼슘 이온 통로의 확률적 개방은 소포체 방출을 유발하는 것으로 알려져 있지만, 명확한 작용기전은 잘 알려진 바 없다. 휴지 상태의 전시냅스 말단에서 칼륨 이온 통로가 칼슘 이온 농도에 미치는 역할은 휴지 막 전위 (RMP)의 변화에 기인하는 것으로 생각되지만 직접적인 실험 증거는 부족한 바 이다. 본 연구는 RMP에 대한 칼륨 이온 통로의 효과와 자발적 글루탐산 방출 사이에 상당한 차이가 있음을 발견하였고, 특정 칼륨 이온 통로가 전시냅스 말단에서 특정 칼슘 이온 통로를 조절할 수 있는 새로운 기전에 대한 증거를 제시한다.

키워드 : autaptic 해마 흥분성 피라미드 신경 세포, 전압 의존적 칼슘 이온 통로, 전압 의존적 칼륨 이온 통로, 세포 내 휴지기 칼슘 농도, 자발적 시냅스 신호 전달, 활동 전위에 의한 시냅스 신호 전달, 칼슘 나노 도메인

학 번 : 2010-31172